University of Potsdam
Institute of Earth- and Environmental Science

Doctoral Thesis

Recurrence Plots and Quantification Analysis of Flood Runoff Dynamics

Author:

Dadiyorto Wendi

Cumulative Dissertation

Submitted for the Doctor of Engineering (Dr.-Ing)
The Faculty of Mathematics and Natural Sciences
at the University of Potsdam

September 2018

Supervisors and reviewers:
Prof. Dr. -Ing. Bruno Merz
Dr. rer. nat. Norbert Marwan

Mentor:
Prof. Dr. rer. nat. Jürgen Kurths

Independent reviewer:
Prof. Dr. -Ing Erwin Zehe

Date of disputation:
5 April 2019

Published online at the
Institutional Repository of the University of Potsdam:
https://doi.org/10.25932/publishup-43191
https://nbn-resolving.org/urn:nbn:de:kobv:517-opus4-431915

Abstract

The main motivation of this study is to develop a method and an elaborate index that are capable of identifying effective changes in flood runoff processes over time. The effective change proxy selected is the stream discharge time series as it is already an integration of spatio-temporal variations of processes within a catchment. As a result of the changes in the boundary conditions of a hydrological system, such as the characteristics of climate, river drainage, and catchments land surface, change in the runoff dynamics is expected. Urbanization, climate change, and different water management practices could have a substantial impact on the characteristics of floods, such that the causative mechanism related process typology of a flood could become unusual from how it is used to be. In addition, different processes can also cascade to cause unprecedented flood dynamics. In this study, the aforementioned effective change discusses on visible characteristics change of the catchment outlet runoff that can be triggered by any modified boundary conditions.

The common practice of analyzing the occurrence of an extreme or rare flood is calculating its return period over a long flood time series. However, this return period is often based upon the index of the peak discharge or maximum water level and therefore is not comprehensive enough to describe the rarity of the process typology. In order to extend the analysis to include more comprehensive runoff characteristics, we introduce the characterization of runoff dynamics that considers the shape of the hydrograph, portrayed as a phase space trajectory. To distinguish the event hydrograph further, the approach is taken to the next level by considering the non-linear and non-monotonic relationship between magnitudes of different time points by using Taken's time delay embedding theorem. This takes the implicit temporal succession of discharge values into consideration, such that the impact of the initial conditions on the flood events is considered as a characteristics vector in the multi-dimensional time delay phase space. This mentioned temporal succession of discharge values is herein called a temporal cascade. This study argues that the proposed characterization of runoff dynamics which includes the continuous shape of hydrograph shape and the temporal cascade is more elaborate and is a better proxy to detect rare flood processes.

As the first application attempt in Hydrology, Recurrence Plot (RP) and Recurrence Quantification Analysis (RQA) are used to visualize and determine the overall similarity between flood runoff dynamics i.e. through a quantitative index as to whether or not a certain dynamic is rare among historical observations. Rooted from the field of theoretical physics, these tools have gained considerable popularity over the past decades in several sci-

entific disciplines, from economics, physiology, neuroscience, paleoclimatology, astrophysics to engineering, especially for non-linear time series analysis and studying the behavior of a complex system. This study includes application examples dedicated to hydrologists to better understand the concept of characterizing runoff dynamics and the usefulness of the additional hydrograph similarity index. This study also extends the current state of RP and RQA with improved robustness towards artifacts and the influence of noise and is adapted to the observation runoff series. This includes the practical method to safely parameterize the time delay embedding and RP, and an extended version of the RP and RQA to reduce the influence of noise, in order to prevent further artifacts. The examples utilize the runoff time series from the Dresden gauging station of the Elbe river catchment located in East Germany from the period of 1901 to 2010. In this study, we showcase examples of rare and unseasonal floods detected by their unusual runoff dynamics that are found to be related to their documented causative mechanism. The advantage of using such a rarity index over the approach of comparing conventional hydrograph indices is assessed and discussed.

Zusammenfassung

Ziel dieser Arbeit ist es, eine Methode und einen umfassenden Index, die die Quantifizierung von Veränderungen in Hochwasserabflüssen über die Zeit ermöglichen, zu entwickeln. Als Proxydaten zur Detektion von Veränderungen dienen Abflusszeitreihen, da diese räumlich-zeitliche Änderungen von Prozessen im Einzugsgebiet integrieren. Einhergehend mit Veränderungen in den Rahmenbedingungen hydrologischer Systeme, beispielsweise Klimaänderungen, Veränderungen im Flussnetzwerk oder der Bodenbedeckung, sind Veränderungen in der Abflussdynamik zu erwarten. Urbanisierung, Klimawandel und veränderte wasserwirtschaftliche Nutzung können erheblichen Einfluss auf Hochwassercharakteristika haben, sodass die auf die abflussverursachenden Prozesse bezogene Hochwassertypologie obsolet wird. Außerdem kann es zur Überlagerung verschiedener Prozesse und der Bildung präzedenzloser Hochwasserdynamiken kommen.

Üblicherweise wird seltenen Hochwasserereignissen eine über einen langen Zeitraum bestimmte Wiederkehrwahrscheinlichkeit zugewiesen. Allerdings wird die assoziierte Wiederkehrdauer häufig nur auf der Grundlage des Höchstwasserstandes ermittelt und ist nicht umfassend genug, um die unterschiedlichen Prozesstypen zu erfassen. Um umfassendere Abflussmerkmale in die Hochwassercharakterisierung aufzunehmen, wird die Charakterisierung der Abflussdynamik mittels der kontinuierlichen Gestalt des Hydrographen und als Kurve im Phasenraum empfohlen. Durch die Berücksichtigung des Taken'schen Satzes zur Einbettung der Zeitverzögerung können ereignisbasierte Hydrographen weiter unterschieden werden. Dieser Ansatz nutzt die zeitliche Abfolge gemessener Abflusswerte, sodass der Einfluss der anfänglichen Werte auf das Hochwasserereignis als charakteristischer Vektor im multidimensionalen Phasenraum interpretiert werden kann.

Im Rahmen dieser Arbeit wurden, erstmals im Bereich der Hydrologie, ‚Recurrence Plot' (RP) und ‚Recurrence Quantification Analysis' RQA eingesetzt, um die Seltenheit bzw. Ähnlichkeit von Abflussdynamiken zu visualisieren und identifizieren. Ebenso werden Anwendungsbeispiele im Bereich der Hydrologie, die das Konzept der Charakterisierung von Abflussdynamiken und den Nutzen des eingeführten Ähnlichkeitsindex verdeutlichen, vorgestellt. Außerdem wurde die Methodik weiterentwickelt und zeichnet sich nun durch erhöhte Robustheit gegenüber Störeinflüssen und eine bessere Anpassung an Abflussmessungen aus. Ein abschließendes Anwendungsbeispiel untersucht den in Dresden gemessenen Abfluss des ostdeutschen Elbe-Einzugsgebietes im Zeitraum von 1901 bis 2010. In dieser Studie werden Beispiele seltener und saisonunabhängiger Hochwasserereignisse, die durch ihre ungewöhnliche Abflussdynamik herausstechen, gezeigt und mit zugrundeliegenden

abflussbildenden Prozessen in Verbindung gebracht.

Acknowledgement

I would like to express my gratitude to my supervisors Prof. Bruno Merz and Dr. Norbert Marwan for their tremendous support, guidance, and critical suggestions alongside the fruitful discussions that contribute to this PhD. This extends to the opportunities and facilities such as the valuable working networks, supporting team and the conducive environment provided under the associated GFZ German Research Centre for Geosciences and PIK Potsdam Institute for Climate Impact Research. This work could not be realized without the expert knowledge inputs of Flood and Hydrology subjects from Prof. B. Merz and the immense methodological guidance and support rooted in Theoretical Physics from Dr N. Marwan.

I would like to thank German Research Foundation (DFG) for the excellent funding and research support provided under the *NatRiskChange* research training group. A big thanks is dedicated for the *NatRiskChange* leaders Prof. Axel Bronstert and Prof. Annegret Thieken and the project coordinator Dr. Theresia Petrow for organizing the training group and provided enormous training supports and facility required to conduct my research. In addition, I truly appreciate Prof. A. Bronstert for his valuable expert inputs and references to my research especially in the causative mechanism of rare flood in Dresden.

A special thanks is dedicated to Dr. Mathias Deutsch for his great archive of the historical floods; Dr. Dung N., S. Ludke., Dr. K. Schröter, Prof. K. Arnbjerg-Nielsen, H. Kraemer, Dr. D. Eroglu, and L. Tarasova for their valuable comments, suggestions, and references to the study. I sincerely appreciate the technical and administrative supports provided by D. Bazant, K. Günther, S. Schrader, R. Zimmer, and H. Prietzel. I am also grateful for the help by M. Heistermann and G. Koc that I could smoothly conduct my teaching duties. Despite not being part of this thesis, I would like to thank all the co-authors for the successful and fun inter-disciplinary taskforce collaboration for the flood disaster in Braunsbach that result in several substantial publications.

I would extend my gratitude to my better half, who shared the adventure with full motivational support and understanding. I am also thankful for the early nurture received by Prof. Liong S.Y., who motivated me to pursue the career of hydro-informatics with the openness towards inter-disciplinary approach. Further thanks is directed to friend Lars for his wholesome motivational support; for Sebastian and Konrad on their introduction to German land use history; Michael and Erwin for their help in German translation, and other friends and colleagues who have accompanied me through the challenging times and kept me entertained.

Declaration of Authorship

I, Dadiyorto Wendi, hereby confirm that I have authored this thesis entitled "Recurrence Plots and Quantification Analysis of Flood Runoff Dynamics" independently and without use of others than the indicated sources. This thesis was carried out at the Institute of Earth and Environmental Sciences, University of Potsdam. All passages which are literally or in general matter taken out of publications or other sources are marked as such.

I confirm that:

- This work was done wholly or mainly while in candidature for a research degree at this University.
- Where any part of this thesis has previously been submitted for a degree or any other qualification at this University or any other institution, this has been clearly stated.
- Where I have consulted the published work of others, this is always clearly attributed
- Where I have quoted from the work of others, the source is always given. With the exception of such quotations, this thesis is entirely my own work.
- I have acknowledged all main sources of help
- Where the thesis is based on work done as a joint work with co-authors, I have specified the scope of contributions in the Introduction chapter, section 1.3.

Dadiyorto Wendi
Potsdam, GERMANY, September 27, 2018

Table of Content

List of Abbreviation

CRP Cross Recurrence Plot

ACF Auto Correlation Function

AMAX Annual maximum of a discharge series

DDET Diagonal Window based Determinism

DEM Digital Elevation Model

FNN False Nearest Neighbour

GHS Global Human Settlement

GIS Geographic Information System (Application Tool)

LM Local Minima Approach for RP and CRP

LMT Local Minima Approach with 2 additional parameters i.e., threshold and minimum distance between minimas

LMT Local Minima Approach with additional Threshold parameter

LOI Line of Identity, the main diagonal line in a RP, i.e. $R_{i,i} = 1$

MI Mutual Information

RP Recurrence Plot

RQA Recurrence Quantification Analysis

List of Symbols

$\beta(t)$	Gaussian white noise
ΔQ_{fall}	falling slope of hydrograph
ΔQ_{rise}	rising slope of hydrograph
Δt	time step or sampling time
σ,ρ and,β	parameters of Lorenz system
τ	time delay
τ_w	lag of the moving/ sliding window starting from LOI
$\tilde{x}(t)$	time series $x(t)$ with induced noise $\beta(t)$
ε	Distance threshold for RP and CRP
$\vec{x}_i$	a phase space vector created from a variable u_i
BFI	baseflow index, ratio of event's baseflow volume over total volume
$CR_{i,j}(\varepsilon)$	cross recurrence matrix (CRP) between two phase space trajectories $\vec{x}_i$ and $\vec{y}_j$ at states i and j correspond to distance threshold ε
D or Δk	diagonal recurrence point distance along the axis k calculated between each consecutive recurrence points
$D(max)$	threshold for maximum gap distance k allowed
DD_{w_i}	alternative determinism indicator for each sliding window
$DDET$	Determinism indicator using sliding diagonal window method
DET	Determinism: diagonal line measure for recurrence quantification; used to defined similarity or synchronization between dynamics in CRP
DET *distance*	distance between DET of each shuffled time series (DET_i) and the original time series (DET_i)
i, j, k	indices

K	storage constant parameter of Muskingum equation [time unit]
l_{min} or d_{min}	predefined minimal length of a diagonal line
LAM	Laminarity: vertical line measure for recurrence quantification to define laminar states in RP
LOI	line of identity (the main diagonal line in a RP, $R_{i,j}$)
m	embedding dimension
Md	median of $DETdistance$
N_{d}	the absolute number of those diagonal lines
N_{v}	the absolute number of those diagonal lines
$P(D_j)$	frequency distribution of the gap distance k between consecutive diagonal recurrence points ($d_k \equiv 1$)
$P(l)$ or $P(d)$	the histogram of the lengths d of connected diagonal lines
$P(v)$	histogram or frequency distribution of vertical line lengths
Q_p)	event discharge or hydrograph peak $[m^3/s]$
Q_t	discharge time series $[m^3/s]$, sometimes separated to Q_a and Q_b to indicate different event discharge series/ hydrograph
R or r	correlation coefficient (Pearson)
$R_{i,j}(\varepsilon)$	recurrence matrix (RP) of a phase space trajectory $\vec{x}$ at states i and j within distance threshold ε
RR	measure for recurrence quantification: recurrence rate (percent recurrence)
RR_{w_i}	recurrence rate of a diagonal window
Sd	standard deviation of $DETdistance$
SNR	signal to noise ratio, calculated as $log(\frac{signal}{noise})$ in decibel (dB)
t_d	event's duration [time unit]
t_f	recession time, time required from the peak discharge to the depletion of direct flow [time unit]
t_p	event's time to peak [time unit]

u_i	time series of variable u of time i
V	event discharge volume, approximated using trapezoidal integration of event hydrograph [m^3]
$vmin$	predefined minimal length of a diagonal line
w_i	sliding window
ws	sliding window size
x	weighing factor parameter of Muskingum equation

List of Figures

List of Tables

1 Introduction

1.1 Motivation

The main motivation of this study is to develop a method and an elaborate index that are capable of quantifying changes of flood runoff processes over time. The particular data interest for the change proxy is the stream discharge time series. This is because stream discharge is already an integration of spatio-temporal variations of processes starting from water input, storage, and routing or transfer within a catchment, and essential to characterize a hydrological regime [Harris et al., 2000, Ternynck et al., 2016]. Therefore the use of catchment outlet streamflow dynamics for the study of flood change allows minimum resources or datasets and appropriate to capture the effective change of a catchment system as it is after all the end result of processes within.

Although there are already variety of indices derived from flood event discharge series, i.e., those used to describe hydrograph characteristics, they are quite limited in characterizing the whole extent of runoff dynamics, such as the continuous shape of the flood hydrograph is not captured and neither is the dynamics influence of its antecedent states being considered. Therefore, arguably, these indices are not elaborate enough to be related to the changes in runoff processes.

The intended use of such elaborate hydrograph characteristics is to be able to compare the similarity of process dynamics between one flood event to another, and also to assess how unusual is a particular flood event to all others that has happened before. For instance this could be hydrograph characteristics that has never been observed before i.e. rare due to unusual process dynamics, or the type of hydrograph that is not usual at a particular season i.e. unseasonal (see illustration of Fig. 1.1). In contrast to just using peak runoff as the indicator for rare events, shape of the hydrograph could further distinct a particular event characteristics as it contains the flow dynamics of how flood water continually build up and recess through time.

The chosen approach is through representing flood hydrographs as phase space trajectories to exploit their time sequence properties and have their similarity or rarity analyzed and quantified using Recurrence Plot (RP) and Recurrence Quantification Analysis (RQA). The concept of phase space to represent hydrograph time sequence property or herein also called runoff dynamics is presented briefly in section 1.1.4. Using both RP and RQA to analyse phase space trajectories has gained considerable popularity over the past decades in several scientific disciplines, from economy, physiology, neuroscience, paleoclimatology,

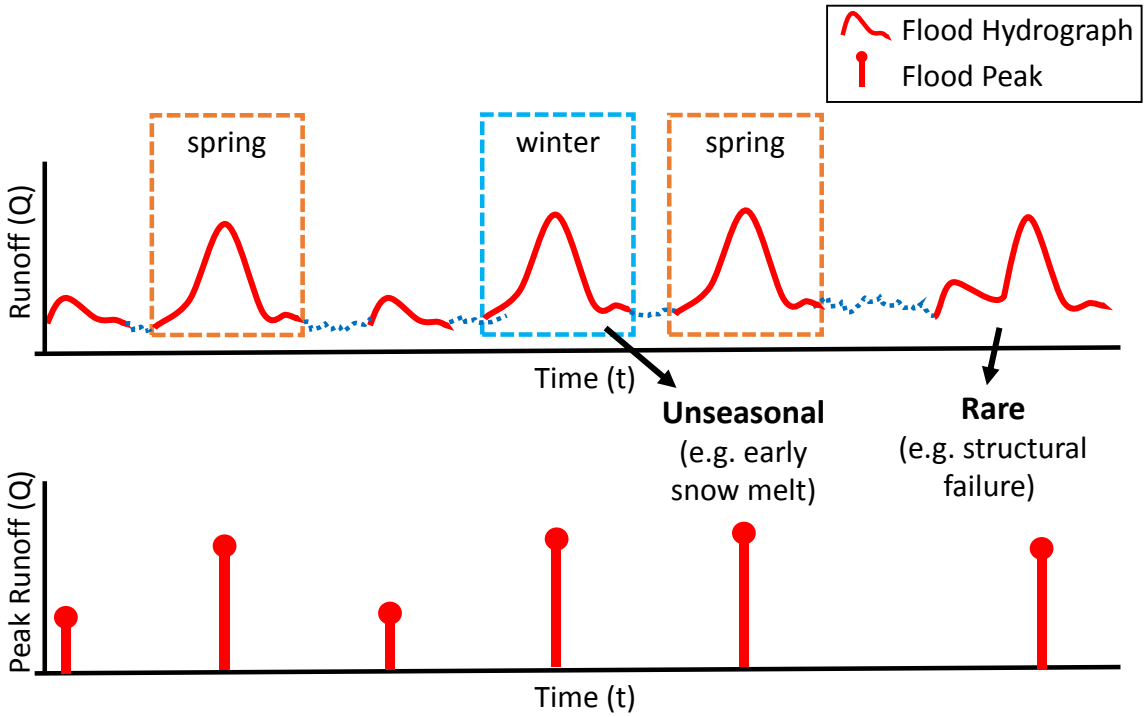

Figure 1.1: Illustration of the intended use of elaborate hydrograph characteristics to assess unseasonal and rare floods within the catalog of historical observations

astrophysics to engineering, especially when focusing on non-linear times series analysis and characterizing the behavior of complex systems [Aceves-Fernandez. et al., 2012, Carrubba et al., 2010, Crowley, 2008, Eroglu et al., 2016, Goswami et al., 2018, Marwan and Meinke, 2004, Oberst and Lai, 2015]. However, such approach is challenged by potential artifacts when not being parameterized properly and can be sensitive to noise that are common in observation series. Furthermore, since such approach has not been used in hydrology, it is therefore important to adapt their application to hydrological data and assess their applicability and usefulness for the intended analysis of change in flood dynamics.

1.1.1 Changes in Boundary Conditions

Along with the changes in the boundary conditions of hydrological system, such as the characteristics of climate, river and catchments land surface, changes in runoff dynamics are expected. Urbanization, climate change, and different water management practice could have a substantial impact on the characteristics of floods, such that the typology of the flood might become unusual and possibly include a cascade of processes. This referred flood typology is mainly the types of causative mechanisms of flood that can be weather related like those defined to include long-rain floods, short rain floods, flash floods, rain-on-snow floods and snowmelt floods [Merz and Blöschl, 2003]. The causative mechanism of flood can also be defined further to include failures and unusual conditions of the catchment or drainage, such as those resulting from dam or levee break, landslide,

ice jam, debris flow, failure of urban drainage, lake and sea level rise, etc. For instance the disastrous extent of flash flood hazard in Braunsbach of Southwest Germany in May 2016 was not just caused by the extreme rainfall intensity fallen over steep slopes alone, therefore the rapid direct runoff, but rather a cascade with debris flow originated from the landslides mass of the unsteady slopes, riverbank incision, and eroded sediment that further destroyed the village [Ozturk et al., 2018].

A report by The Climate Service Centre in Germany, showed that overall amount of precipitation in Germany has increased by 10.2 percent relative to the long term average from 1961 to 1990 and this is mainly contributed by the high increase of the precipitation during winter [Brasseur et al., 2017]. The average wintertime precipitation has increased by 47 mm between 1881 and 2014. Green house gases based future projections from this study also show most simulations lead to a further increase in the next one hundred years. Moreover, the study also indicate an increased potential of severe storms and hail. Heavy and intense rainfall during winter is rather untypical for the season. Such could also lead to rare flood typology, for example where unseasonal heavy rainfall falls shortly upon cold frozen ground in the winter. This frozen ground reduces infiltration and hence water flows rapidly as surface runoff and result in a flashy and pronounced peak discharge. Another example of a rare flood typology is ice jam, where ice debris are being carried downstream by rainfall inflow and accumulate at a particular river section and jam the system to cause inundation, although due to the increased temperature during winter, such typology is expected to become less.

The impact of the increased intensity of precipitation would be more pronounced had the change of land surface become more impervious, thus leading to faster response of discharge with dominant surface runoff. Such surface imperviousness can be contributed by soil sealing which is dominantly a byproduct of urbanization with the examples of increased road networks, paved surface, and buildings [European Commission, 2012]. Germany for instance has experienced the conversion of land to urban use at a rate of 80-130 hectares per day between 1993 and 2004 [European Commission, 2012]. The increase of built-up areas can also be further supported through satellite imagery, for instance the built-up index dataset of Global Human Settlement (GHS) derived from Landsat imagery. Fig. 1.2 shows a side by side comparison of the built-up index in Germany between 1975 and 2014, where the built-up footprint proportion are shown as a ratio from 0 to 1, has shown the noticeable increase over the whole country, and especially in the west side.

However, the moderate impact of land cover change towards flood peak and volume is predominantly within the boundary of convective rainfall (i.e usually during summer) and hence quite local, as compared to the advective ones especially in meso-scale catchment scale i.e. above 100 km^2. Moreover, its impact gets smaller with the increase of catchment size due to the superimposition of flood waves from different tributaries as concluded by Bronstert et al. [2007] on the Rhine catchment study. In addition, it is also worthy to note

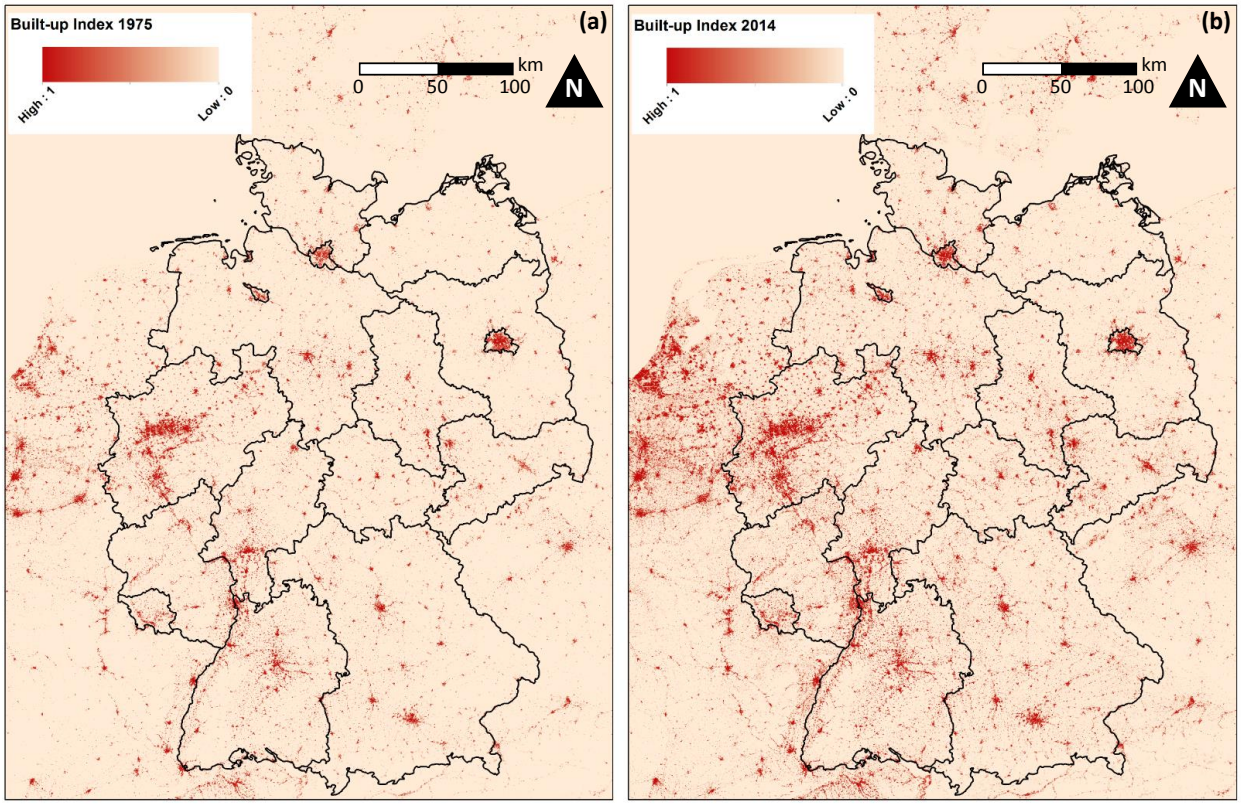

Figure 1.2: Comparisons of satellite based (Landsat) GHS built-up index between 1975 and 2014, dataset downloaded from Joint Research Centre of European Commission, with 250m resolution, and the index indicates a proportion (or ratio) of the built-up area within a grid cell

that there has been an increased of forest cover in Germany with an approx. 10,000 km^2 over the past 4 decades [Federal Ministry of Food Agriculture and Consumer Protection (BMELV), 2011]. However, according to Bronstert et al. [2007], although forested areas would naturally increase the water retention capacity, the forests in Central Europe often grow in mountainous regions with thin soils and low-permeable bedrock. Therefore the overall storage capacity of the soil in these areas is limited to a smaller scale impact. Their study also indicates that the highest relevance towards the magnitude of flood peaks is rather the antecedent soil moisture prior to the storm, and yet a flood peak or its return period is not a suitable indicator to assess the impact of land-cover on floods as it provides a very limited insights on the runoff generation processes in a catchment. Possibly, this is in line with the research shown by Bormann et al. [2011], Petrow and Merz [2009], where no increase consensus of flood peak magnitude and frequency is concluded for the second half of the 20th century in Germany, and that the observed changes are more pronounced in the winter as compared to the summer.

Moreover, to complicate the matter, alterations in the river are also known to have dominated European history for hundred of years, in particular with the motivation for navigation, flood protection and, more recently, hydropower and environmental restoration

[Hall et al., 2014]. Bronstert et al. [2007] suggested that river training measures might affect floods at a similar level or larger, than land use change for large basin in the past decade. The floodplains of the larger rivers in Germany have lost on average two-thirds of their former area [BMU/ BfN, 2009, Follner et al., 2010]. In Rhine catchment for instance, where floodplains have been reduced by 60% [UBA/ UBA, 2013], study by Vorogushyn and Merz [2013] showed that river training had caused a systematic superposition of flood waves of the Rhine and its tributary, the Neckar River, which had increased the annual maximum floods by about 10% for the analysis period between 1950-2009.

However, in line with the view of Bronstert et al. [2007] the assessment of changes in flood process with respect to runoff generation process dynamics might require a more elaborate indicator instead of flood peak index alone. Furthermore, the analysis of flood seasonality is commonly attached to the season classified strictly based on calendar months e.g. summer is defined to be from June to August, instead of the real flood typology. Therefore, if any of the typical summer flood typology i.e. convective rainfall flood is occurring beyond the calendar season, this method is unable to capture this interesting aspect of change. In the study of Vormoor et al. [2015] for instance, it is concluded that the increased winter temperatures have replaced snow-melt with rainfall as the dominant causative mechanism of the flood in the Norwegian catchments, and in line with the change of flood seasonality.

In case the changing boundary have a pronounced and effective impact on the increase rarity of flood typology and shift of seasonality, this study is to develop method and index to quantify any effective change observed from the discharge series of the catchment's outlet through the elaborate characteristics of their flood hydrographs.

1.1.2 Conventional Hydrological Signatures for Flood Event and Their Limitations

A range of indicators extracted from discharge time series, in the following called hydrological signatures, have been used to describe rainfall-runoff event hydrographs. The hydrograph peak (Q_p) for instance is the most popular hydrological signature in flood risk assessment due to its close relationship with the socio-economic impact of floods. Other important hydrological signatures are mean flow (Q_{mean}), discharge volume (V), event duration (t_d), time to peak (t_p), recession time (t_f), base flow index (BFI), or the rising and falling limb slope of the hydrograph (ΔQ_{rise} and ΔQ_{fall}) and could provide more information to the flood causative mechanism. For instance, the attempt from Gaál et al. [2015] to classify intra-seasonal flood typology using volume to peak discharge ratio. However, they are rarely incorporated to the analysis of flood change. These signatures have been used mainly as general similarity indices of hydrological characteristics, that are not necessarily flood, i.e. required for classification, regionalisation, prediction, and model calibration [Bárdossy, 2006, Merz and Blöschl, 2003, Peel and Blöschl, 2011, Sawicz et al., 2014, Westerberg and McMillan, 2015, Westerberg et al., 2016]. Although the

consideration of other hydrological signature would provide more insight to the runoff causative mechanism or the typology of the flood, just like flood peak they represent only a single element of the hydrograph (Q_p, t_d, t_p, and t_f), or their derivations are resulted from statistical aggregate of a hydrograph (Q_{mean}, V, BFI and ΔQ_{rise}, and ΔQ_{fall}). For instance, as also discussed in Chapter 4, slope based indices often provide a misleading depiction of the flood hydrograph with multi-peaks, as its derivation lump or average across characteristics of several sub-events i.e. referred by the multi-peaks. Furthermore, we argue that these signatures are not comprehensive enough to describe the flood causative mechanism implied by the shape of the hydrograph.

1.1.3 Sequence as a Substantial Information

What makes a certain English word unique to provide a specific meaning is its sequence of letters or characters. For instance when the 6 letters combination word 'LISTEN' is shuffled (see Fig. 1.3), it could generate a permutation of 720 words, mostly non-meaningful words and some words that have totally different meaning. Further we can also consider shuffling phrases like 'ELEVEN PLUS TWO' into one of the possibilities 'TWELVE PLUS ONE'. Although the two phrases contains the same histogram of letters, and can be summarized with a value of 13, the process mechanism and reasons why they are 13 are not the same.

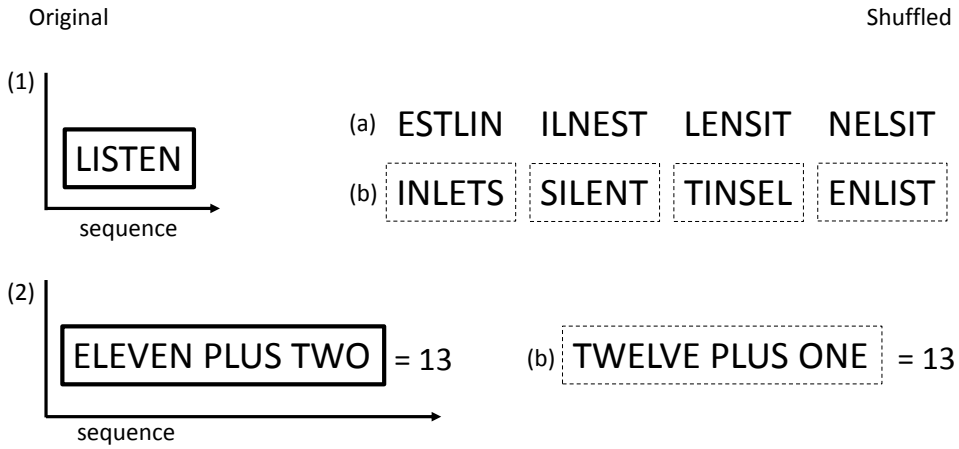

Figure 1.3: The important sequence of letters in a word and a phrase, examples from shuffling 'LISTEN' and 'ELEVEN PLUS TWO' into non meaningful words and words or phrase with different meaning

Similar to the information in words and phrases, the distinct information of hydrograph also depends on the sequence of the runoff magnitude in time. This essentially translates into the shape of the hydrograph, and known to vary on climatic inputs, catchment and river conditions or characteristics. For instance, the high rising slope of the hydrograph represents how flashy is the river flow possibly correspond to short intensive rainfall or even the catchment steep slope and sealed surface that prevent much infiltration. Moreover, the shape of a particular flood hydrograph is sensitive to its antecedent condition. For

instance if prior to a flood, there existed a moderate rainfall-runoff event that already sufficient to saturate the catchment's soil moisture and hydraulics capacity, the subsequent event, i.e. flood would easily build up upon the existing condition and easily overflow the system and trigger a flashier hydrograph and hence a more severe flood (see illustration in Fig. 1.4). In this study, the implicit effect of such antecedent condition(s) towards the subsequent event is herein called a temporal cascade.

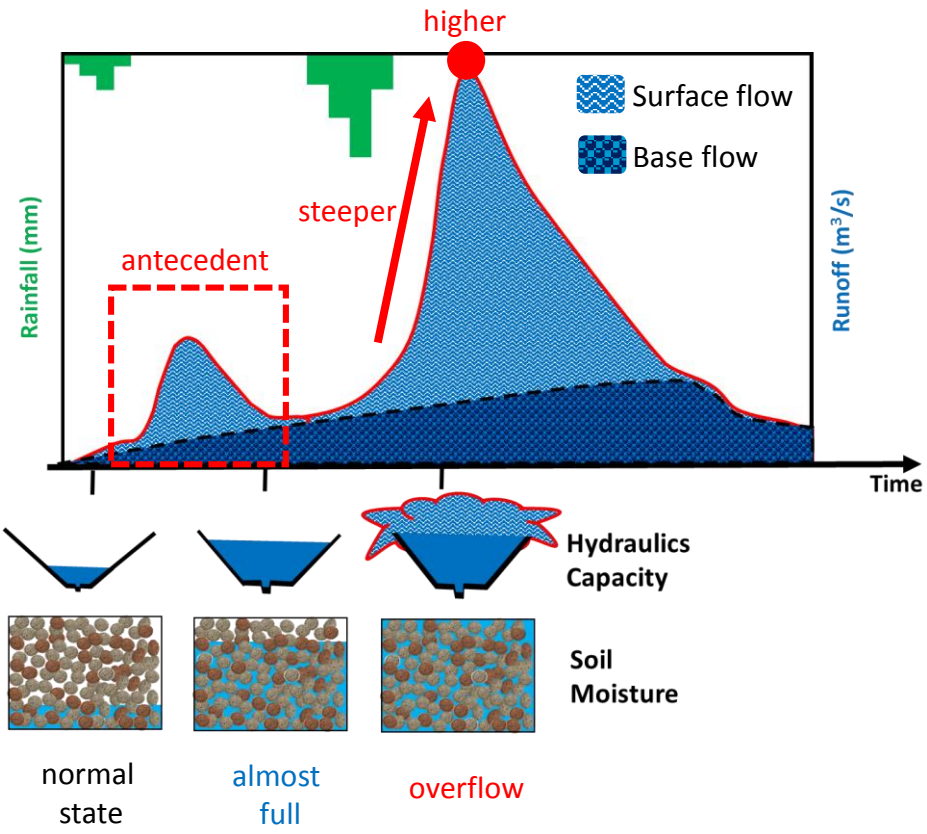

Figure 1.4: The impact of antecedent conditions towards the severity of a flood or an event

1.1.4 Runoff Dynamics Derived from Hydrograph Time Sequence Property and Represented by Phase Space Trajectory

Motivated by the need of a more elaborate hydrological signature and the recent assessment for state-of-the art flood analysis tool [Hall et al., 2014] which suggests the exploration of non-linear time series analysis tools to reveal the underlying dynamics that are more comprehensive to explain the degree of complexity, this study investigates the potential of characterizing flood dynamics from the perspective of phase space construction. By doing so, the characterization of a hydrograph envelopes the whole continuous shape of the hydrograph instead of its partial elements. In addition, with the help of Taken's time delay embedding method [Takens, 1981], a multi dimensional phase space trajectory can be created to include the relationship of different magnitudes in time. For instance, a

2-dimensional phase space vector can be regarded as an autocorrelation scatter plot where the x and y axes are the extracted values of the original time series that are separated by a shift of τ, however the trajectory is the set of connected vector based on their time sequence instead of scattering points. A 3-dimensional phase space contains three variable, i.e. x, y and z with time delay of τ and 2τ, and so on for higher dimensions (see illustration Fig. 1.5).

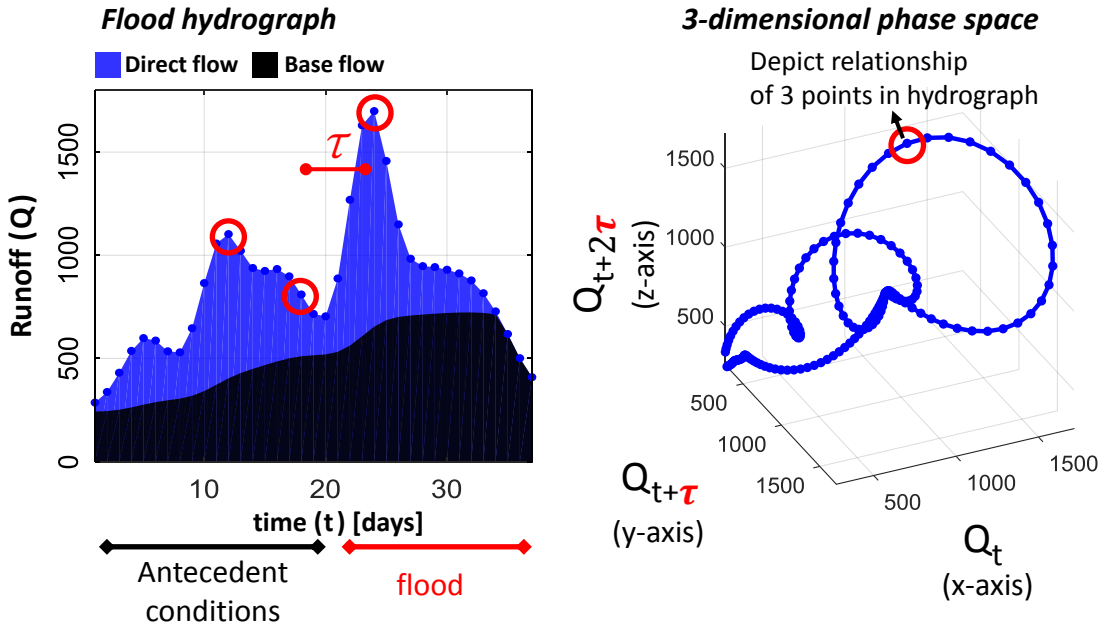

Figure 1.5: Illustration example of a phase space trajectory constructed from a flood hydrograph

In another words, A 1-dimensional phase space trajectory is simply the continuous shape of a hydrograph, while higher dimensional phase space further include the the mentioned relationship of discharge magnitudes at different time to capture a temporal cascade. By using this approach we are able to consider the relationship of antecedent conditions towards a flood magnitude illustrated in 1.4. Further illustration and example of this time delay embedding approach are shown in Chapter 4, section 4.2.1. The mentioned time sequence property of hydrograph represented through phase space trajectory is herein called runoff dynamics.

1.1.5 Challenges in the Assessment of Recurring Runoff Dynamics

Recurrence Plot (RP) and its quantification (RQA) are powerful tools that are able to analyze and quantify the recurrence of similar dynamics portrayed by phase space trajectory [Marwan et al., 2007] and therefore is of our interest to use for analyzing flood runoff dynamics. Although both RP and RQA's applications are known in wide range of disciplines in analyzing processes in a complex system, to the authors' knowledge, they

have not been used in hydrology. Therefore, their applications for hydrology need to be adapted to the corresponding observation data.

In general, the application of time delay embedding method and RPs, require proper parameters set that is well-suited for the dataset. Sub-optimal parameters can result in artifacts and therefore mislead an evaluation [Marwan, 2010]. Although conventional methods to determine optimum embedding parameters exist, Marwan [2010] concludes that these method often overestimate the required parameters. Optimum distance threshold (ε), required in defining similar dynamics for the construction of RP, is also essential. Besides, in the real world application, observation signals are often induced by noise, and that can lead to further artifacts in RP and RQA. Therefore it is of our interest to properly setup the method with correct parameters and ensure its robustness before any conclusive application.

1.2 Specific Objectives and Structure

The main objective of this method development is to derive a more elaborate index capable of quantifying the similarity of runoff dynamics between flood hydrographs, that provides a better association to a flood causative mechanism in contrast to conventional hydrograph indices.

The specific objectives formulated in this doctoral study are emphasized on the method development that is well-suited to hydrological data, instead of the application to evaluate flood change e.g. in a specific region. The developed method is directed at analyzing rare or unusual flood runoff dynamics from the perspective of phase space trajectories, that accounts the whole continuous shape of the hydrograph, and considers relationships between different runoff magnitudes in time to possibly include the characteristics impacts of antecedent events. The chosen tool and measure to compare these trajectories are Recurrence Plots (RP) and Recurrence Quantification Analysis (RQA). However further development to properly utilize and adapt this method to the runoff dataset is necessary. Parameters uncertainty for example is still an issue, as wrong choice of parameters can result in artifacts and therefore mislead a conclusion. Furthermore, the method is also known to be sensitive to noise. Therefore, further development is needed because of the aforementioned challenges faced and that its application in hydrology is not yet available as reference. This study also attempts to provide application examples dedicated to hydrologists without theoretical physics background and intend to use such method for analyzing runoff dynamics.

These specific objectives are formulated as forms of questions listed below:

1. What does phase space trajectory and time delay embedding mean for hydrological time series, i.e. discharge?

2. How to determine a safe parameters set when creating a phase space trajectory using time delay embedding?

3. How to define a threshold for similar runoff dynamics in order to properly construct an RP and what are the pitfalls to avoid?

4. Are the current RP and RQA methods robust for noise-present observational series and how to improve its robustness to prevent artifacts?

5. How to apply RP and RQA to evaluate similar runoff dynamics between floods?

6. How to adapt the method to evaluate a common or rare flood runoff dynamics?

7. What are the advantages of using such approach to quantify similar runoff dynamics, and how does it compare with other existing similarity index, e.g. hydrological signatures?

8. What is the implication of rare runoff dynamics in its relation to causative mechanism?

The following Fig. 1.6 presents the structure of how these specific research questions are discussed and presented in the doctoral thesis. Please note that the actual chapter name is different from the summarized topics shown in this figure.

In the Chapter 2 and 3, the focus of the research will be in the method development, where parameterization tool and artifact avoidance technique related to the method will be introduced and discussed. In particular, research question 2 will be addressed. Chapter 2 will cover the topic of phase space reconstruction and its parameterization by addressing research questions 3 and 4, while Chapter 3 will discuss the robustness of the method (i.e. RP and RQA) for observation dataset with regards to the questions 1, 5, 6, 7, and 8. The application for hydrograph similarity and rare flood dynamics will then be discussed in chapter 4 along with examples and analysis.

The application example of Chapter 4 uses the runoff time series extracted from the Dresden gauging station of the Elbe river catchment located in the East Germany from the period of 1901 to 2010. The example compares the runoff dynamics between all the flood events happening in February and March that are commonly separated into winter and spring flood typology but in fact easily coincide. This is done by constructing inter-comparison matrix of runoff dynamics between each flood in a pair-wise manner. This study showcases examples of rare and unseasonal flood dynamics indicated by the approach and are related to their documented unusual causative mechanism or herein referred to as typology. The resulting similarity and rarity indication derived from this approach are also compared with those using conventional hydrological signatures. Added values of such approach are then analyzed and discussed.

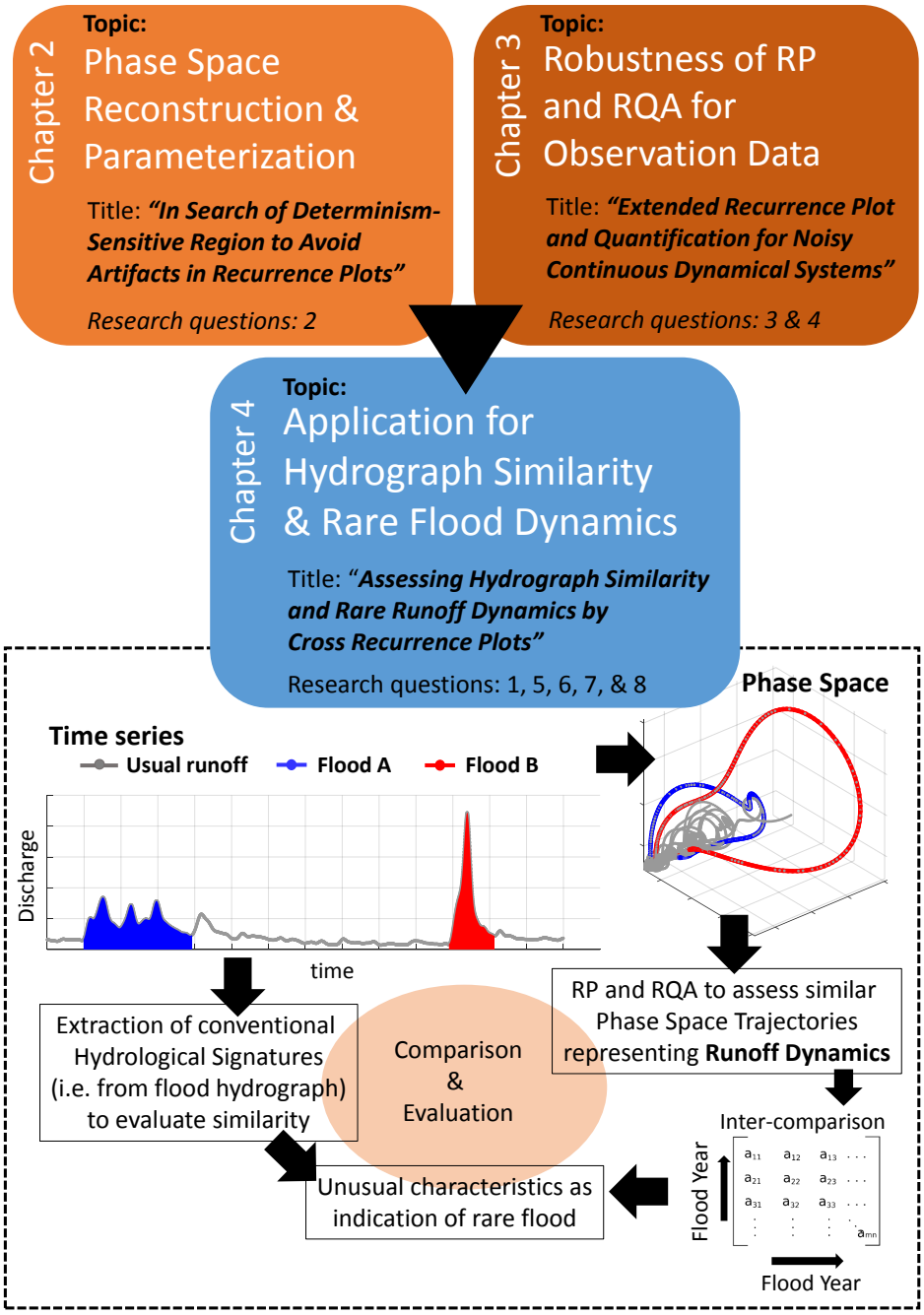

Figure 1.6: Structure of the thesis presentation with regards to the specific research questions

1.3 Author Contribution

Most of the works presented in this thesis have been performed by the author of this thesis (D. Wendi). Though, all co-authors of the manuscripts (see Chapter 2 to 4) have helped to develop and accomplish this research. Valuable feedbacks, questions and comments from colleagues within the associated research institution i.e. *NatRiskChange* research training group of the University of Potsdam, Hydrology section of German Research Centre for Geosciences (GFZ) and Potsdam Institute for Climate Impact Research (PIK) have

provided insights in approaching the research questions.

The three studies i.e. presented in Chapter 2 to 4 of this PhD thesis have been submitted to international and peer reviewed journals. In fact two of these manuscripts have been accepted and published by the time of this thesis submission. These manuscripts layouts have been adjusted to the formatting of this thesis, yet main text and figures remain as published, except with the standardized equation for e.q. 3.2 with the additions of summarizing key points of each manuscript where it was not available in the published version of Chapter 2 and 3.

Specific author contributions are as follows,

Chapter 2 - Research questions and rough conceptual idea of overcoming artifacts in embedding were suggested by N. Marwan followed by his methodological advice and consultation. D. Wendi carried out the actual design of the embedding parameterization framework, programmed and implemented the parameterization method, evaluated the method with test cases or datasets, and wrote the manuscript with inputs of all co-authors. B. Merz provided inputs, comments, and proofread the manuscript.

Chapter 3 - D. Wendi drafted the problem statements with regards to RP and RQA artifacts and their issues with noise, developed conceptual idea, designed method, formulating equations, programmed and tested the new or extended methods with various test cases and compared with the existing ones, conducted evaluations of the method robustness, and wrote the manuscript along with the inputs from co-author. N. Marwan brainstormed along and provided specific suggestions and feedbacks to the method design, testing framework, and the manuscript.

Chapter 4 - D. Wendi suggested and developed the main idea of analyzing runoff dynamics to evaluate hydrograph similarity and rarity, evaluated and presented the CRP and the RQA added value in contrast to traditional methods, conducted the method applications for Dresden flood series, evaluated the proposed similarity and rarity index in comparisons with conventional hydrograph indices and wrote the manuscript with inputs of all co-authors. B. Merz provided expert knowledge, inputs and suggestions on the presentations of the method and evaluations, and provided comments, corrections, and feedbacks to the manuscript. N. Marwan provided method expert knowledge to the study, comments and feedbacks to the manuscript.

2 In Search of Determinism-Sensitive Region to Avoid Artifacts in Recurrence Plots

Published as: Wendi, D., Marwan, N., and Merz, B. (2018). In Search of Determinism-Sentitive Region to Avoid artifacts in Recurrence Plots. International Journal of Bifurcation and Chaos, 28. https://doi.org/10.1142/S0218127418500074

Keypoints:

- Recurrence Plot parameterisation and how to avoid artifacts
- Deriving determinism sensitive parameter sets region using random shuffling technique

Abstract

As an effort to reduce parameter uncertainties in constructing recurrence plots, and in particular to avoid potential artifacts, this paper presents a technique to derive artifact-safe region of parameter sets. This technique exploits both deterministic (incl. chaos) and stochastic signal characteristics of recurrence quantification (i.e. diagonal structures). It is useful when the evaluated signal is known to be deterministic. This study focuses on the recurrence plot generated from the reconstructed phase space in order to represent many real application scenarios when not all variables to describe a system are available (data scarcity). The technique involves random shuffling of the original signal to destroy its original deterministic characteristics. Its purpose is to evaluate whether the determinism values of the original and the shuffled signal remain closely together, and therefore suggesting that the recurrence plot might comprise artifacts. The use of such determinism-sensitive region shall be accompanied by standard embedding optimization approaches, e.g. using indices like false nearest neighbor and mutual information, to result in a more reliable recurrence plot parameterization.

2.1 Introduction

Recurrence is a fundamental property of many dynamical systems, which can be exploited to characterize the system's behavior in phase space, while a recurrence plot (RP) is the visualization tool for the analysis of this property. In this study, the phase space reconstruction method of time delay embedding [Packard et al., 1980, Takens, 1981] is used (Eq.4.1). Such a reconstruction is particularly useful when not all variables required to describe the system are available (i.e. data scarcity or limited set of observation variables), and where the topology of the system dynamics $\vec{\hat{x}}_i$ can still be created using only a single variable or observation u_i.

$$\vec{\hat{x}}_i = \sum_{i=1}^{m} u_{i+(j-i)\tau} \vec{e}_j. \tag{2.1}$$

where m is the embedding dimension and τ is the time delay. The vectors $(\vec{e}_j)$ are unit vectors and span an orthogonal coordinate system $(\vec{e}_i \cdot \vec{e}_j) = \delta_{i,j}$. The calculation of recurrence as elements of the RP is based on Eq.2.2:

$$R_{i,j}(\varepsilon) = \Theta(\varepsilon - \|\vec{x}_i - \vec{x}_j\|), i, j = 1, ..., N. \tag{2.2}$$

where N is the number of measured points $\vec{x}_i, \varepsilon$ is a threshold distance, $\|\cdot\|$ is a norm and $\Theta(\cdot)$ the Heaviside function.

The RP is basically the visual representation of the square matrix, in which the matrix elements correspond to those times at which a state of a dynamical system recurs (columns and rows correspond then to a certain pair of times). RPs are especially useful for non-stationary pattern in time series [Eckmann et al., 1987, Marwan et al., 2007]. Besides using RPs for the visual analysis of time series, RPs can also quantify structures hidden within the series through recurrence quantification analysis (RQA)[Marwan et al., 2007, Zbilut and Webber, 1992]. In RQA, important elements are the diagonal and vertical/horizontal straight lines because they reveal typical dynamical features of the investigated system, such as range of predictability, chaos-order, and chaos-chaos transitions [Trulla et al., 1996]. One of the prominent diagonal line measures is called determinism (DET, Eq.4.3), from which the system predictability can be inferred.

$$DET = \frac{\sum_{l=lmin}^{N} lP(l)}{\sum_{i,j}^{N} R_{i,j}} \tag{2.3}$$

where $P(l) = \{l_i; i = 1, ..., N_l\}$ is the histogram of the lengths l of diagonal structures, and N_l is the absolute number of those diagonal lines.

For a deterministic signal (including chaos), many diagonal lines in the RP are typical, leading to high value of DET [Marwan, 2010]. However, single, isolated recurrence points

can occur if states are rare, if they do not persist, or if they fluctuate heavily. For instance, stochastic or random signals would comprise such single points and result in a very low DET.

Since the use of RPs relies on the reconstructed phase space, its parameters uncertainty includes those of the phase space reconstruction method, such as embedding dimension (m) and time delay (τ), in addition to the recurrence threshold (ε). Standard approaches for finding optimal embedding parameters are false nearest neighbours (FNN) for m, and auto-correlation or mutual information (MI) for τ [Fraser and Swinney, 1986, Kantz and Schreiber, 2005, Kennel et al., 1992]. Other methods include wavering-products, fill-factor or integral local deformation [Buzug and Pfister, 1992]. Moreover, Marwan [2010] concludes that τ is sometimes overestimated by auto-correlation and mutual information, and that the choice of the embedding dimension has to be considered with care, as a wrong choice artificially increases diagonal lines, and hence DET, and leads to artifacts. For instance, a RP resulting from a random series should exhibit scattered or non-deterministic patterns (i.e. single points). However, when m increases to 2 and beyond with $\tau = 1$, the number and the length of diagonal lines start to increase and dominate the plot as artifacts. This may be misinterpreted as if the series was highly deterministic (Fig. 2.1).

In this study, we focus on the artifacts related to these embedding parameters. The impact of the recurrence threshold (ϵ) is not elaborated, since the selection of the optimal values of the recurrence threshold has been discussed earlier Gao2009, Koebbe1994, Zbilut1992, Zbilut2002, Mindlin1992, Schinkel2008, Thiel2002. Hence, the recurrence threshold is fixed to a 10% recurrence rate (recurrence points density). Supplementary information on the impact of changing this threshold is enclosed in the appendix. The appendix also includes the evaluation of DET values of a correlated random series, using an AR1 series as example, to showcase that high DET values are indeed associated with deterministic systems instead of its auto-correlation structures, although there are also cases at certain parameter values where the number / length of diagonal lines artificially increase. It is important to note that the proposed technique is not intended to be used as a new, independent method, but rather as an additional consideration during parameterization, when the dynamical system is known to be deterministic.

2.2 Methodology

Artificially biased line length distributions due to the embedding can overlay the true line length distributions and lead to wrong conclusions. Hence, it would be desirable to separate the contribution of the embedding induced line length distributions from the real underlying dynamics. However, separating both contributions is not possible without additional knowledge about the system (such as precise model or amount of observational noise). Therefore, we propose an approach that minimizes the contribution

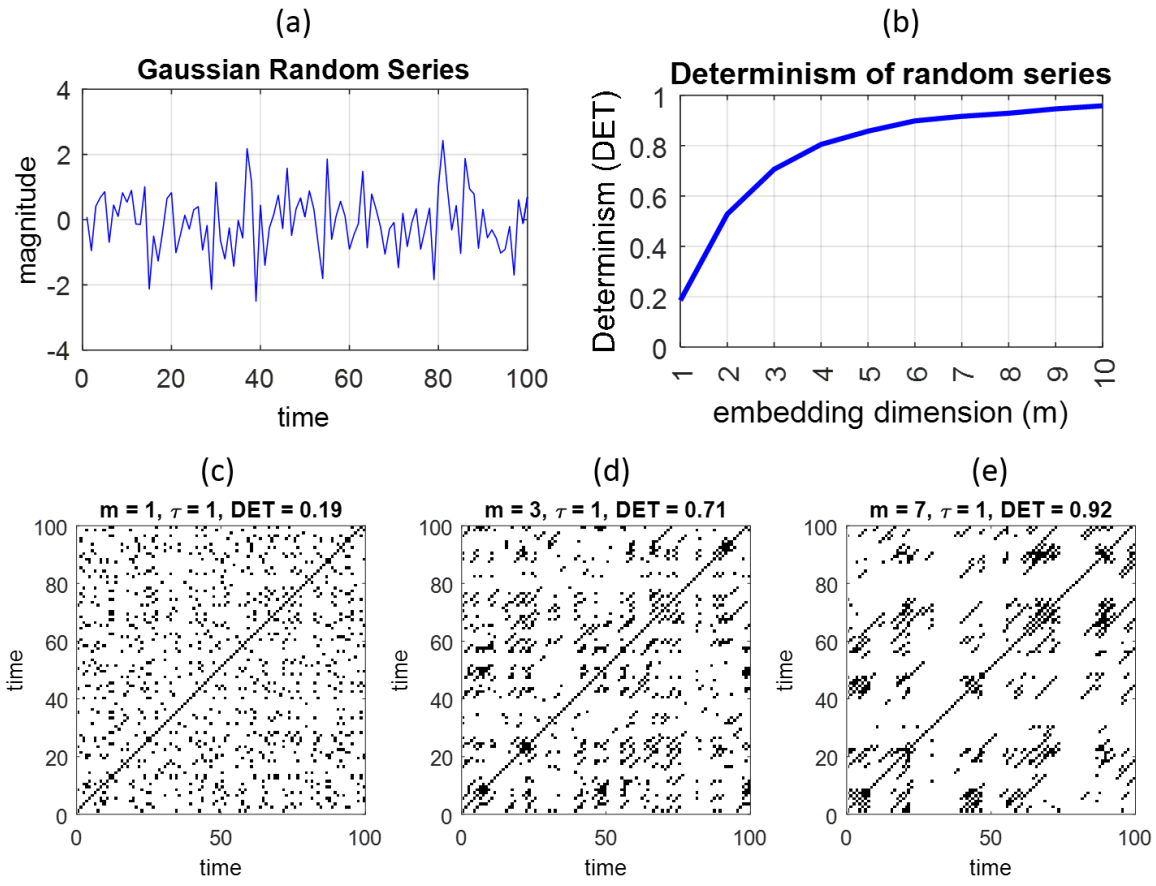

Figure 2.1: Misleading DET values of random series (a); sub-figure (b) shows the artificial increase of DET when embedding dimension (m) increases, while (c) to (e) show the corresponding RP with the increase of diagonal line structures at high embedding dimension ($m = 7$).

of the embedding. This approach is based on comparing the fraction of recurrence points that form diagonal lines in the RPs of the original time series (which includes both the real underlying dynamics as well as the embedding effect) with that of a random time series (which consists of the embedding effect only). As random time series we use simply shuffled versions of the original time series, because this preserves its value distribution and, thus, allows to use the same recurrence threshold and allows to compare the resulting RPs. As mentioned above, RPs of random time series should consist mainly of single points, but embedding artifacts would increase the fraction of recurrence points that form diagonal lines in the RP. Thus, this fraction measure is well suited for our purpose. Moreover, this measure is equal to the DET measure. Other measures that use the line length distribution (e.g., average and longest line length, entropy of the length distribution) would be possible but are less intuitive and interpretable. The advantage of the DET measure is that it considers the influence of scattered points that appears within the RP as well in addition to just the diagonal lines. While the index of average and longest line length could easily suffer from large statistical uncertainty and are easily influenced by a few extreme values.

In order to compare the line length distributions of the original and the shuffled time series, we define DET_o for the original time series and DET_i for the shuffled version. For a number of shuffling iterations (i.e. n times), the resulting difference (called determinism distance, see Eq. 2.4) is calculated for each shuffle (Fig. 2.2).

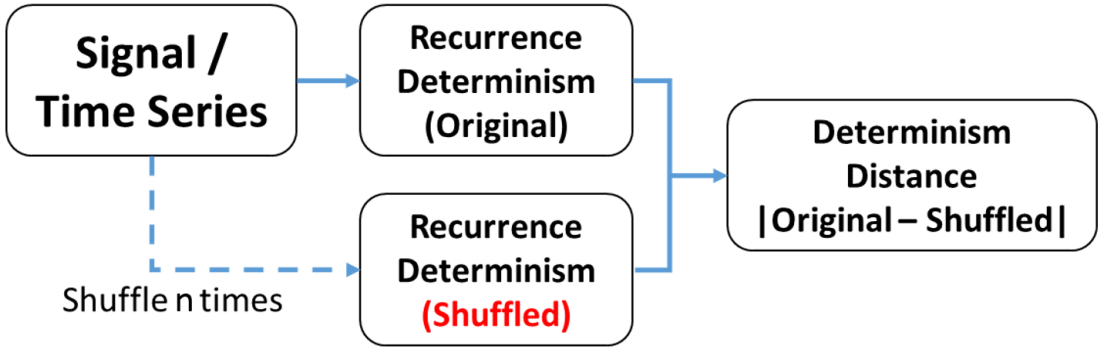

Figure 2.2: Scheme of the proposed artifact avoidance method.

For non-optimal embedding, we expect a rather high contribution of the embedding in the line length distributions in both, the original time series and in the shuffled version. Therefore, DET should have high values in both cases and should not differ so much from each other. For optimal embedding, and if there are deterministic structures in the RP of the original time series, the DET_i of the shuffled time series should be very low whereas DET_o of the original time series has still larger values. The distinctive high and low values of DET in deterministic and stochastic systems are exemplified in this paper using Lorenz and Gaussian random series. In this example, both the original and embedded Lorenz systems show DET values of around 0.8 to 0.9 with τ fixed at 3 following the first minimum of its auto-mutual information, with m varying from 1 to 10. In contrast, for the Gaussian random series, the DET values are shown to be between 0 to 0.2 (Fig. 2.3).

The resulting difference (determinism distance) between DET_i and DET_o would therefore be high. The undesired effect by the embedding should be minimal for the difference between DET_i and DET_o. Both median (M_d) and standard deviation (S_d) of these distances are used for identifying this determinism-sensitive region (Eqs. 2.4 and 2.5). The further (larger) the M_d of each parameter combination, the safer it is in terms of avoiding the mentioned artifacts, under the condition that S_d should be reasonably small (e.g. within 0.1).

$$M_d = \text{Median}_{i=1\ldots n}(|DET_o - DET_i|). \tag{2.4}$$

$$S_d = \sqrt{\frac{1}{n-1}\sum_{i=1}^{n}\left[|DET_o - DET_i| - \frac{1}{n}\sum_{i=1}^{n}|DET_o - DET_i|\right]^2}. \tag{2.5}$$

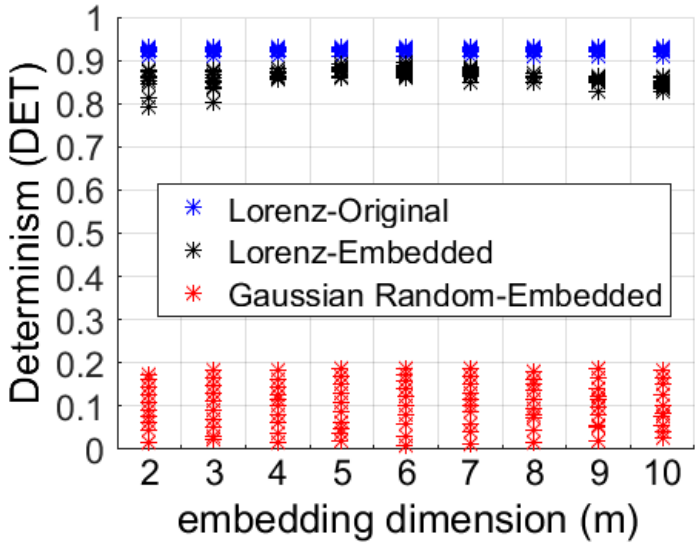

Figure 2.3: Examples for high and low DET values from deterministic (Lorenz) and stochastic (Gaussian random) signals.

where DET_o and DET_i are the recurrence determinism values of the original series and each shuffled iteration (i), and n is the total number of shuffling iteration.

2.3 Case study applications

This paper presents 2 application examples using Lorenz series derived from a mathematical model, and daily runoff observations from the station Burghausen at the Salzach River in south Germany. These signals are chosen for its non-linear characteristics with known presence of determinism [Martins et al., 2011, Sivakumar, 2000]. The resulting region of artifact-safe parameter set will be presented and discussed in section 4. Caution should be taken when $\tau = 1$ because artificially high DET values can lead to misinterpretations (Figs. 2.1b, d, and e), and hence should be excluded. In addition to the resulting artifact-safe region as the boundary of the parameter sets, the final choice of the parameter set is still necessary to be optimal, i.e. being able to reconstruct the topology of system dynamics and minimal in the sense not to over-reduce data points in the signal. There are many approaches to find optimal embedding parameters, such as the standard approaches mentioned in section 2.1.

2.3.1 Lorenz Series

The Lorenz system with known non-linear, non-periodic, 3-dimensional and deterministic chaos behaviour (i.e. with parameters $\alpha = 10$, $\rho = 28$, $\beta = 8/3$ and sampling time

$\Delta t = 0.05$) is chosen as the first application example, following Eq.2.6) [Lorenz, 1963, Sparrow, 1982]. Its RP and characteristics have also been studied by Marwan et al. [2007]

$$\frac{dx}{dt} = \alpha(y - x);\ \frac{dy}{dt} = x(\rho - z) - y;\ \text{and}\ \frac{dz}{dt} = xy - \beta z. \tag{2.6}$$

This Lorenz system is described by 3 variables and integrated using the Euler scheme, and hence, we know the 3-dimensional phase space that describes the topology of the system dynamics. In this study, the x variable is used as our Lorenz series test set (Fig. 2.4a) with its phase space reconstructed using the time delay embedding method. Thereafter, its DET is calculated. The reliability of these DET values is checked by using median and standard deviation of their determinism distance values (M_d and S_d) to qualitatively evaluate how much the constructed RP of a certain parameter set is influenced by artifacts.

This Lorenz series is derived from a mathematical model with well-known phase space topology and recurrence characteristics, whereas real world observations are most likely contaminated by noise. Therefore, we also investigate the impact of noise on the method, i.e. in respect to the values of determinism and determinism distance. Gaussian white noise with a magnitude range corresponding to the standard deviation of the Lorenz signal is applied, i.e. added to the signal (Eq. 2.7).

$$\tilde{x}(t) = x(t) + k\beta(t). \tag{2.7}$$

where, $\tilde{x}(t)$ is the resulting new series with the addition of noise and $x(t)$ is the original series (Lorenz); k is the noise level, while $\beta(t)$ is the Gaussian white noise with magnitude range corresponding to the standard deviation of $x(t)$. The noise levels used are 5%, 10%, 30% and 50%. For each of the noise-added signal, its determinism and determinism distance are calculated.

2.3.2 River Runoff Series

The second test application uses daily river runoff observations extracted from station Burghausen in south Germany for the year 1961. This station measures the streamflow of the Salzach River with a catchment area of 6,600 km^2. The time series (Fig. 2.4b) is used as a test set representing real world data, i.e.it is potentially non-stationary and contaminated by noise and observation error.

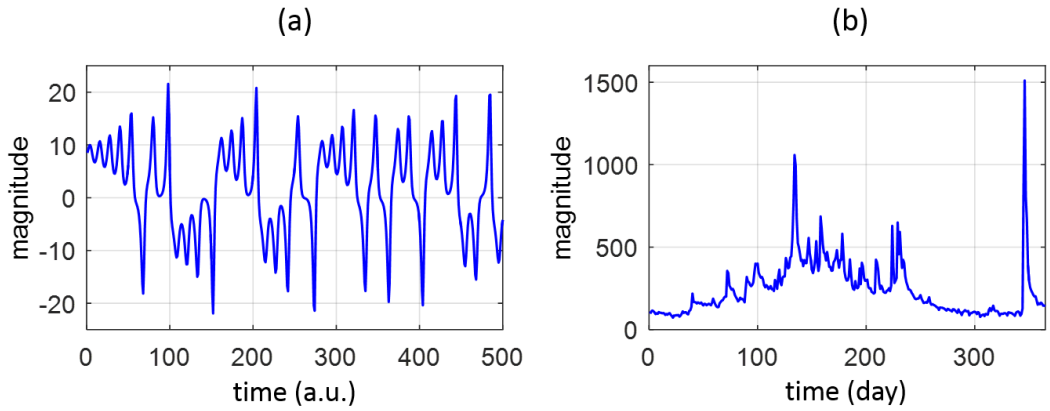

Figure 2.4: Test applications of (a) Lorenz - x variable and (b) Burghausen daily runoff series (1961).

2.4 Results and Discussion

This section presents the results of our proposed method for selecting an artifact-safe parameter region with the assumption of recurrence rate fixed at 10%. The range of embedding parameters bounds embedding dimension (m) from 1 to 10 and time delay (τ) from 1 to 20.

2.4.1 Lorenz Series

The Lorenz series is known for its deterministic feature, i.e.high determinism value, yet certain parameter combinations can give incorrect, low determinism values, e.g.when $m = 1$ or $m = 10, \tau = 6$ (Figs.2.5a, b, and c). Increasing the time delay at high embedding dimension is also seen to thicken the line structures of the RP (Fig. 2.5i). Low determinism values reflect non-optimal parameterization, and hence, misleading RP structures (Figs.2.5d and g) with diagonal lines structures as wobbly and perpendicular to the main diagonal [Marwan et al., 2007]. In order to assess the reliability of the resulting RP corresponding to the m and τ parameter combinations, the proposed shuffling techniques is applied to find the determinism-sensitive region.

Using the proposed technique ($n = 100$ shuffles), M_d is low for the case without embedding ($m = 1$) as well as for $\tau = 1$, when $m > 1$ (Fig. 2.6). The latter suggests artifacts due to embedding. Those parameter values where M_d is high, e.g. for $\tau \geq 2$, when $m > 1$, can be considered to be less influenced by embedding artifacts. It can be noticed that when τ and m are higher, M_d starts to decrease and to fluctuate, as indicated by S_d. In this case, the use of the median is quite reliable due to the low S_d value (i.e. below 6%).

The identified determinism-sensitive region is suggested to be referenced with the standard approaches, such as FNN and MI, to find the optimal parameter set. This

also serves to prevent the use of unnecessarily high parameter values that result in the reduction of data points (i.e. by $(m-1)\tau$). For instance, in the case of the Lorenz series, the optimal parameter set found by the standard approach is $m = 3$ and $\tau = 3$ (Fig. 2.7) which coincides well with the domain of high M_d values.

To investigate the impact of noise as in a real world scenario, Gaussian white noise with different noise levels is added to the signal as described in section 2.4.1. Figs. 2.8a and b show both false nearest neighbor and mutual information characteristics for the added-noise signal. The false nearest neighbor approach slightly increases at the optimal dimension of 3 causing a shift to the next dimension value, i.e. $m = 4$). When the noise level reaches 30 and 50%, the mutual information characteristics start to differ from the original, whereas the noise levels of 5 and 10% still preserve the original signal characteristics. Noise needs to be handled with care, as high level noise contamination potentially alters the determinism of the signal. It decreases in this case when Gaussian white noise is added, hence the determinism distance between the original and the shuffled series gets smaller.

2.4.2 River Runoff Series

A river runoff series is used to represent an example for field observations which are usually contaminated with noise. River runoff is typically a non-linear deterministic series and exhibits chaos properties [Martins et al., 2011, Porporato and Ridolfi, 1997, Sivakumar, 2000], hence, its DET is expected to be high. However, its recurrence determinism is low when parameter $m = 1$ and when both m and τ reach high values, e.g. $m > 8$ and $\tau > 9$ (Fig. 2.9a). For instance, for $\tau = 10$ the DET value starts to decrease when $m > 7$ (Fig. 2.9b), while for $m = 10$ the increase of τ (i.e. above 4) also starts to reduce DET values (Fig. 2.9c).

When evaluated through 100 shuffles, the parameter set of $\tau = 1, m > 1$ should not be used due to the clear artifact potential suggested by its low determinism distance (see Fig. 2.10a: first column and Fig. 2.10c: black line). The artifact-safe region could then be deduced from the high determinism distance domain corresponding to different combination parameter sets. For example when median determinism distance values above 0.8 imply high dissimilarity between the recurrence of the original signal and the shuffled ones (see Fig. 2.10a). The S_d values in this case are also low to safely use the median values (see Fig. 2.10b).

As cross-checked with the standard approach of parameter identification (Fig. 2.11a), the suggested optimal embedding parameters in this case would be $\tau = 10$ days and $m = 5$.

2.5 Summary

We propose a method to identify a determinism-sensitive parameter region with minimal impact of artifacts due to embedding when constructing a Recurrence Plot (RP). The method utilizes both deterministic (incl. chaos) and stochastic characteristics of recurrence quantification, i.e. diagonal structures, as indicated by their determinism values. It is useful when the evaluated signal is known to be deterministic. The method involves randomly shuffling the time series for an abundant number of times in order to destroy its original characteristics and its determinism. Thereafter, determinism values are calculated for each shuffle iteration and compared with the determinism of the original signal at a range of parameters, resulting in a measure called determinism distance.

The matrix of the median values of this measure is plotted to depict the determinism-sensitive parameter region. The larger the determinism distance, i.e. the closer to 1, the safer the parameter set is to avoid potential artifacts. The optimal parameter set can be selected from the consideration of this artifact-safe region together with the standard approach of using false nearest neighbors and mutual information and auto correlation.

Noise needs to be handled with care, since it affects the determinism structures of the signal or decreases the determinism values, therefore reducing the determinism distance between original and shuffled series. One could apply this method as an artifact-precautionary measure especially when intending to choose high values of embedding parameters.

Acknowledgement

This research was carried out within the Research Training Group "Natural Hazards and Risks in a Changing World" (NatRiskChange; GRK 2043/1) funded by the "Deutsche Forschungsgemeinschaft" (DFG).

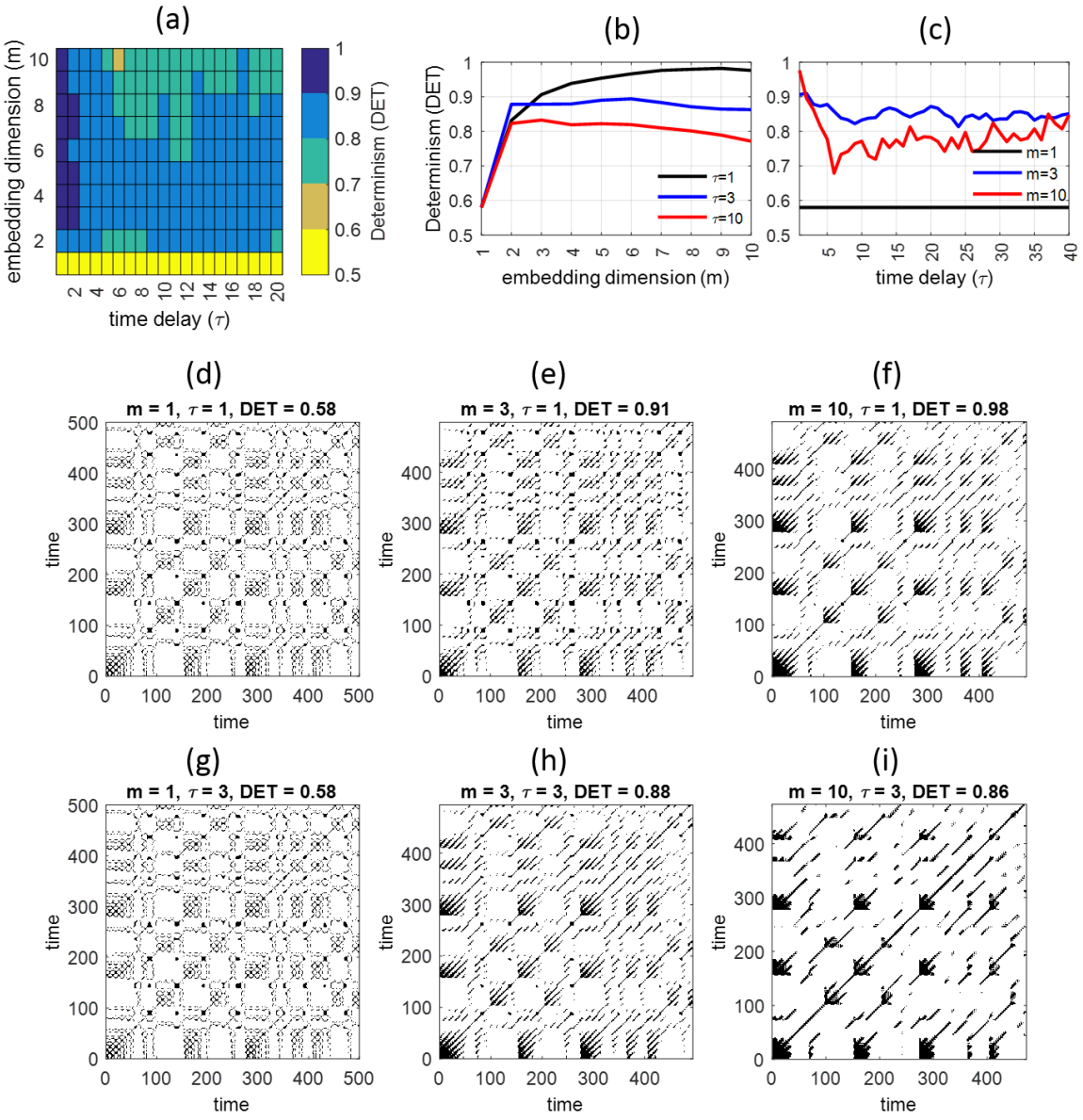

Figure 2.5: Recurrence characteristics of the chaotic, deterministic Lorenz signal: (a) determinism corresponding to m and τ; (b) change in determinism corresponding to an increase of the embedding dimension (m) from the RP, with $\tau = 1$, 3, and 10; (c) change in determinism corresponding to an increase of the time delay (τ), with $m = 1$, 3, and 10; (d) to (f) RP of different embedding dimension with fixed $\tau = 1$; and (g) to (i) RP of different embedding dimension with fixed τ=3. All RPs and recurrence measures are calculated based on fixed 10% recurrence rate.

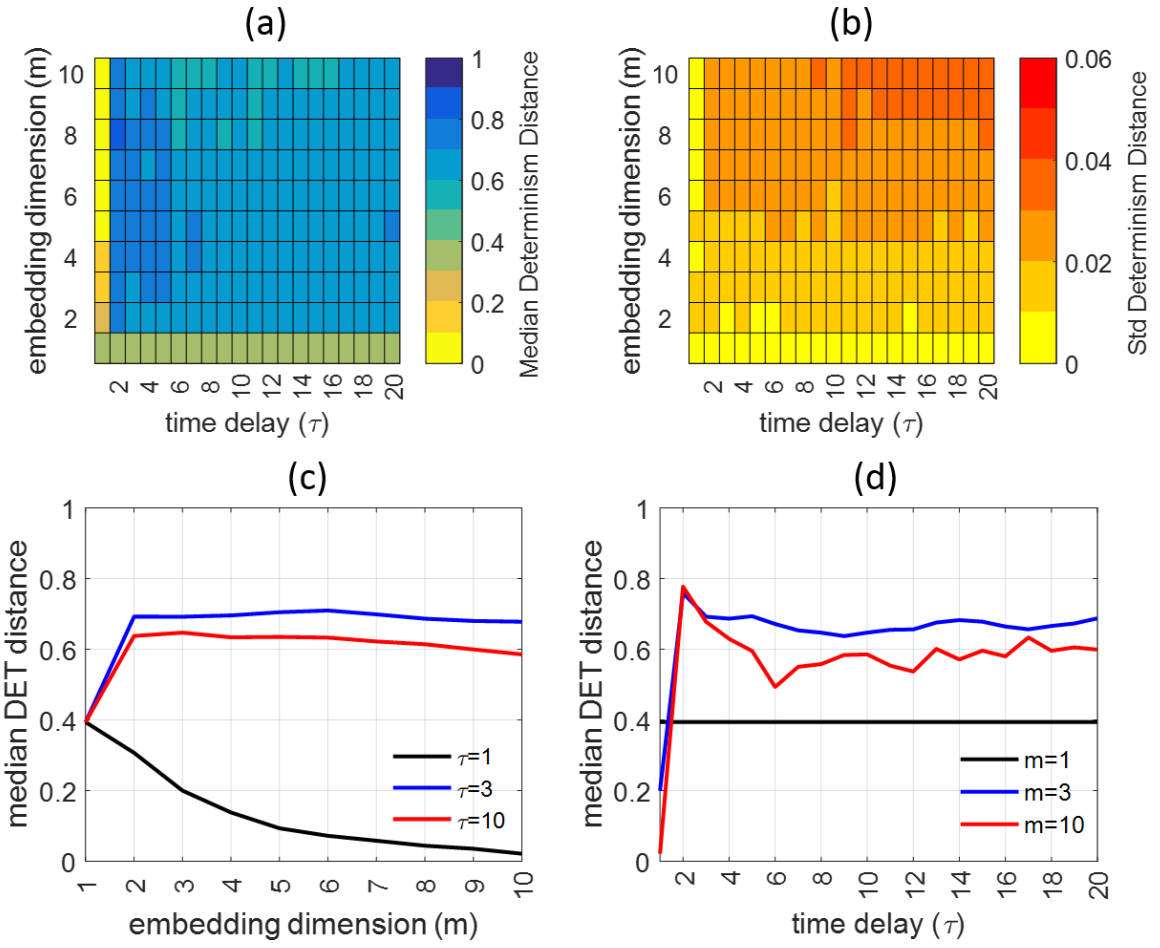

Figure 2.6: Determinism distance of the Lorenz series: (a) median (M_d) and (b) standard deviation (S_d) of determinism distance between the RP of shuffled and original Lorenz series. (c) and (d) show the median determinism distance corresponding to $\tau = 1, 3, 10$ and $m = 1, 3, 10$.

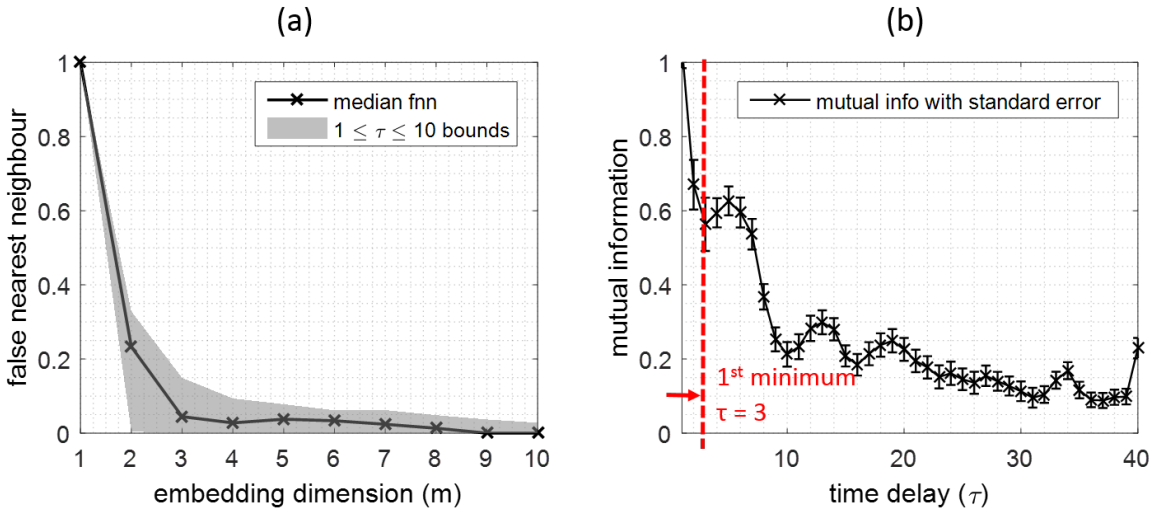

Figure 2.7: Embedding parameters for the Lorenz series resulting from standard approaches: (a) false nearest neighbor (FNN) with median and bounds derived from parameter set $1 \leq \tau \leq 10$, and (b) mutual information (MI).

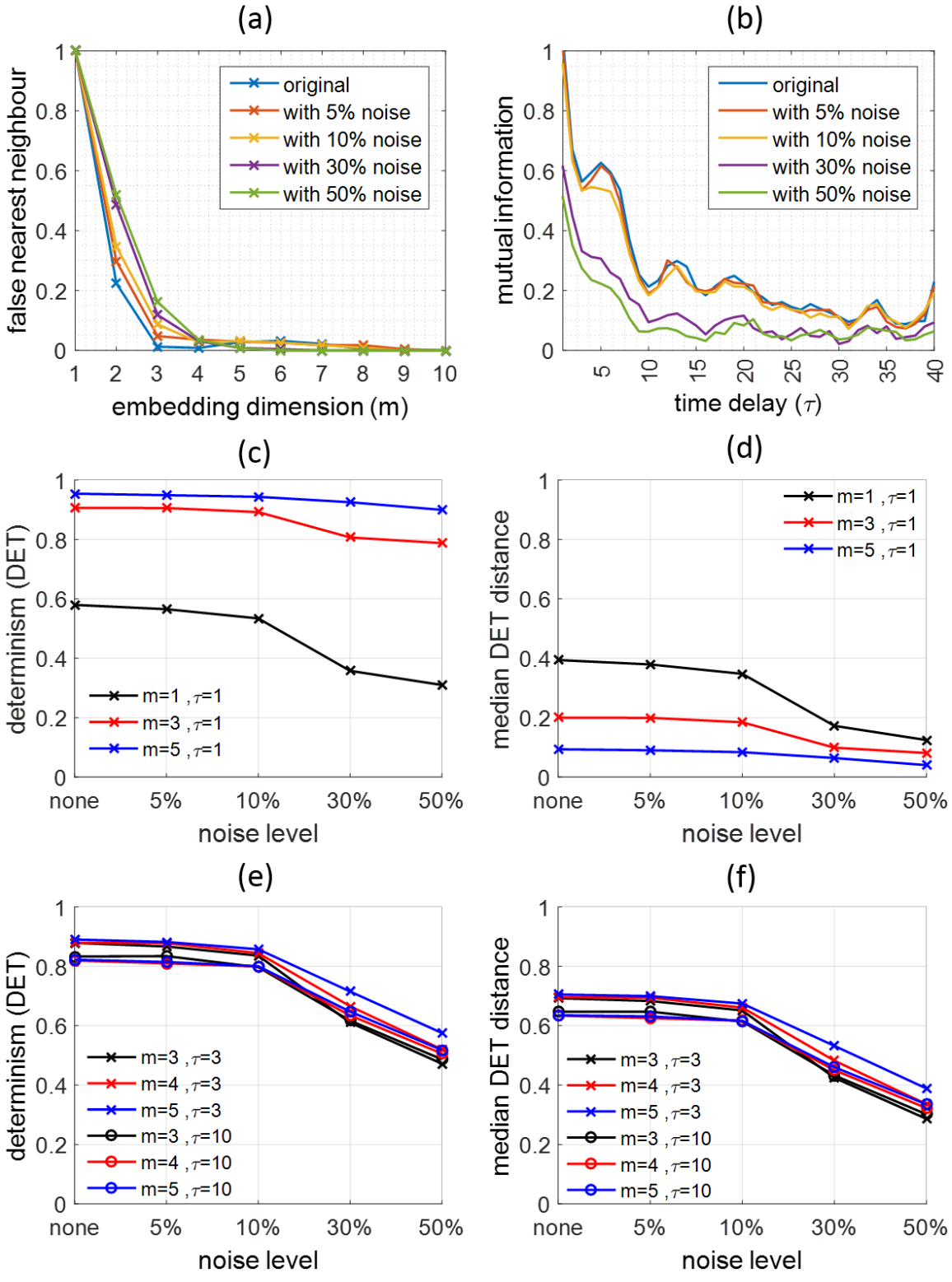

Figure 2.8: Impact of noise levels of the Lorenz series on (a) false nearest neighbor, (b) mutual information, (c) determinism, and (d) median determinism distance extracted at m=1, 3, 5 with τ=1. (e) and (f) present the extracted values with parameter bounds of $3 \leq m \leq 5$, τ=3 and 10, and 10% recurrence rate (ϵ). Noise added is Gaussian white noise with noise levels derived from the percentage of the signal standard deviation.

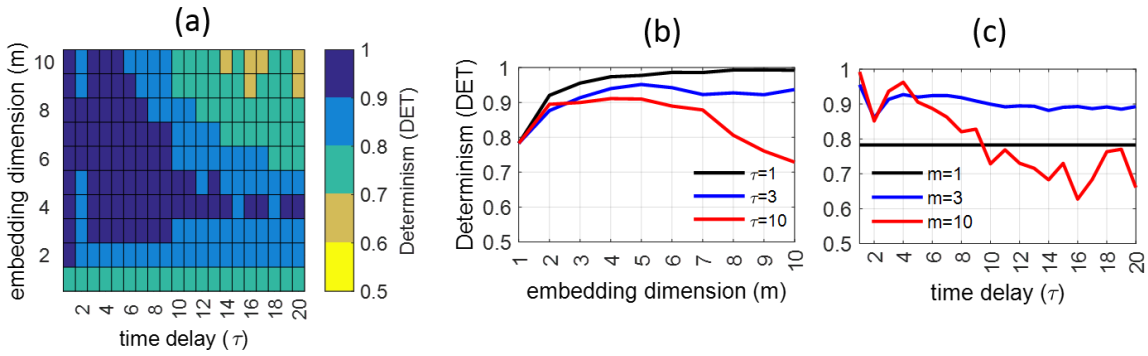

Figure 2.9: Recurrence characteristics of daily river runoff series: (a) determinism corresponding to m and τ, (b), change in determinism corresponding to increasing embedding dimension (m) from the RP, with tau=1, 3, 7; and (c) change in determinism corresponding to increasing time delay (τ), with m=1, 3, 7.

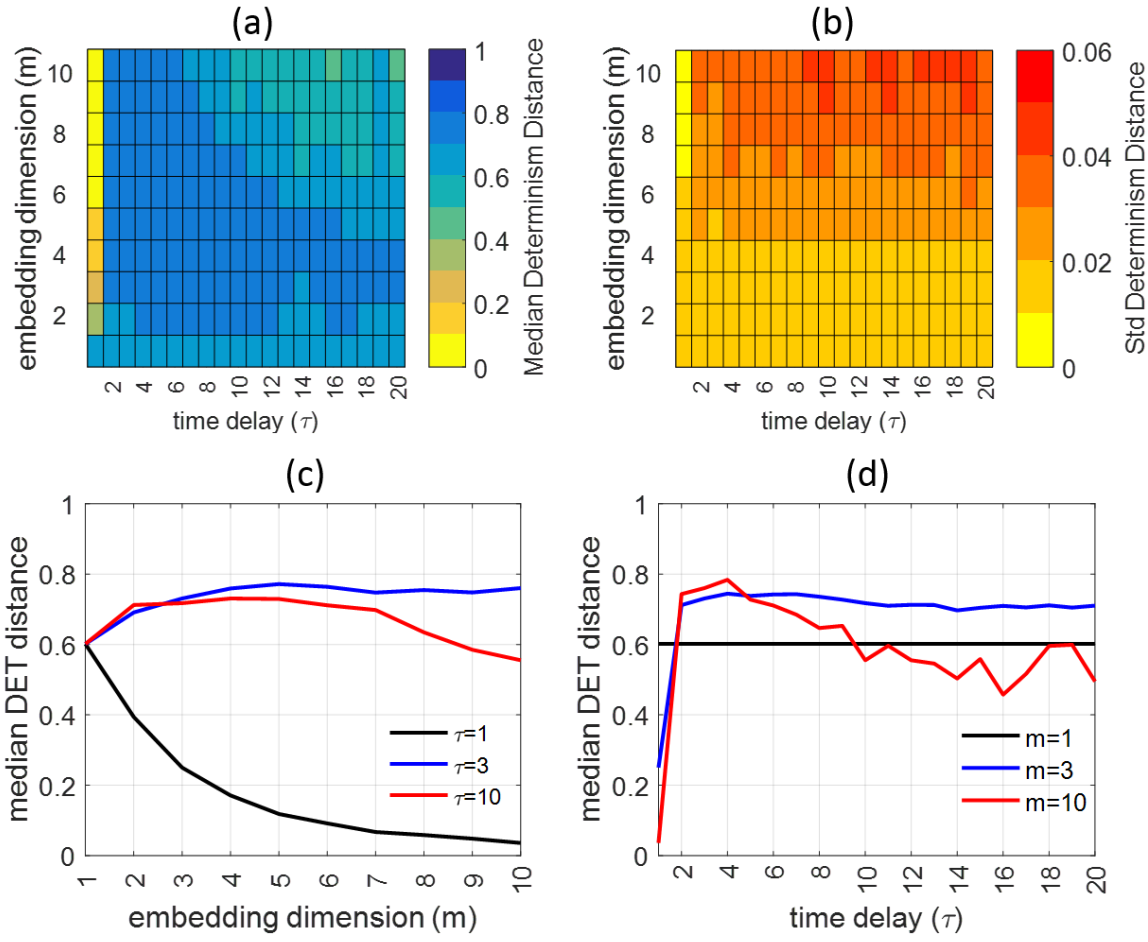

Figure 2.10: Determinism distance of runoff series: (a) median and (b) standard deviation of the determinism distance between the RP of shuffled and original runoff series. (c) and (d) show the median determinism distance corresponding to τ = 1, 3, 10 and m = 1, 3, 10.

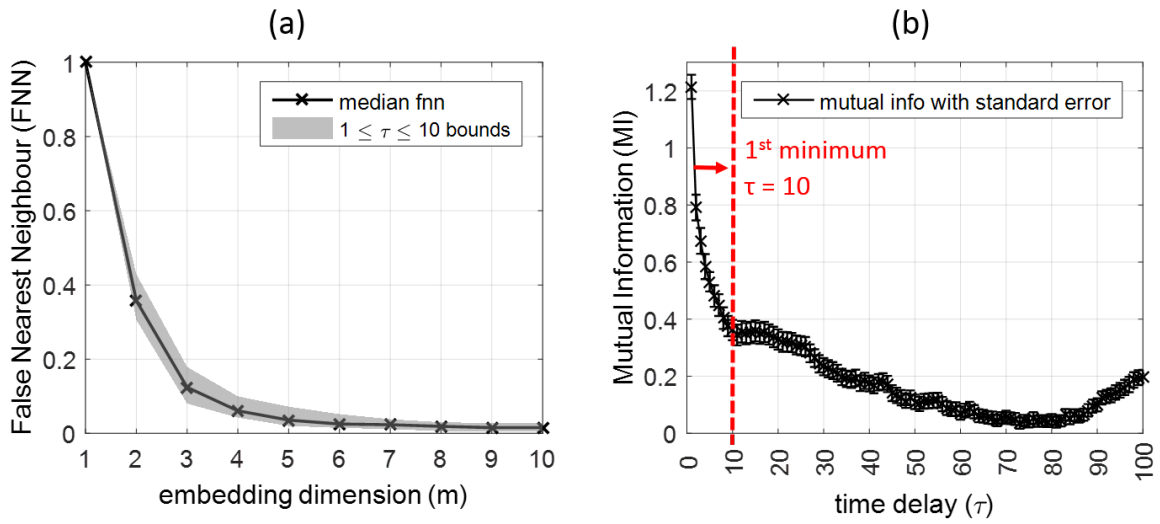

Figure 2.11: Embedding parameter selection for daily river runoff using the standard approach: (a) false nearest neighbor with median and bounds derived from parameter set $1 \leq \tau \leq 10$ and (b) mutual information with first minimum found at $\tau = 10$

.

3 Extended Recurrence Plot and Quantification for Noisy Continuous Dynamical Systems

Published as: Wendi, D. and Marwan, N. (2018). Extended recurrence plot and quantification for noisy continuous dynamical systems. Chaos: An Interdisciplinary Journal of Nonlinear Science, 28(8), 085722. https://doi.org/10.1063/1.5025485

Keypoints:

- Reducing thick line artifacts in Recurrence Plot (RP)
- Local minima based Recurrence Plot with 2 parameters
- Overcoming disrupted and deviated diagonal Lines due to noise
- Alternative Determinism index for noisy signals based on sliding diagonal window approach

Abstract

One main challenge in constructing a reliable recurrence plot (RP) and hence its quantification (RQA) of a continuous dynamical system is the induced noise that is commonly found in observation time series. This induced noise is known to cause disrupted and deviated diagonal lines despite the known deterministic features and, hence, biases the diagonal line based RQA measures and can lead to misleading conclusions. Although discontinuous lines can be further connected by increasing the recurrence threshold, such approach triggers thick lines in the plot. However, thick lines also influence the RQA measures by artificially increasing the number of diagonal and the length of vertical lines (e.g., Determinism (DET) and Laminarity (LAM) become artificially higher).

To take on this challenge, an extended RQA approach for accounting disrupted and deviated diagonal lines is proposed. The approach uses the concept of a sliding diagonal window with minimal window size that tolerates the mentioned deviated lines and also considers a specified minimal lag between points as connected. Such is meant to derive a similar determinism indicator for noisy signal where conventional RQA fails to capture. Additionally an extended local minima approach to construct RP is also proposed to further reduce artificial block structures and vertical lines that potentially increase the associated RQA like LAM. The methodology and applicability of the extended local minima approach and DET equivalent measure are presented and discussed respectively.

3.1 Introduction

As a fundamental property of many dynamical systems, recurrence can be exploited to characterize the system's behavior from their phase space topology. A recurrence plot (RP) is a visualization tool for the analysis of this property. In this study, the phase space reconstruction method of time delay embedding Packard et al. [1980], Takens [1981] is used to create the topology of the system dynamics $\vec{x}_i$ from a variable u_i (Eq.3.1).

$$\vec{x}_i = \sum_{i=1}^{m} u_{i+(j-i)\tau} \vec{e}_j. \tag{3.1}$$

where i is the current time point and j is other time point, m is the embedding dimension, and τ is the time delay. The vectors $(\vec{e}_j)$ are unit vectors and span an orthogonal coordinate system $(\vec{e}_i \cdot \vec{e}_j) = \delta_{i,j}$.

The RP is basically the visual representation of the square matrix, in which the matrix elements correspond to those times at which a state of a dynamical system recurs (columns and rows correspond then to a certain pair of times). The calculation of a recurrence point as an element of the RP matrix $\mathbf{R}$ is usually based on Eq. (3.2). RPs are especially useful for analyzing non-stationary time series Eckmann et al. [1987], Marwan et al. [2007].

$$R_{i,j}(\varepsilon) = \Theta(\varepsilon - \|\vec{x}_i - \vec{x}_j\|), i, j = 1, ..., N. \tag{3.2}$$

where N is the number of measured points $\vec{x}_i, \varepsilon$ is a threshold distance, $\|\cdot\|$ is a norm and $\Theta(\cdot)$ the Heaviside step function.

Besides using RP for the visual analysis of time series, RP can also be used quantitatively to unveil hidden structures from the series through recurrence quantification analysis (RQA)Marwan et al. [2007], Zbilut and Webber [1992]. In RQA, important elements are the diagonal and vertical lines because they reveal typical dynamical features of the investigated system, such as range of predictability, chaos-order, and chaos-chaos transition Trulla et al. [1996]. One of the prominent diagonal line measures is *determinism* (DET), from which the system's predictability can be inferred:

$$DET = \frac{\sum_{d=d_{\min}}^{N} dP(d)}{\sum_{i,j}^{N} R_{i,j}} \tag{3.3}$$

where $P(d) = \{d_i; i = 1, ..., N_\mathrm{d}\}$ is the histogram of the lengths d of connected diagonal lines, and N_d is the absolute number of those diagonal lines.

In addition, *laminarity* LAM is a measure based on the distribution of the RP's vertical lines:

$$LAM = \frac{\sum_{v=v_{\min}}^{N} vP(v)}{\sum_{i,j}^{N} R_{i,j}} \tag{3.4}$$

where $P(v) = \{v_i; i = 1, ..., N_\mathrm{v}\}$ is the histogram of the lengths v of connected vertical

structures, and N_v is the absolute number of those vertical lines.

For a deterministic continuous dynamical system (including chaos), many diagonal lines in the RP are typical, leading to a high value of DETMarwan [2010]. However, single, isolated recurrence points can occur if states are rare, if they do not persist, or if they fluctuate heavily. For instance, stochastic or random signals would comprise such single points and result in a very low DET.

Nevertheless, pitfalls and artifacts are not unusual when constructing RP such as those occurred with wrong choice of embedding parameters or high threshold (ε) Marwan [2010], Schultz et al. [2011], Wendi et al. [2018]. Thick lines for instance could easily occur in continuous dynamical systems due to the temporal correlation of the phase space trajectory and hence causing the RP to contain redundant information Schultz et al. [2011]. Such thick lines artificially increase the number of diagonal lines and even introduce vertical lines that lead to artifacts in RQA such as an increase in DET and LAM. With regards to these thick lines Schultz et al. suggested a local minima based RP with additional threshold ε to overcome this issue and demonstrated the benefits on the Lorenz system as an example. The minima are found in each column of the RP and should correspond to the closest neighbors of a state (within the range ε). Such method is shown to minimize line thickness without requiring much computational effort as would be necessary for perpendicular or iso-directional RPs that had also been suggested to overcome the line thickness problem. Additionally, Schultz et al. concluded that such local minima based RP resulted in less dependency when choosing the ε. In our study we call this approach LMT (i.e., local minima with threshold), while we refer the local minima without any constraint parameter as LM. LM and LMT method difference is further illustrated on (Fig. 3.1d, such that LM would considers all local minima found while LMT only considers the local minima below the ε, indicated by the region of orange shade).

However, in the real world application, observation signals are often induced by noise, and that can lead to further artifacts in our RP and RQA. Especially, in the regular RP (using a distance threshold ε), the induced noise could easily disrupt and deviate the position of recurring points (Fig. 3.1). Nevertheless, such is no exception when using LM approach, the mentioned artifacts are still present due to the induced noise. It is also important to note that in this study we only consider the contamination of noise by adding Gaussian to a one dimensional input signal (i.e. of a continuous dynamical systems or in this case Lorenz) given the desired signal SNR (signal to noise ratio) in decibels.

The impact of noise is obvious in the traditional distance threshold based RP, LM, and LMT (Fig. 3.2). Visible block clusters can be observed in the threshold based RP (Fig. 3.2c) especially along the lines of identity (known as LOI, i.e. the middle diagonal line) where perfect continuous line is expected) and in the LMT (Fig. 3.2e) despite the reduction of thick lines (marked with red rectangles). Despite the thick lines in threshold based RP result in the visually clearer diagonal lines, this is not necessarily correct as they

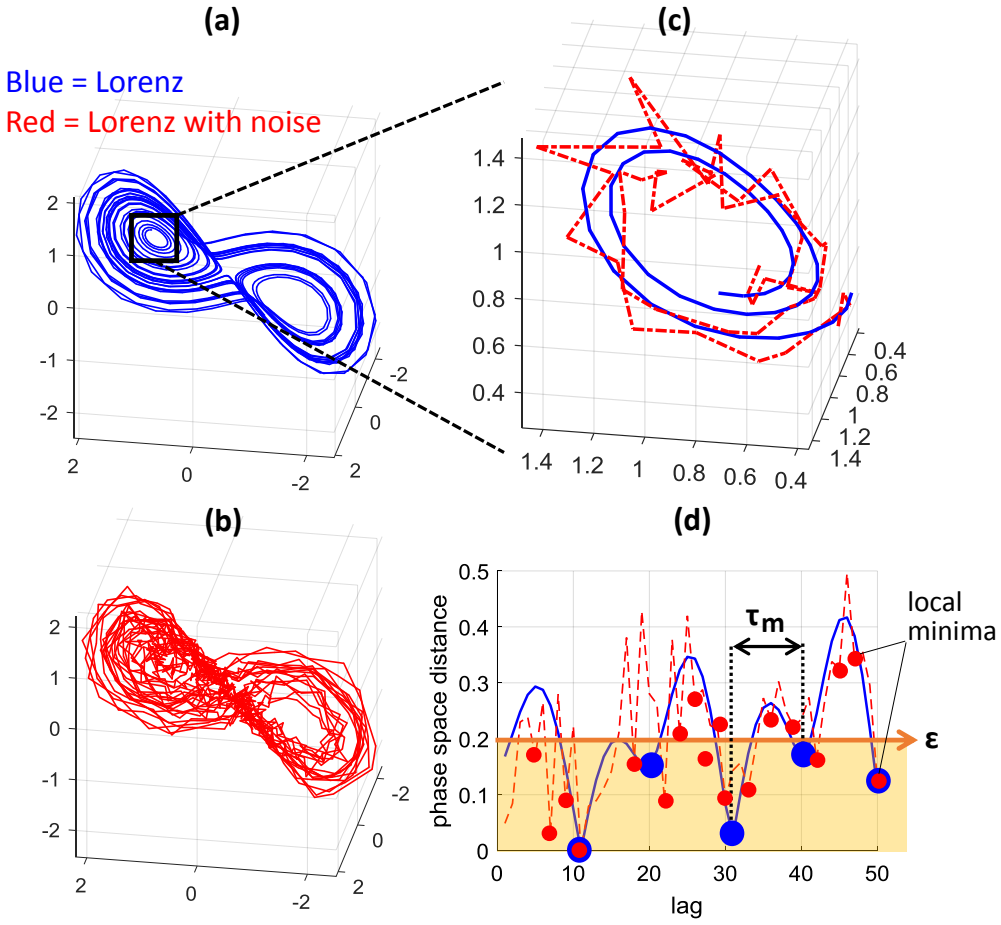

Figure 3.1: Phase space trajectories of Lorenz series ($\frac{dx}{dt}$, with $\sigma = 10, \rho = 28, \beta = \frac{8}{3}$): (a) without noise and (b) with noise (SNR=20dB); (c) zoom-in view of both signal trajectories; (d) extracted phase space distance (y-axis) between a selected point at the phase space trajectory and all other trajectory points by time lag (x-axis) and corresponding local minima (blue and red points, indicating local minima of no noise and noisy Lorenz recpectively). The shaded orange region refer to the region where local minima with threshold (ε) are used for RP with LMT approach. The embedding parameters of all phase space are fixed at $m = 3$, $\tau = 3$.

artificially introduce more diagonal lines and block structures that increase vertical lines and hence artificially increasing LAM (i.e. in our example and increase by 0.35). This is a problem because such laminarity characteristics is not expected for the Lorenz system. The increase of LAM is also noticed in the LMT approach (by 0.11). Meanwhile, the LM RP (Fig. 3.2d) is dominated by visible long vertical lines which, therefore, drastically increase the LAM when compared to the RP of the Lorenz without noise (increase by 0.69).

As to tackle the problems with noisy continuous signals (blocks and vertically extended structures), we propose an additional constraining parameter to the LMT in order to

reduce the mentioned artifacts (i.e., block cluster and increase in LAM) and we call this method local minima based RP with 2 parameters (LM2P). This LM2P approach is further explained in section 3.2. Although LM2P is found to improve the reliability of RP and RQA as evaluated from its deviation from the RP constructed from uncontaminated signal (i.e., without noise), the disrupted or discontinuous diagonal lines due to noise are, however, still a bottleneck in deriving a system representative DET value, e.g., such that the deterministic Lorenz would still yield a very low DET value despite its RP deterministic pattern (i.e., DET of 0.24 instead of 0.59 found in the RP of Lorenz without noise). Such is also noticed in different Lorenz system with varying ρ parameters (Fig. 4.3), where DET of the noise induced signals (both LMT and LM2P) show a very low DET values closer to the stochastic system rather than the reference DET generated from the RP of Lorenz with no noise. This reference RP (shown in all figures as Lorenz no noise) is generated using LM2P approach, although there is hardly any difference to the one generated using LMT approach (i.e. when no noise is present). Therefore, we also propose a new measure to account this mentioned diagonally clustered points that do not necessarily form strict diagonal lines as required for the conventional RQA calculation of, e.g., DET. The methods and findings are presented and discussed in the following sections.

3.2 Local Minima based RP with 2 Parameters (LM2P)

Vertical distance between recurrence points in the RP correspond to the time between recurring states (recurrence time). However, noise can reduce these recurrence times by introducing many new local minima in the distance matrix, and by this artificially adding many new recurrences (visible as the clusters and vertical structures in Fig. 3.2). In order to reduce the number of these noise-induced minima, we introduce a minimum distance τ_m required between the local minima as a new additional parameter. This τ_m in addition of ε is also illustrated on Fig. 3.2d. Because the local minima approach now consists of two parameters (i.e. ε and τ_m), we call this approach "local minima with 2 parameters" (LM2P). By doing so, we exclude the minima that are found next to each other due to the induced noise. The resulted minima with reasonable τ_m are expected to separate the potentially recurring pattern despite the local noise. This selection of τ_m however should be minimized that one does not exclude the recurring pattern due to large τ_m that potentially overlaps the sequence of the signal. It should also be reasonably sized to avoid the noise artifact. The optimal τ_m as implied by Fig. 3.3a has to be larger than the maximum of the local minima of the phase space distances as found in a random system (i.e., Gaussian white noise) and smaller than the one of the assessed deterministic signal (in this case Lorenz). Such criterion can be found by using the auto-correlation function (ACF) of the assessed signal. This should be chosen larger than the first minimum lag of white noise, and lower than the first minimum lag of the assessed signal. In this case we obtained the

first minimum by using a threshold of autocorrelation value less or equal to 0.1, and we infer the safe choice of τ_m to be below 15 at Lorenz with $\rho = 80$ (see Fig. 3.3b). Since the τ_m of Gaussian noise is found to be around 3, we could infer the safe τ_m for our noisy Lorenz signal to be above 3 (lets say 5) (see Fig. 3.3a) and below 15 as guided by ACF. The RP based on the LM2P approach solves the mentioned issues on thick lines and block patterns as well as the vertical artifacts due to noise. First, for the noisy signal the LM2P RP (Fig. 3.2f) yields a closer pattern to the one of the uncontaminated time series (i.e., without noise) as seen in Fig. 3.2a and b. Furthermore, the block clusters are now removed and vertical lines due to noise disappeared (Fig. 3.2f). This is confirmed by the low LAM value that is similar to the one of the signal with no noise (difference only 0.02). However disrupted lines due to noise are still visible to cause low diagonal line based RQA measures (e.g., DET, difference 0.35) despite the agreement of the RP patterns. The conventional RQA measures based on strict diagonal structures (i.e., connected points with 45° slope) are not always satisfactory especially in the case of noisy signals, where diagonal lines can be disrupted by the noise. The disruption of line is prominent and shown to vary with the noise level (see Fig. 3.4). For instance noise impact with SNR of 30dB already causes the median values (probability exceedance of 0.5) of the line length to 1 (i.e. no connected points) and that the relative longest diagonal line within the RP already drops to 30%. Despite the solution in increasing ε could be promising in connecting the disrupted and deviated lines Thiel et al. [2002], such approach undesirably thickens the structures in the RP and eventually causes an artificial increase in diagonal and vertical lines, and, therefore, biases RQA.

3.3 Determinism Indicator Using Diagonal Sliding Window

In order to resolve the aforementioned reliability issues (i.e., DET sensitivity to disrupted and deviated diagonal lines), we propose another approach to derive a more robust determinism indicator that is less sensitive to noise. This approach uses a sliding window (w_i) of size ws and iterates at a lag of τ_w (distance from the main diagonal LOI) from the left corner of the RP until the end point of the RP (right corner) minus the window size ($N - ws$). The conceptual diagram of this method is presented in Fig. 3.5a. The RP of a deterministic signal tends to form a cluster of diagonal structures despite the wiggly and disrupted lines (i.e., up to the user tolerance deviation criteria set by ws, and maximum gap or discontinuity distance of $D(max)$ as exemplified in the rotated view of the window for sub-figure (Fig. 3.5b) RP of Lorenz without noise, (c) Lorenz with noise using LM2P, (d) Lorenz with noise using LMT, and (e) RP of a random signal (i.e., Gaussian noise) with typical scattered recurrence points all over the space.

For each w_i the fraction of recurrence points, (RR_{w_i}) is calculated as the ratio of the number of recurrence points (R_{w_i}) over the area of the window A_{w_i}, Eq. (3.5). In this

approach ws should be set considerably small (2 or 3) to consider only small wiggling or deviation of the diagonal lines due to noise. Such limited window, e.g., with $ws = 2$ allows each perpendicular cell or point (i.e., R_{d_i} binary values) along the length of the window $(i, ..., i + ws - 1\ )$ to be aggregated like a logical OR function as d_k. In addition, for every d_k at window w_i, the diagonal recurrence point distance along the axis k is calculated between each consecutive recurrence points as D or Δk (Fig. 3.5f). The ratio of frequency distribution of the gaps distance that is within the threshold $D(max)$ is the emphasis for our calculation. In this case, user should allow minimal gap tolerance to consider the such discontinuity as diagonal line (e.g. gap of 1 or 2 point distance). These variables are then used to formulate an alternative determinism indicator DD_{w_i} for each window (w_i) and $DDET$ as the index for the whole RP:

$$RR_{w_i} = \frac{1}{A_{w_i}} \sum_{i,j=w_i}^{n} R_{w_{i,j}} \tag{3.5}$$

where A_{w_i} is the area of the diagonal window (i.e., number of cells in each window), $R_{w_{i,j}}$ is the recurrence point within the window calculated from the starting point of the window (w_i) up to the maximum possible length $(N - ws)$.

$$DDET = log\left(\frac{\frac{1}{N}\sum_i^N DD_{w_i}}{\frac{1}{N}\sum_i^N RR_{w_i}} \right)$$

$$DD_{w_i} = \frac{\sum_j^{D(max)} D_j P(D_j)}{\sum_j^N l_{w_i} - D_j P(D_j)} \tag{3.6}$$

$$D = \Delta k, \text{ for } \{d_k \in \mathbb{B} : d_k = 1\}$$

$$d_k = \vee_i^n R_{d_i},\ n = i + ws - 1$$

where d_k is calculated as the logical OR aggregate function of horizontal cells R_{d_i} within the window size ws (from $R_{d_{i...n}}$ where $n = i + ws - 1$. $P(D_j);,\ j = \{1, ..., N_D\}$ is the frequency distribution of the gap distance k between consecutive diagonal recurrence points $(d_k \equiv 1)$ where $D(max)$ is the maximum threshold of distance allowed, and l_{wi} is the maximum length of w_i $(l_{w_i} = n_k)$, and N_D is the absolute number of those distances stored in D.

The calculated RR_{w_i} and DD_{w_i} of every window are then compared for their probability of exceedance. Based on Lorenz with parameter $\rho = 80$, the distributions of the exceedance are distinct between those of Lorenz and Gaussian process, with better performance of LM2P over LMT (i.e., closer to the one of Lorenz with no noise) especially for DD_{w_i}

(Fig. 3.6a, b). Furthermore, the correlation coefficient (r) of RR_{w_i} and DD_{w_i} between the RP of the Lorenz signal with no noise as reference and the other RPs are assessed respectively for varying ρ (Fig.3.6c, d). Unlike the conventional RQA (i.e. DET is low for the noisy Lorenz signal and appear closer to the one of Gaussian noise and thus, the correlation to the reference is low), the correlation between LM2P RP of the reference (i.e., no noise) and the noisy signal is higher.

Furthermore, the resulted DDETs for varying ρ are also plotted in comparison with the DET values of Lorenz with no noise as reference (Fig. 3.7b). Although the DDET values of Lorenz with noise (both LMT and LM2P) are slightly lower than the one without noise, their values are rather distinctive from the one of Gaussian noise. Meanwhile, two periodic windows ($P1$ and $P2$) of the Lorenz system as indicated by maximum Lyapunov exponent below 0 (Fig. 3.7a (red)) are also captured by the DDET measure, while the RQA DET could only capture the high deterministic features of Lorenz in the 2nd periodic window ($P2$). DDET values can be seen to range from approx. 2 to 3 for the periodic system, fluctuating around a value of 1 for the chaotic regime, and dropped to almost -1 when it is Gaussian noise or stochastic process.

Although a higher embedding dimension could further insinuate the implicit deterministic features and, hence, increase DET values, the impact of induced noise as shown in Fig.3.8 would still result in distinct difference (i.e., underestimation) as compared to the signal without noise. In contrast, DDET values of the noisy Lorenz are found to be much closer to the Lorenz without noise regardless of the embedding dimension. Such differentiates stochastic systems like white noise further from the deterministic signal. Furthermore, applying LM2P in this case does not require to choose high embedding. The LM2P approach outperforms the other approach for all ρ parameters (Fig.3.7b) and with varying embedding dimension (Fig.3.8).

Despite the selection of optimum ws could be attributed to the amount of noise, i.e. the lower the signal to noise ratio (SNR) the expected deviation is larger, the large choice of ws could result in recurring sequence being aggregated within a window. In our test case, we focus on the example of Lorenz series with 20dB SNR which is already considered to be quite a prominent noise contamination case. With this SNR, the choice of $ws = 2$ is already shown effective to derive a representative DDET (i.e. close to the signal without noise), and as shown in Fig.3.9 the increase of ws would only decrease the reliability of DDET (i.e. DDET values between non noisy and noisy signal start to distant apart and that the DDET values of the deterministic signal start to decrease). In this figure, it is also shown that the LM2P approach would yield more robust DDET values with respect to the increase of ws in contrast with LMT approach where the decrease of DDET deviate further from the non-noisy signal.

Moreover, this example can be used to study the sensitivity of the new approach with respect to noise. The DDET values for SNR ranging from 30 to 20dB are still close to the

DDET values of the non-noisy signal (Fig. 3.10). On the contrary, DET is very sensitive to noise and the drop in SNR to 20dB causes a drastic change in the DET and implies a closer relationship to a stochastic process. However, in the case of extremely noisy signal i.e. SNR below 20dB, even DDET cannot be longer deemed to be reliable.

3.4 Conclusion

1) RP artifacts such as thick lines can be reduced using the LMT (i.e. introduced by Schultz et al. [2011]) and LM2P method (i.e. introduced in this paper). However, when noise is present in the continuous system, the LMT approach is still shown to contain block like clusters and artificial vertical lines that eventually increase the RQA measure LAM. This however can be resolved by using the LM2P approach, where an additional parameter constraint (i.e., minimum distance τ_m between the local minima) is introduced in addition to the threshold. The parameter τ_m can be guided by using the location of the first zero auto-correlation function (ACF). The recommended τ_m should be smaller than the first zero ACF but larger than the ACF of the stochastic process.

(2) Although the LM2P (and LMT) approach reduce the mentioned artifacts and visually appear to have agreement between RPs created from pure and noisy signals (i.e. closer representation of LAM values), their conventional RQA calculated based on diagonal lines lengths (i.e. DET) is heavily underestimated. Such is due to the impact of the induced noise that disrupts and deviates the recurrence points. Therefore the strict quantification based on connected points that form 45° diagonal lines would fail to capture the recurring dynamics' property.

3) To resolve the RQA reliability with mentioned disrupted and deviated diagonal lines, an alternative approach for calculating a determinism indicator is proposed. This uses a diagonal sliding window concept with minimal window size (ws) designed to capture the mentioned deviated lines at each window time lag (τ_w).

4) As to account the disrupted lines (i.e., cluster of points with minimal distance), we propose an index measured from the distribution of this minimal diagonal point distance, and their recurrence rate at each window iteration (w_i). Such allows disrupted points with minimum distance to be considered as a diagonal line and, hence, providing a DET equivalent measure.

5) The new measure is able to capture the deterministic property of the Lorenz system (for varying parameter ρ from 80 to 110) despite the induced noise with signal to noise ratio of 20dB, as assessed from their window's RR_w and DD_{w_i} correlation agreement, distribution, and $DDET$ variation for different ρ values as compared to the system without noise. In addition, it also captures the two periodic windows of the Lorenz system in both noisy and non-noisy signal, where the conventional RQA-DET measure fails to capture them. The conventional DET measure also tends to distinctly underestimates the

determinism and, hence, appears to be closer to the indication of a stochastic process when the induced noise is present. Furthermore, the use of DDET allows minimal embedding dimension to match the noisy system with the non-noisy one, and their performance are in general rather constant in spite of the embedding.

6) However, it is worth to note that the magnitude range of this measure differs from the conventional DET measure. The challenge remains to set up a standard of range for which a more intuitive scale of determinism can be easily inferred. Nevertheless, the new DDET measure and the diagonal sliding window is a promising concept when the known continuous system dynamics is induced by noise, which is very common in real world observations. More research could focus on the more specific attribution of the measures and different types of noise. Furthermore, the relation of the signal to noise ratio to the window size (ws) necessary to capture the expected deviation and the maximum diagonal distance to consider for the tolerance of line disruption should be elaborated in future studies.

Acknowledgement

This research was carried out within the Research Training Group "Natural Hazards and Risks in a Changing World" (NatRiskChange; GRK 2043/1) funded by the Deutsche Forschungsgemeinschaft (DFG). In addition, this work has been financially supported by the German Research Foundation (DFG projects no. MA 4759/9-1 and MA4759/8) and the European Unions Horizon 2020 Research and Innovation programme under the Marie 499 Skłodowska-Curie grant agreement No. 691037 (project QUEST).

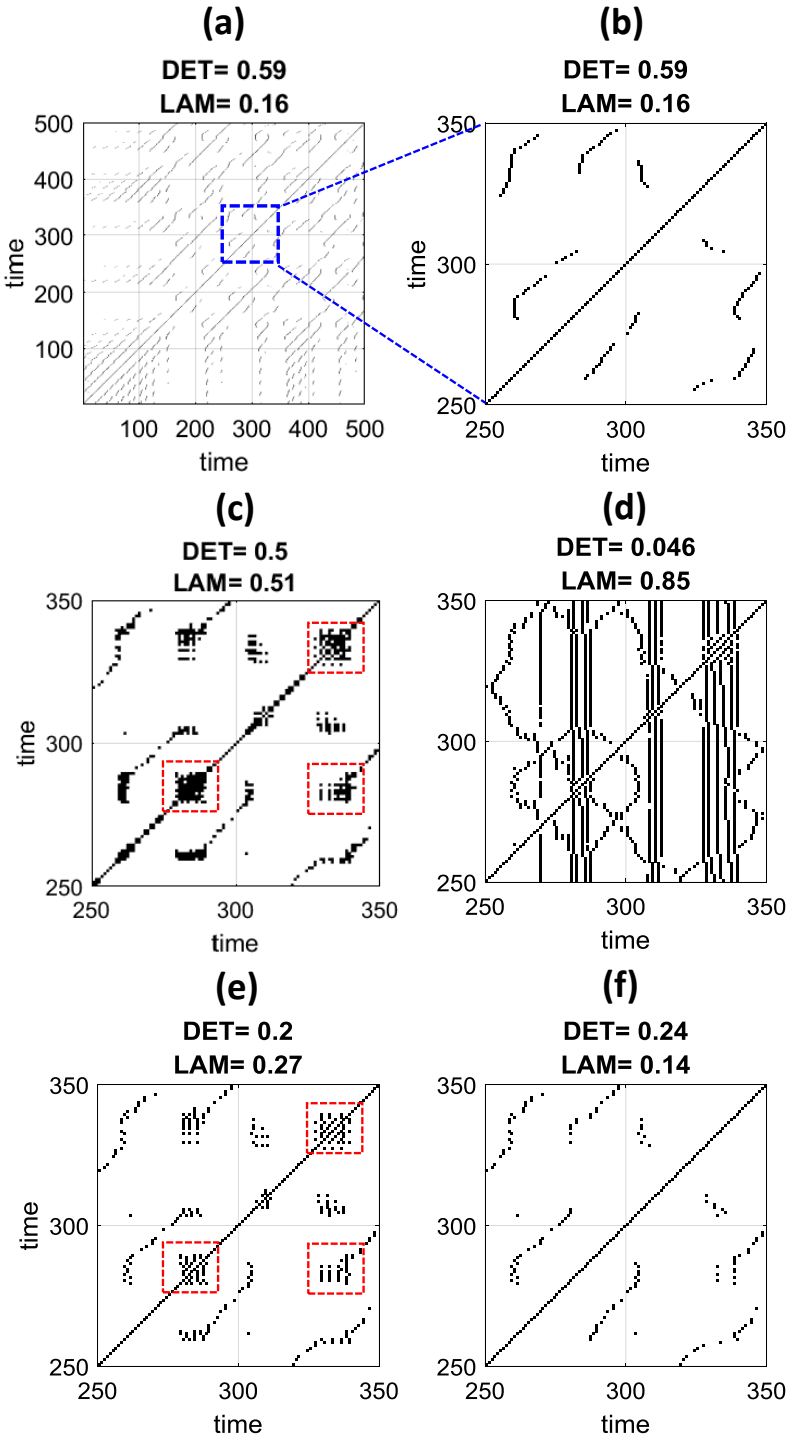

Figure 3.2: RPs of the Lorenz series ($\frac{dx}{dt}$, with $\sigma = 10, \rho = 28, \beta = \frac{8}{3}$), and additionally induced with noise (SNR=20dB). The following RPs are constructed using (a) LMT of Lorenz with no noise, while (b) is the zoomed-in view of the same RP, (c) distance threshold of $\varepsilon = 5^{th}$ percentile of phase distances, (d) LM only, (e) LMT with same ε parameter used in (a), and (f) LM2P with the same ε and $\tau_m = 10$. The red rectangles in (c) and (e) are used to indicate the mentioned block clusters. The embedding parameters of all RP are fixed at $m = 3$, $\tau = 3$

.

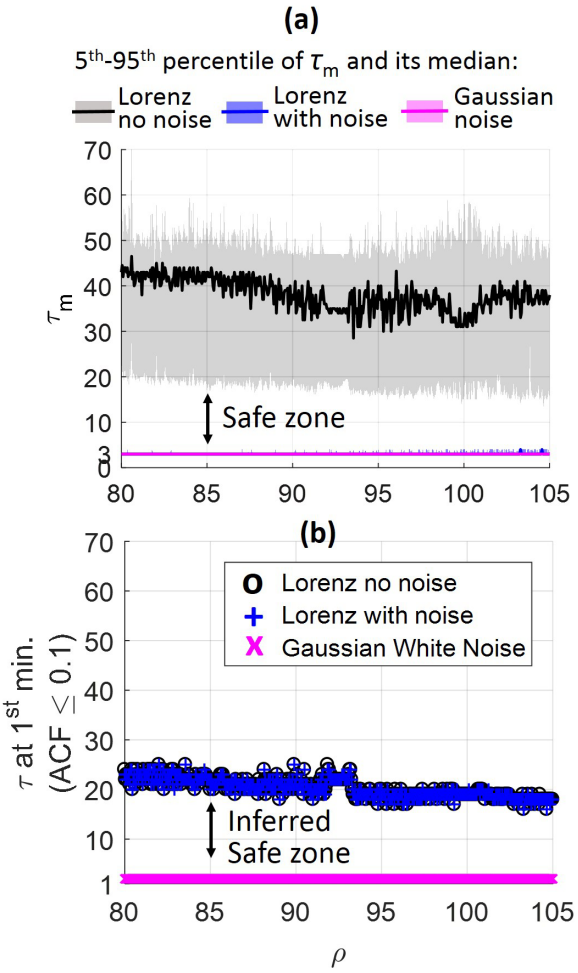

Figure 3.3: Safe choice of parameter τ_m by using ACF: (a) Local minima of the phase space distance for Lorenz and Gaussian noise. While (b) is the inferred safe τ_m to choose based on first minimum τ of auto-correlation (chosen threshold, $ACF \leq 0.1$).

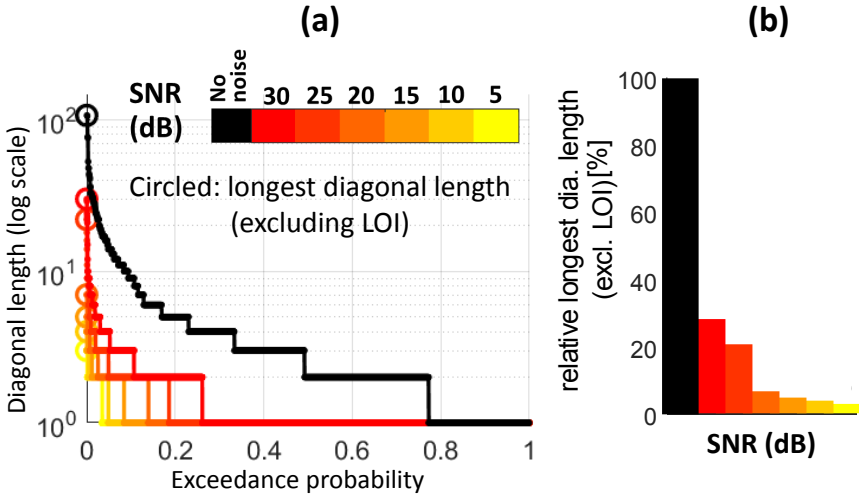

Figure 3.4: (a) Probability exceedance of diagonal line lengths and (b) relative longest diagonal line length (%) of Lorenz of $\rho = 80.$ with response to induced noise, i.e. indicated by signal to noise ratio (SNR)

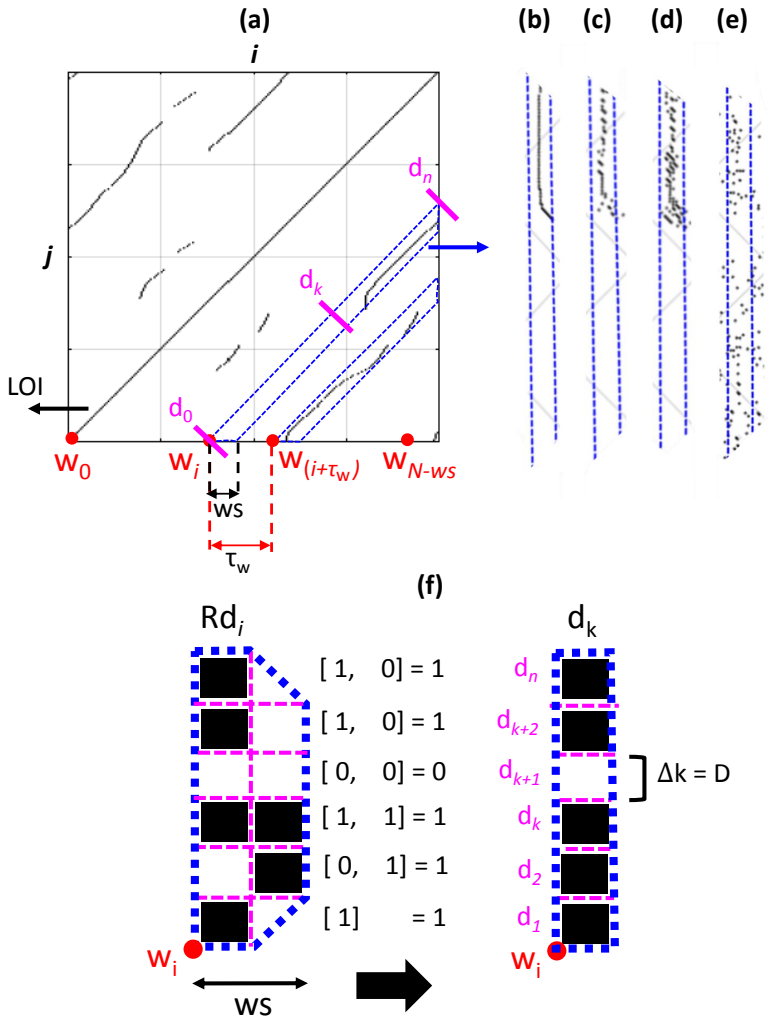

Figure 3.5: Concept of diagonal sliding window: (a) A considerably small ws size window (w_i) slides diagonally through the RP. For each window, RR_{w_i} and $DDET_{w_i}$ are calculated (Eqs. (3.5) and (3.6)). Sub-figures (b) to (e) show a zoom in rotated view of a diagonal window to exemplify an RP of Lorenz without noise, RPs with noises constructed with LMT and LM2P, and a RP of Gaussian white noise respectively. Sub-figure (f) with reference to (a) shows the calculation concept of diagonal distance between (D or Δk) recurring points at each window (rotated view) derived from an aggregate of cells (OR logic) from i to $i + ws - 1$.

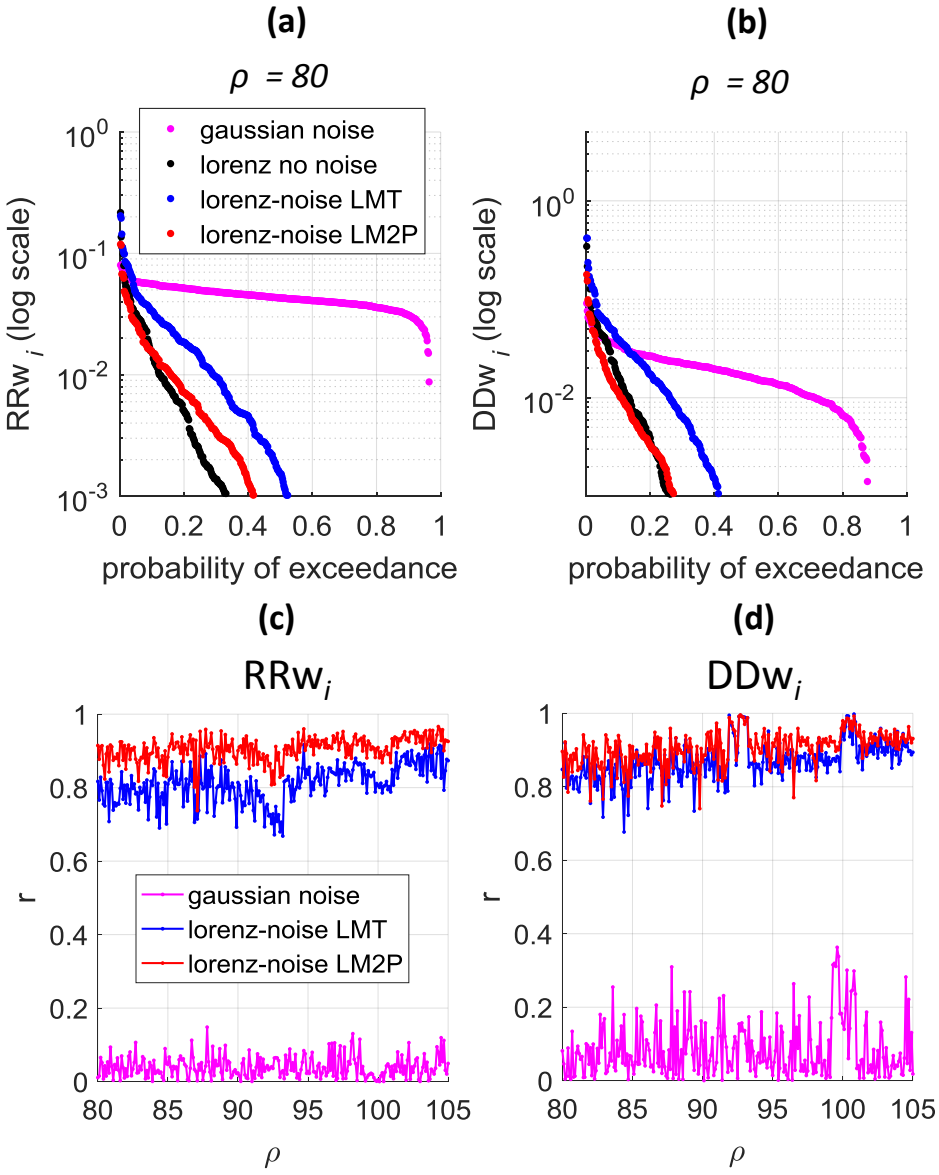

Figure 3.6: Probability of exceedance of (a) RR_{w_i} and (b) DD_{w_i} values of diagonal windows between Lorenz no noise and the LMT and LM2P of the one with noise (shown here is only Lorenz with $\rho = 80$), and Gaussian noise. Correlation coefficient r of (c) RR_w and (d) $DDET$ for all RPs with reference to the RP of Lorenz with no noise. The embedding parameters of all the assessed RPs are fixed at $m = 3$, $\tau = 10$, $\varepsilon = 5^{th}$, $\tau_m = 10$ $ws = 2$, $\tau_w = 2$.

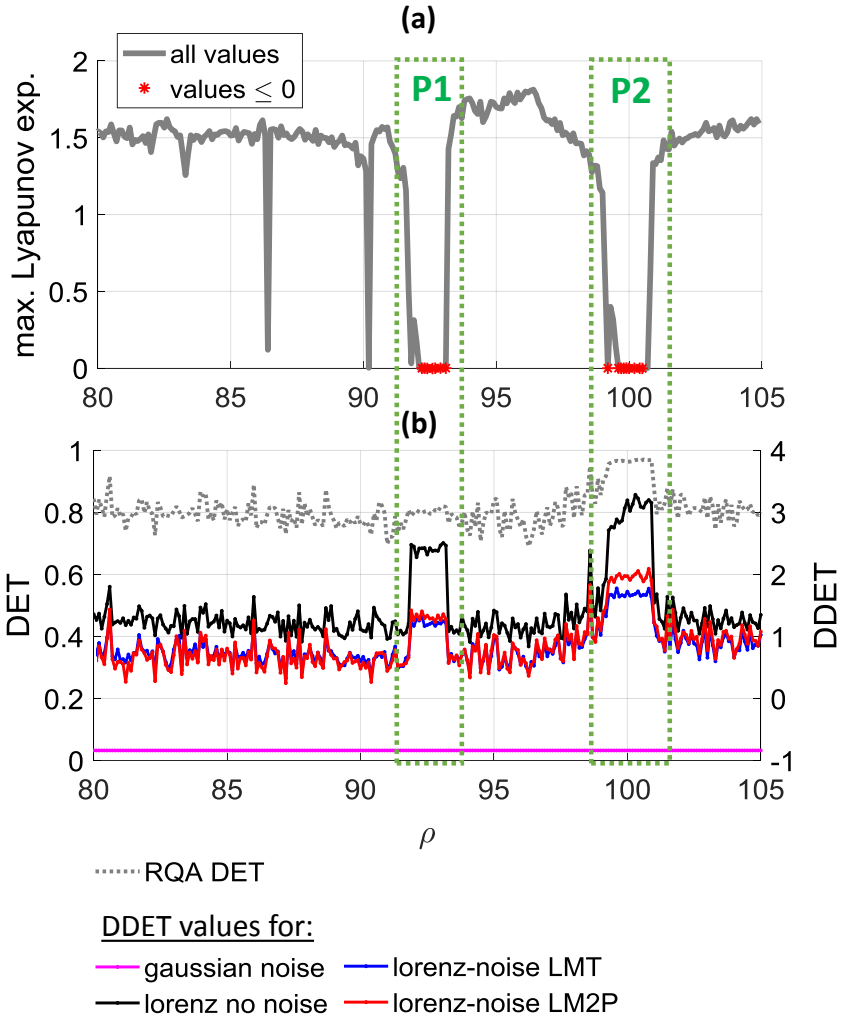

Figure 3.7: (a) Maximum Lyapunov exponent of the Lorenz system with varying ρ parameters (with values below 0 indicating periodic dynamics highlighted as red). (b) DDET values of Gaussian noise, and Lorenz with varying parameters with reference to DET. Green boxes emphasize the two Lorenz periodic windows P1 and P2 (indicated by max.Lyapunov exponent below 0). The RP measures are calculated based on embedded approach: $m = 3$, $\tau = 10$, $\varepsilon = 5^{th}$, $\tau_m = 10$ (for LM2P), and $ws = 2$, $\tau_w = 2$ (for DDET calculation).

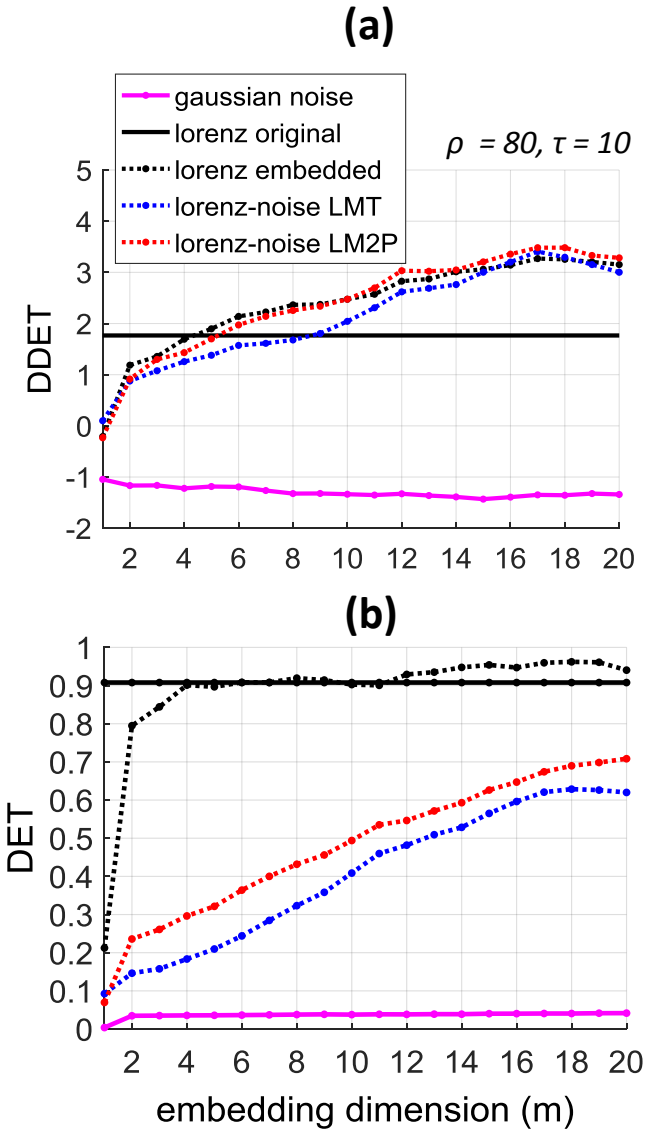

Figure 3.8: (a) Impact of embedding parameter (m on the DDET measure. Shown here is the example of ws for full Lorenz system (i.e. created without embedding, using 3 variables) RP (LM2P) set for $2 \leq ws \leq 10$ and additionally $ws = 50$ and Gaussian noise with $ws = 2$ as reference.

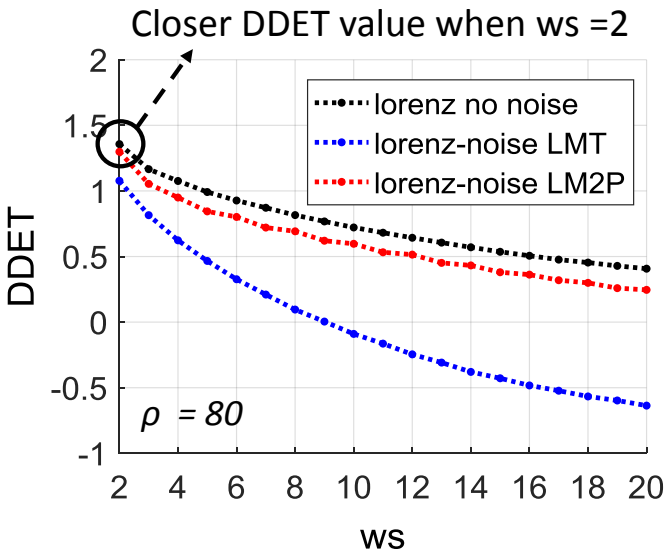

Figure 3.9: (a) Impact of window size parameter (ws on the DDET measure. Shown here is the example for DDET of embedded Lorenz system using LMT and LM2P approach in response to changing ws in comparison with Lorenz without noise

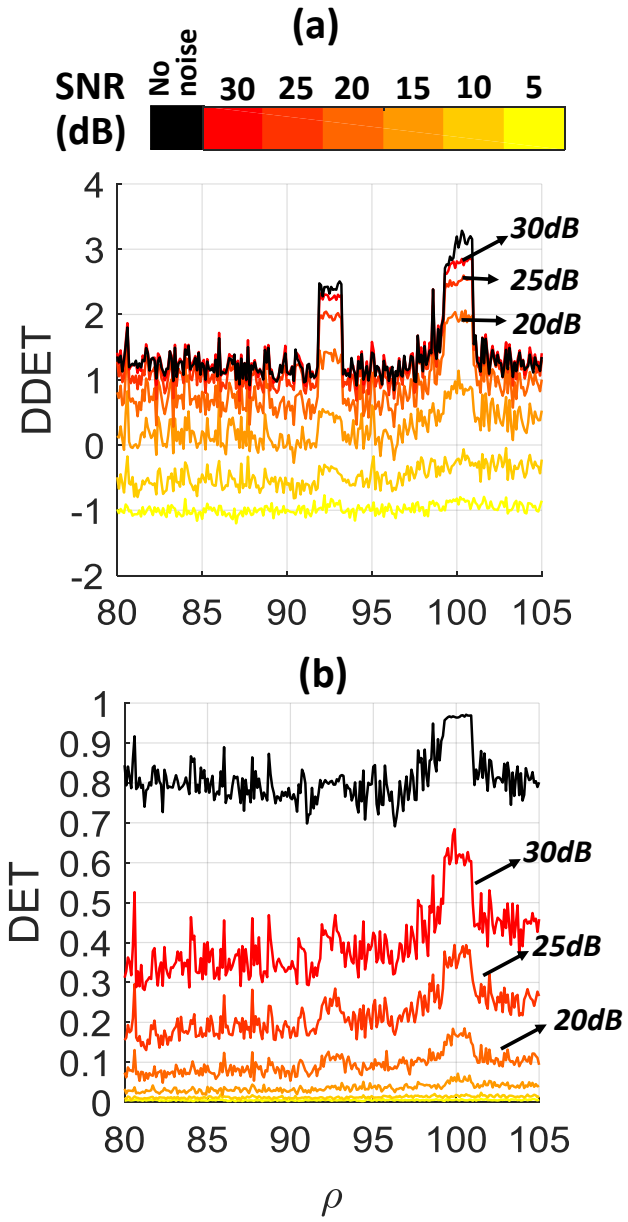

Figure 3.10: (a) Impact of induced noise SNR level on the DDET and DET measure. Shown here is the example of noisy Lorenz series with SNR from 5 to 30db as compared to Lorenz with no noise. All measures are based on RPs generated using LM2P and embedded approach with $m = 3$, $\tau = 10$, $\varepsilon = 5^{th}$, $\tau_m = 10$ $ws = 2$, $\tau_w = 2$.

4 Assessing Hydrograph Similarity and Rare Runoff Dynamics by Cross Recurrence Plots

Submitted as: Wendi, D., Merz, B., and Marwan, N. Assessing Hydrograph Similarity and Rare Runoff Dynamics by Cross Recurrence Plots. Water Resources Research, September 2018.

Keypoints:

- First application of Recurrence Plots in hydrology
- Novel method for quantifying hydrograph similarity based on runoff dynamics
- Time delay embedded phase space trajectory allows to consider relationships between magnitudes of different point in time

Abstract

This paper introduces a novel measure to assess similarity between event hydrographs. It is based on Cross Recurrence Plots and Recurrence Quantification Analysis which have recently gained attention in a range of disciplines when dealing with complex systems. The method attempts to quantify the event runoff dynamics and is based on the time delay embedded phase space representation of discharge hydrographs. A phase space trajectory is reconstructed from the event hydrograph, and pairs of hydrographs are compared to each other based on the distance of their phase space trajectories. Time delay embedding allows considering the multi-dimensional relationships between different points in time within the event. Hence, the temporal succession of discharge values is taken into account, such as the impact of the initial conditions on the runoff event. We provide an introduction to Cross Recurrence Plots and discuss their parameterization. An application example based on flood time series demonstrates how the method can be used to measure the similarity or dissimilarity of events, and how it can be used to detect events with rare runoff dynamics. It is argued that this methods provides a more comprehensive approach to quantify hydrograph similarity compared to conventional hydrological signatures.

4.1 Introduction

The shape of flood event hydrographs can vary substantially between regions and between events for a given catchment, depending on catchment and event characteristics. Variations in hydrographs can be expected for different event types, e.g. driven by different climatic factors, and for different catchment conditions. For instance, short-rain floods triggered by moderate to substantial rainfall tend to show a faster response compared to snowmelt driven floods [Merz and Blöschl, 2003]. Hence, the hydrograph is a fingerprint of the processes involved in the rainfall-runoff event [Blöschl et al., 2011]. Quantifying the similarity or dissimilarity of event hydrographs has received increasing attention in the field of surface water hydrology [Haaf and Barthel, 2018], for example within the 'Predictions in Ungauged Catchments' initiative [Hrachowitz et al., 2013], or for assessing the performance of hydrological models [Ehret and Zehe, 2011].

A range of indices, herein also called hydrological signatures, have been used to describe rainfall-runoff event hydrographs. The hydrograph peak (Q_p) is the most popular hydrological signature in flood risk assessment and flood design due to its close relationship with the socio-economic impact of floods. Other important hydrological signatures are discharge volume (V), event duration (t_d), time to peak (t_p), recession time (t_f), base flow index (BFI), or the rising and falling limb slope of the hydrograph (ΔQ_{rise} and ΔQ_{fall}). These signatures have been used as event similarity indices required for classification, regionalisation, prediction, change and extreme event analysis, and model calibration [Bárdossy, 2006, Merz and Blöschl, 2003, Peel and Blöschl, 2011, Sawicz et al., 2014, Westerberg and McMillan, 2015, Westerberg et al., 2016]. However, these indices either represent a single element of the hydrograph only (Q_p, t_d, t_p, and t_f), or they are a statistical aggregate of the hydrograph (V, BFI and ΔQ_{rise}, and ΔQ_{fall}). Other studies have introduced the consideration of multi-variate signatures altogether to better exploit the information contained in the hydrograph, for examples the studies of Brunner et al. [2017], Ehret and Zehe [2011], Hannah et al. [2000], Ternynck et al. [2016].

In this study we propose a more elaborate hydrological signature to quantify similarity between event hydrographs. Our signature is based on the phase space representation of discharge hydrographs and attempts to consider the event runoff dynamics more comprehensively. Instead of using a single element index or a joint considerations of statistical aggregates of the hydrograph signatures, it considers the entire, continuous hydrograph shape, i.e. the time sequence and additionally its dependence on the antecedent conditions of the flood event.

In our approach a phase space trajectory is reconstructed from the corresponding hydrograph using Taken's time delay embedding method [Takens, 1981]. Please note that the official term 'reconstruct' is used instead of 'construct' because the theory claims that this embedding allows recreating the system behavior, represented by the phase space

geometry, by just using the time series of one of the system variables [Packard et al., 1980, Takens, 1981]. However, we apply the embedding method in a more practical manner, such that the reconstructed phase space trajectory allows the analysis of the multi-dimensional relationship between discharge values in different points in time. This means that we can implicitly consider antecedent conditions of the flood, i.e. discharge values prior to the flood peak. Their consideration are important for flood analysis, as for instance, a moderate rainfall prior to a flood may partially saturate the catchment and lead to a high flood event peak – much higher than would be expected from the event precipitation alone.

The specific method we propose are Cross Recurrence Plots (CRP), as a variation of Recurrence Plots (RP), and their quantification (RQA - Recurrence Quantification Analysis) as the basis for quantifying hydrograph similarity. RP and RQA are used in order to visualize and quantify phase space trajectories especially at higher dimensions where such trajectories cannot be visualized anymore [Marwan et al., 2007]. Both RP and RQA have gained considerable popularity over the past decades in several scientific disciplines, from economy, physiology, neuroscience, paleoclimatology, astrophysics to engineering, especially when focusing on non-linear times series analysis and characterizing the behavior of complex systems [Aceves-Fernandez. et al., 2012, Carrubba et al., 2010, Crowley, 2008, Eroglu et al., 2016, Goswami et al., 2018, Marwan and Meinke, 2004, Oberst and Lai, 2015]. However, to the authors' knowledge, RP, CRP and RQA have not been used in catchment hydrology, let alone in comparing hydrograph dynamics, despite the popular exploration of chaos theory, which also builds on phase space trajectories. Such phase space trajectories for example have been used for hydrological forecasting or gap-filling of hydrological time series [Sivakumar, 2000].

This paper introduces Cross Recurrence Plots (CRP) as a novel approach for assessing the similarity or dissimilarity of rainfall-runoff events based on the phase space representation of their hydrographs. We argue that this approach better captures the underlying runoff dynamics compared to the traditional hydrological signatures. Not only the comparison method is based on the entire shape of hydrograph, but also configurable to capture the relationships of magnitudes at different time through time delay embedding. Since such methodological application in catchment hydrology has no references yet, the paper first provides a practical introduction to CRP and RQA. To introduce the methodology, we contrast it with the traditional way of comparing time series, i.e. through correlation analysis using scatter plots and correlation coefficients. It is important to note that, in contrast to correlation analysis, CRP and RQA are not restricted to comparing time series of the same length

Our application example, using historical floods at the Elbe River runoff station at Dresden, Germany, compares flood events of varying durations that occured in February and March during the period 1901-2010. These two months show the highest number of annual maxima at the gauge Dresden. The application example illustrates the potential

of the method to quantify similarity of hydrographs between events and to detect their unusual runoff dynamics. This could be events with unseasonal runoff dynamics, i.e. an unexpected flood type for a certain season, or events with rare event characteristics, i.e. never seen before runoff dynamics.

We see the potential of this method to be used for a wide range of questions in hydrology. An obvious extension would be to quantify the similarity of longer epochs, e.g. annual periods, instead of flood events. Another example would be the detection and attribution of change in hydrological time series by investigating whether changes in the runoff dynamics can be identified.

4.2 Methodology

4.2.1 Cross Recurrence Plot

The Cross Recurrence Plot (CRP) is a variation of the Recurrence Plot (RP). RP was first introduced by Eckmann et al. [1987] to visualize the recurrence behavior and properties of dynamical systems through their phase space topology. A dynamical system is represented by a phase space trajectory, and RP is used to identify recurring states of this system, i.e. whether a certain pattern recurs in time. This recurring states are represented by the diagonal lines in the 2 dimensional plot where x and y axis represent time. In contrast, CRP is a tool to analyze time synchronization and similarity between two time series by comparing their phase space trajectories that can also be reconstructed through time delay embedding [Marwan et al., 2002a].

In CRP, continuously connected points that form diagonal lines indicate that (parts of) the time sequence patterns of the two hydrographs are similar to each other. Hence, the longer these diagonal lines, the longer are the patterns that are similar between the hydrographs. Time delay embedding can also be additionally implemented to allow the reconstruction of a high-dimensional phase space trajectory from univariate time series. This means that multiple subsets of values within a single time series are extracted according to a time delay τ and plotted in the phase space to describe the relationships of magnitudes at different time distanced by τ.

For instance, a 2-dimensional phase space vector can be compared to an autocorrelation scatter plot where the x and y axes are the subset values of the original time series that are separated by a shift of τ. A 3-dimensional phase space contains a third variable, i.e. x, y and z with time delay of τ and 2τ, and so on for higher dimensions. Fig. 4.1a shows an extracted flood hydrograph with three peaks or sub-events. The rising slope at each sub-event i (defined as the gradient from the start of the sub-event to its peak) is higher for the second and third peaks. This can be explained mainly by the increasing wetness of the catchment from the first to the third sub-event. This kind of cascading relationships in time where the initial or antecedent conditions are important information motivates the

use of multi-dimensional, time delay embedded, phase space analysis.

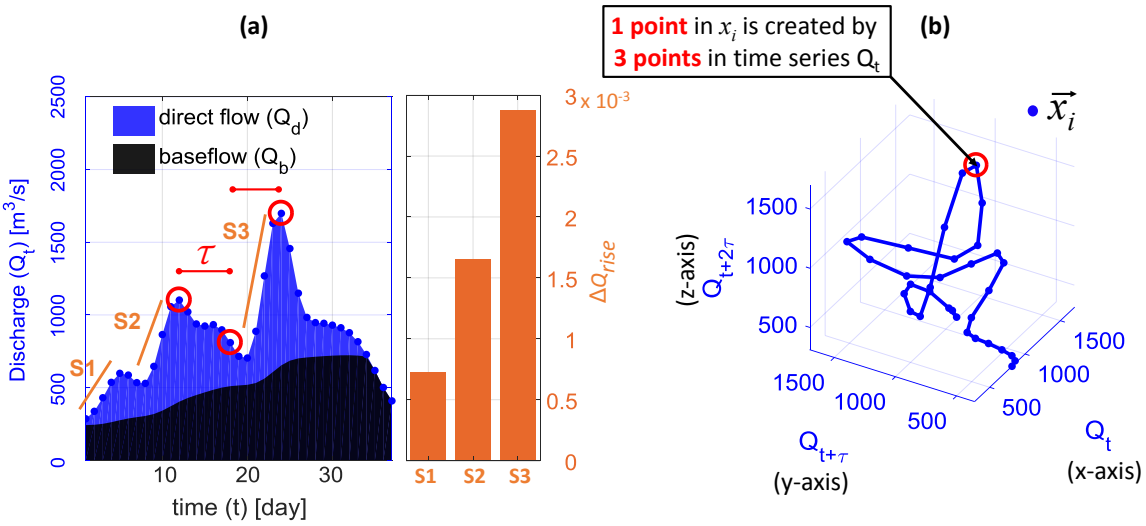

Figure 4.1: Multiple-peak flood event (a) and its 3-dimensional phase space reconstruction (b). The phase space vector consists of three dimensions, whereas each axis shows the values of the original hydrograph separated by the time delay τ and 2τ. Red circles show exemplarily the reconstruction for one point in the phase space.

This time delay phase space reconstruction follows Takens' embedding theorem [Packard et al., 1980, Takens, 1981]:

$$\vec{x}_i = (u_i, u_{i+\tau}, ..., u_{i+(m-1)\tau}) \tag{4.1}$$

where m is the embedding dimension and τ is the time delay, and u_i is a univariate time series or in this case our discharge series (Q_t).

When comparing two time series, phase space trajectories (x_i and y_j) are reconstructed from both time series, and the pointwise similarity of the two trajectories can be assessed based on their distance and visualized with CRP (see Fig. 4.2). The CRP is a 2-dimensional matrix encoding the similarity structure of two high-dimensional, embedded systems. It is a visual representation of a rectangular matrix in which the matrix elements (recurrence points $CR_{i,j}(\varepsilon)$) correspond to times at which the states (i, j) of the two dynamical systems are equal or similar (defined by their phase space distance and a threshold ε):

$$CR_{i,j}(\varepsilon) = \begin{cases} 1, & \text{if } \|\vec{x}_i - \vec{y}_j\|_2 < \varepsilon \\ 0, & \text{otherwise} \end{cases} \qquad i = 1, ..., N, \quad j = 1, ..., M \tag{4.2}$$

where N and M are the number of measured points in the compared phase space vectors $\vec{x}_i$ and $\vec{y}_j$, ε is a cutoff threshold for distances between the vectors, and $\|\cdot\|_2$ is the Euclidean norm.

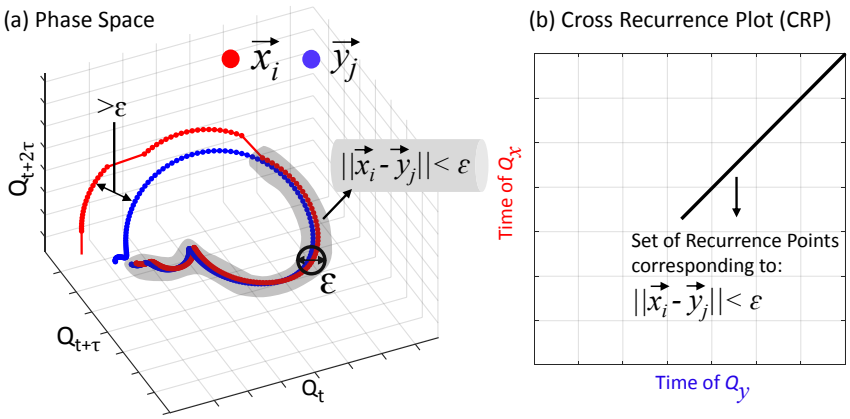

Figure 4.2: Comparison of two phase space trajectories $\vec{x}_i$ and $\vec{y}_j$ constructed from time series Q_x and Q_y using distance threshold ε (a) to define recurrence points in the CRP (b).

To exemplify the concept of CRP and to demonstrate its differences to the widely used tools scatter plot and cross correlation analysis, Fig. 4.3 compares two hydrographs using scatter plots and CRP. One of the differences between the CRP and the scatter plot is that the scatter plot axes represent magnitudes, while in the CRP they represent the time of occurrence of the two series. When two identical time series are compared, CRP shows a single diagonal line (45° angle) that divides the CRP matrix symmetrically (Fig. 4.3.1c, green line). As differences increase this straight diagonal line will become more and more distorted, e.g., becoming perforated and wiggled. Then this line could be quantified by *DET* in order to derive a similarity measure (section 2.2). Further, it is worth to note that the high-dimensional embedding results in embedding loss with a size of $(m-1)\tau$. This embedding loss is a result of reconstructing the phase space vectors corresponding to the number of dimension (m) and time delays (τ) and, thus, the size of the CRP is shorter by $(m-1)\tau$ and needs to be cautioned.

The first example shows the CRP when comparing two identical hydrographs patterns Q_a and Q_b which occur at different times, i.e. Q_b is shifted by 17 time units (Fig. 4.3.1a). Despite the time shift, the CRP still indicates the similarity of the two time series as indicated by the diagonal line. In addition, it shows the time shift. This similarity cannot be derived from the scatter plot without knowing the time shift in advance. Hence, the scatter plot and correlation analysis (Pearson correlation coefficient $R = 0.17$) could lead to the wrong conclusion that there is no similarity between Q_a and Q_b. The CRP approach is useful for detecting recurring runoff dynamics, possibly related to the same causative mechanism, which do not necessarily happen at the same season. It should also be noted that the CRP is useful for comparing hydrographs regardless of their, possibly dissimilar, duration.

The second example compares Q_a with a random system dynamics where Q_b is a randomly shuffled time sequence of Q_a (Fig. 4.3.2a - 2c). In this case, the CRP does not

show any diagonal lines. Similarly, the scatter plot does not indicate a relationship, but it should be cautioned that the correlation analysis suggests a substantial anti-correlation (Pearson correlation coefficient $R = -0.28$).

The third example (Fig. 4.3.3a - 3c) compares two hydrographs with different runoff dynamics where Q_b represents an increased storage capacity in the catchment that dampens the flow. This could result from a perturbation to the catchment such as dam construction. Q_b is obtained by a storage-based Muskingum transformation that is commonly used for flow routing in hydrological modelling [Hattermann et al., 2014]. The parameters of the Muskingum transformation are set as: storage constant $K = 15$ time units; weighting factor $x = 0.01$. Due to the different runoff dynamics, the resulting CRP shows a rather high dissimilarity in contrast to the substantial correlation coefficient $r \approx 0.4$. Although this CRP contains an inclined line, this line is rather broken and not tilted with 45° which would indicate similarity.

Furthermore, It is important to note that, unlike correlation analysis and scatter plots, CRP and RQA do not require that the two time series have the same length. In the case of cross correlation analysis the lag would be constant for the complete piece of time series, where CRP allows temporal changes of the temporal relationship between the two considered time series and, thus, also non-monotonic changes in the relationship.

When working with real world observations, the presence of noise might cause the diagonal in CRP to be discontinuous. Two examples are given Fig. 4.4, where the hydrograph Q_a is compared to similar hydrographs that have been constructed by imposing white Gaussian noise on Q_a with a signal to noise ratio (SNR) of 25dB and 20dB respectively. These values are represented in decibels (dB), a logarithmic ratio between the signal and noise level. The diagonal line of the CRP becomes broken or contains gaps, and these gaps are larger when the signal is more noisy. When dealing with noisy signals, one can consider noise reduction methods, such as filtering or smoothing; for an overview see [Elshorbagy et al., 2002].

4.2.2 Recurrence Quantification Analysis

Similar to the correlation coefficient which summarizes the information of a scatter plot, patterns within a CRP can be quantified by Recurrence Quantification Analysis (RQA). In our study, RQA is used to provide a similarity index for flood hydrographs. RQA can also be used to reveal typical dynamical features of the investigated system, such as range of predictability, chaos-order, and chaos-chaos transition [Marwan et al., 2002b, Trulla et al., 1996]. The RQA measure *d*eterminism (*DET*) describes the similarity (or dissimilarity) of two dynamical systems using the distribution of connected recurrence points that form diagonal lines, i.e. lines in the CRP with slope 45°, over all the points within the CRP:

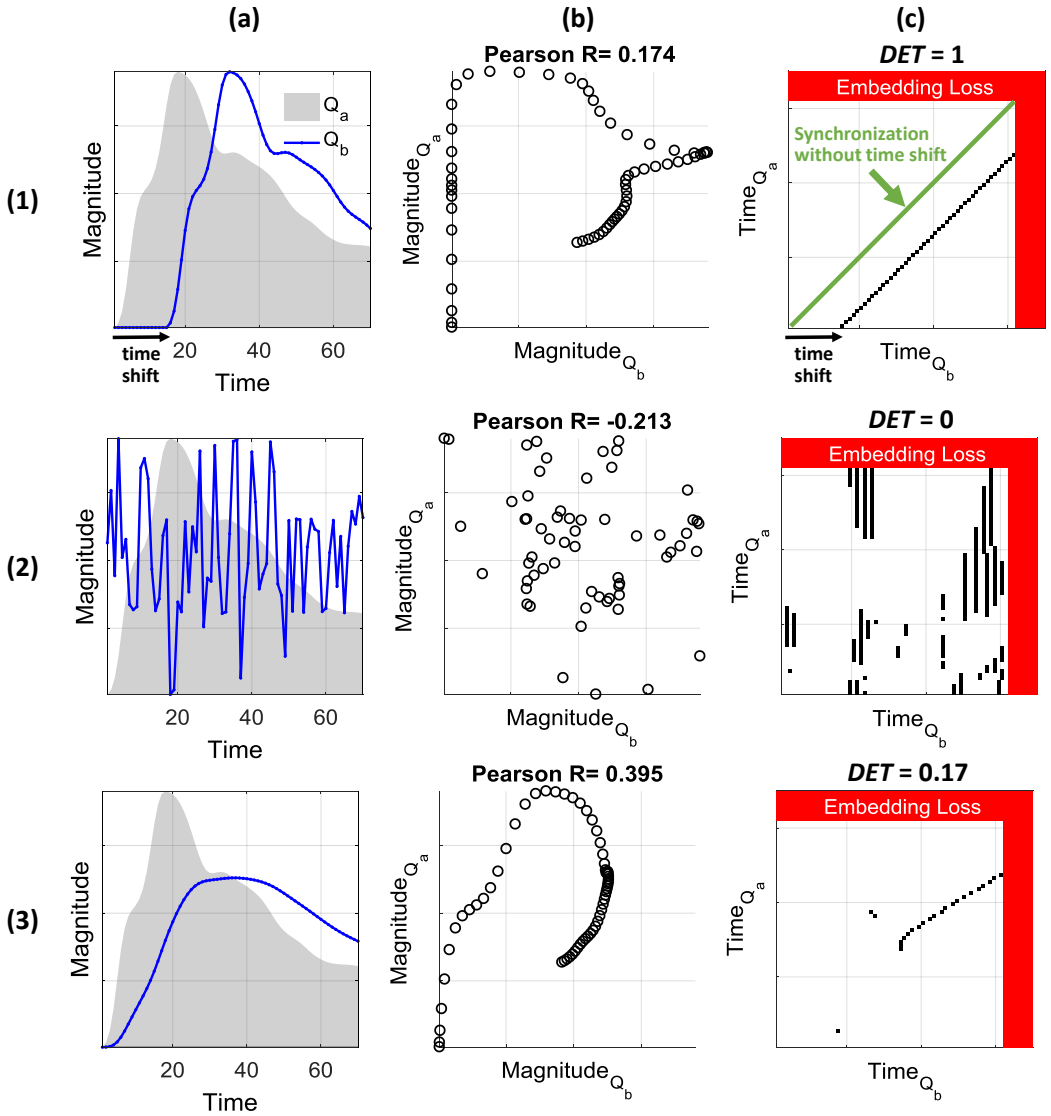

Figure 4.3: Comparison of two discharge time series (a) with scatter plot and correlation coefficient R (b) and CRP and *d*eterminism DET (c). Example (1) compares two identical hydrographs with a shift in their timing, example (2) compares a hydrograph with a randomly shuffled version of the same hydrograph, and example (3) compares two different runoff dynamics where Q_b results from a storage-based Muskingum transformation of Q_a representing an increased storage capacity in the catchment. The embedding losses are shaded in red.

$$DET = \frac{\sum_{l=l_{\min}}^{N} lP(l)}{\sum_{i,j}^{N} CR_{i,j}}, \tag{4.3}$$

where $P(l) = \{l_i;\ i = 1, \ldots, N_l\}$ is the relative frequency of the lengths l of diagonal structures, N_l is the total number of those diagonal lines in the CRP, and $l_{\min}$ is the minimum length of diagonal lines (usually two recurrence points).

This quantification based on the fraction of diagonal lines among all recurrence points ($CR_{i,j}$) considers the influence of scattered single recurrence points that occur by chance.

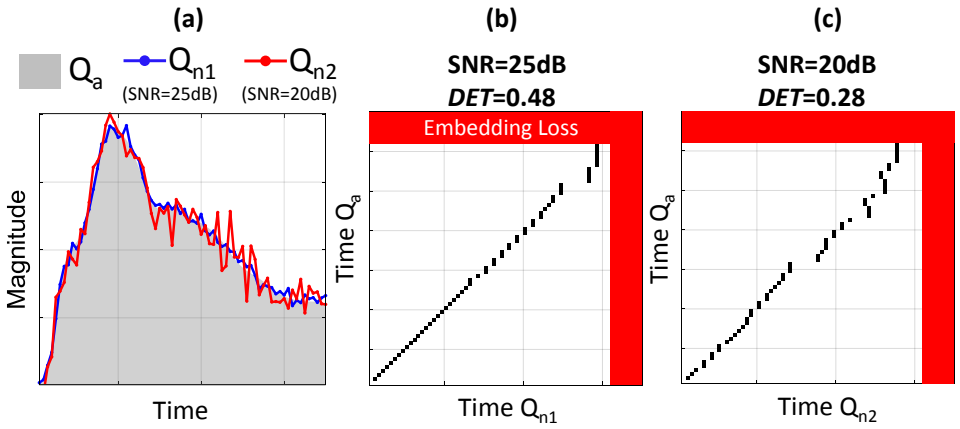

Figure 4.4: Comparison of a hydrograph with noise-induced versions of the same hydrograph (a). CRP for a signal to noise ratio (SNR) of 25dB (b) and 20dB (c), respectively.

DET varies between 0 and 1, indicating the range from low to high similarity in the dynamics of the two times series. For similar continuous dynamical systems, many diagonal lines in the CRP are typical, leading to a high value of *DET* [Marwan, 2010]. The similarity of the two continuous states in the phase space is strictly defined by the 45° diagonal line, and any other lines are not relevant for the quantification of similarity. Single, isolated recurrence points can occur if states are rare, if they do not persist, or if their distance fluctuate heavily. For instance, two signals with the same magnitudes but different time sequence, and hence different dynamics, would lead to single points and result in a low *DET*. For the two identical but shifted hydrographs (Fig. 4.3.1), *DET* is 1. Hence, this measure correctly identifies the identical runoff dynamics of the two hydrographs in contrast to the correlation coefficient which suggests little similarity ($R = 0.17$). This is because correlation analysis is unable to capture the non-monotonic pattern in the scatter plot. When comparing the hydrograph with its randomly shuffled version (Fig. 4.3.2), $DET = 0$ in contrast to the, possibly misleading, value of the correlation analysis ($R = -0.28$).

When comparing the two hydrographs with different runoff dynamics in Fig. 4.3.3, *DET* shows a low value of 0.17 suggesting little similarity in contrast to the correlation analysis ($R \approx 0.4$).

4.2.3 Construction and parameterization of CRP

Three parameters are required in constructing the CRP. These are the two parameters for the time delay embedding, i.e. embedding dimension m and time delay τ, as well as the phase space distance threshold ε that defines a recurrence point. In a specific context, m and τ can be chosen according to the requirement of the analysis, i.e. by the number of interrelated points in time. For example, the description of events consisting of complex, multi-peak hydrographs would require a higher number of points than regular events. The sub-events within a multi-peak hydrograph have possibly different characteristics.

Initial sub-events, for instance, can be regarded as antecedent conditions and might affect the following sub-events, i.e. increase their magnitude. Therefore, their relationships are valuable in the characterization of the event dynamics. In general, the higher the embedding dimension and the smaller the time delay, the more complete the dynamics can be described by the phase space trajectories. However, artifacts from the suboptimal choice of parameters and embedding loss, which also increases with higher m and τ, should be avoided. Two unrelated random signals for instance (Fig. 4.5a) should yield zero or near zero value of *DET* and be represented by scattering recurrence points in the CRP (Fig. 4.5b), but improper parameters could artificially increase number of diagonal lines and hence result in artifacts, i.e. high *DET* value (Fig. 4.5c).

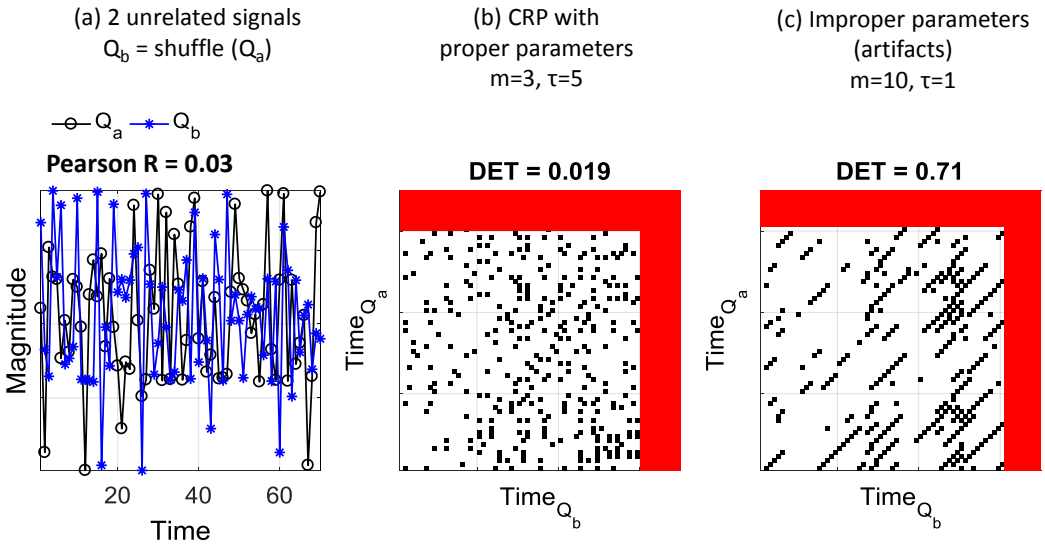

Figure 4.5: Example of artifacts in CRP due to improper embedding parameters: comparing (a) 2 unrelated random signals result in (b) CRP with proper embedding parameters and (c) CRP with artifacts caused by improper parameters.

The standard approaches for finding the optimal embedding parameters are the method of false nearest neighbours (FNN) for m, and the auto-correlation or mutual information (MI) for τ [Fraser and Swinney, 1986, Kantz and Schreiber, 2005, Kennel et al., 1992]. However, Marwan [2010] concludes that τ is sometimes overestimated by auto-correlation and mutual information, and that the choice of m has to be considered with care, as a wrong choice artificially increases diagonal lines and *DET* values.

To prevent such artifacts, we have proposed a random shuffling method to determine the safe region of embedding parameters [Wendi et al., 2018]. However, this method was developed for the RP assessing the recurring dynamics within a single system or time series. Here, we adapt this method for the CRP by comparing two identical time series and shuffling the time sequence of only one of the two time series. The basic idea is, similar to the CRP example of Fig. 4.3.2, that shuffling destroys the original sequence information about the process, thus changing its dynamics to a different and random one. The *DET*

value from the CRP of the hydrograph Q_a and the shuffled one Q_b should be small. A high *DET* value for a certain set of parameters m and τ indicates that the CRP contains artificially long diagonal lines and, therefore, this parameter set is assumed to be unsafe. Safe parameter sets can be found using a *DET* distance matrix. The *DET* distance is the absolute difference between the *DET* values of the original CRP i.e. constructed from the two identical time series without shuffling, where *DET* is expected to be 1, and multiple iterations of shuffling, with expected low *DET* values. These multiple iterations are then summarized based on the median. The median *DET* distance varies from 0 to 1; the larger the *DET* distance, the safer the parameter set. The optimal choice is a trade-off between the requirements for a safe parameter region and for small embedding loss.

To demonstrate the parameterization of CRP, we use the hydrograph example in Fig. 4.1. It has a daily resolution, but is resampled with linear interpolation to a finer resolution of 6 hours to allow the evaluation of higher embedding parameters (m and τ). We calculate the median of the *DET* distances for 100 shuffling iterations for each set of embedding parameters within the range of $1 \leq m \leq 10$ and $6 \leq m \leq 60$ hours (Fig. 4.6a) and the resulting embedding loss, i.e. ratio of the loss to the time series length (Fig. 4.6b). We select the parameter set from the region with high median *DET* distances (above 0.8) and small embedding loss (below 10%). In this example, since we have decided to fix the embedding dimension m to 3, therefore best candidates for τ selection derived from this safe parameter region are 30 and 40 hours. Should a higher m be desired in order to quantify the relationship of more points in time, then τ should be adjusted to match the mentioned trade-off.

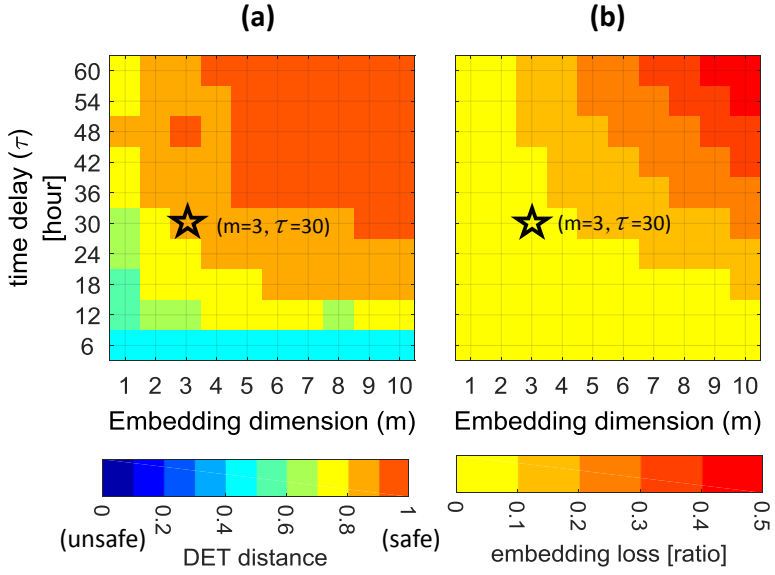

Figure 4.6: Safe regions and optimal parameter sets: (a) median *DET* distance, (b) embedding loss. The parameter set used in this study is marked with a star.

In addition to the embedding parameters, an optimal threshold for the phase space

distance ε is also essential to prevent artifacts. Thick lines, for instance, can easily occur in continuous dynamical systems due to the temporal correlation of the phase space trajectory, causing the CRP to contain redundant information when ε is not defined properly [Krämer et al., 2018, Schultz et al., 2011, Wendi and Marwan, 2018a]. Fig. 4.7 illustrates this problem for the hydrograph comparison in Fig.4.3-1. Sub-figure (a) shows the distance matrix of the two phase space vectors ($\|\vec{x}_i - \vec{y}_j\|$), while sub-figure (b) shows exemplary three slices of the distance matrix at rows 20, 40 and 60, i.e. distances relative to Q_a at time 20, 40 and 60. Using simply a distance threshold ε in defining the recurrence points leads to thick lines in the CRP for those periods where the local variance of the hydrograph is low, i.e. at the time of Q_b around 40-50 (Fig. 4.7c). Such thick lines artificially increase the number of diagonal lines, yielding unreasonably high *DET* values. Schultz et al. [2011], Wendi and Marwan [2018a] suggested a local minima-based recurrence definition to solve this problem. The minima are found in each row of the distance matrix and should correspond to the closest neighbors of a state within the threshold ε. This method minimizes the line thickness (compare Fig. 4.7c and d), and requires much less computational effort compared to alternative solutions [Schultz et al., 2011]. Moreover, Schultz et al. [2011] shows that the local minima-based CRP is less dependent on the selection of the threshold ε, making the method more robust. Therefore, we select and recommend this method for calculating the CRP for comparing runoff dynamics.

4.3 Application Example and Comparison with Conventional Indices

We apply CRP and RQA to evaluate the similarity of flood hydrographs measured at Dresden gauge from 1901 to 2010. This gauge is located in the city of Dresden, Germany, on the Elbe River which flows from the Krkonoše Mountains in the Czech Republic to the North Sea at Cuxhaven, Germany. This application is meant to show the potential of the method to quantify similarity taking into account the underlying runoff dynamics, and to detect unusual events. We also compare the results with frequently used hydrological signatures individually and and altogether. Using this example, we attempt to provide a practical introduction to CRP and RQA, as these methods have not been used in hydrology so far but have been beneficial in several other disciplines.

To compile a set of flood events, we first identify the annual maximum values from the times series of daily streamflow observations. Thereafter we select only those events with peaks in February and March. These are the months where the highest number of annual streamflow maxima occur. Although the same flood types, e.g., snow-melt flood or rain-on-snow flood, may occur in these months, February and March are often classified in different seasons, i.e. December-February (DJF) for winter and March-May (MAM) for spring [Matti et al., 2017]. Hence, it is interesting to our analysis to which extent events with similar dynamics occur in these two months. We further select only those events

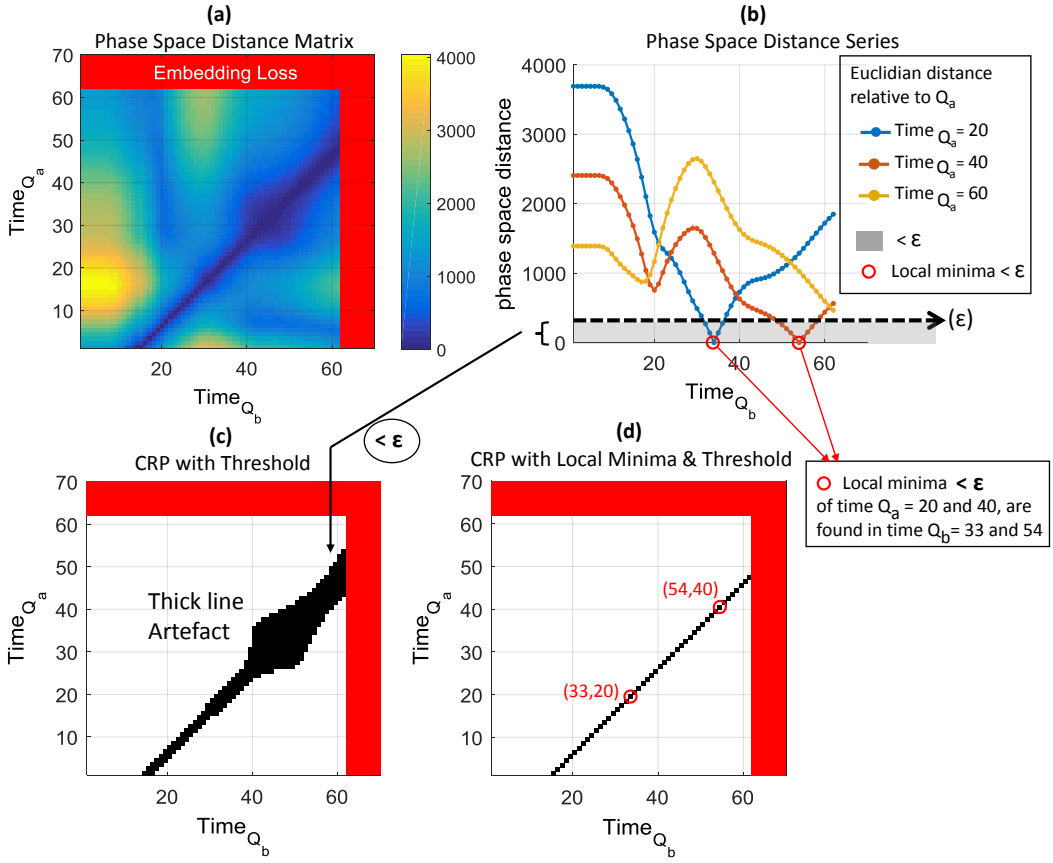

Figure 4.7: Illustration of the local minima approach [Schultz et al., 2011, Wendi and Marwan, 2018a] to define recurrence points for the CRP example shown in Fig. 4.3-1. (a) recurrence distance matrix ($\|\vec{x}_i - \vec{y}_j\|$), (b) phase space distance with reference to Q_a at time 20, 40 and 60, and their corresponding local minima below the applied threshold ($\varepsilon = 5^{th}$ percentile), (c) and (d) CRPs resulting from the distance matrix below the threshold and from the local minima below the threshold, respectively

.

with a peak of at least 1000 m^3/s to exclude minor events. The next step consists in deriving the complete event hydrograph for each selected peak. To this end, we partition the streamflow into direct flow and base flow using the Boughton 2-parameters separation method [Boughton, 1993]. The start of the flood event is defined as the day when the direct flow reaches a minimum threshold of 50 m^3/s within 30 days prior to the peak flow. The event ends when the direct flow falls below a second threshold of 30 m^3/s within 40 days after the peak. These thresholds have been subjectively determined after multiple trials with visual inspection. This procedure results in a series of 45 event hydrographs (shown in Fig. B.3 in Appendix B.3).

The first analysis of this event set compares the event in February 1953, which has a commonly seen single-peak hydrograph, with all other flood events in a pairwise manner. We construct the CRP for each hydrograph pair and use the *DET* measure as similarity index. For the CRP construction in this application example, we choose $m = 3$ to allow

the visual comparison of the reconstructed phase space, and $\tau = 30$hours. This parameter set is considered as a safe choice for all events. It is determined via the *DET* distance (section 2.3), i.e. by comparing each event hydrograph to itself and its shuffled versions, and by ensuring that the embedding loss does not exceed 10%. Each event's median *DET* distance is calculated for different parameters sets. In appendix 6 we provide the median *DET* distances for all 45 events based on the selected parameter set ($m = 3$; $\tau = 30$hours), and the possible maximum *DET* distance for different parameter sets. For our fixed parameter set, all median *DET* distances fall into a considerable safe range, i.e. above 0.6, and the majority is above 0.8. It would be possible to maximize our *DET* distances by changing their parameter sets, but this would require higher embedding dimension (m). For instance, for the events 1937 and 1942, a higher *DET* distance could be attained by increasing m to 5. Overall, longer multi-peaks events tend to have lower *DET* distance for the fixed parameter set, and would require higher m values to maximize their *DET* distance. Although in this example m is fixed to 3 for the purpose of phase space visualization, it is recommended to utilize parameter sets that yield the maximum median DET distance for a more reliable assessment.

Fig. 4.8 shows the time series of resulting *DET* values. Two events with high *DET* values, suggesting high similarity to the 1953 event, are exemplary shown in Fig. 4.8c (February 1916) and Fig. 4.8e (March 1969). Just like the 1953 event, their hydrographs consist of a single peak with similar shape. In contrast, the comparison with the event in February 1937 (Fig. 4.8d) results in a low *DET* value as expected by the very different hydrograph shape with multiple peaks and considerably longer duration. A low *DET* value is also noticed for the March 1992 event (Fig. 4.8f); this time the hydrograph slope is milder with lower flow magnitude. Fig. 4.8g – f show the phase space trajectories for these four pairwise comparisons. They illustrate that the phase space trajectories of the events in 1916 and 1969 are much more similar to the 1953 event compared to the events in 1937 and 1992. Fig. 4.8l – o plot the CRPs for these four event pairs; the comparison with 1916 and 1969 shows extended 45° diagonal lines. In contrast, the CRP of 1937 shows several short lines, however only the first one has an angle of 45°. The CRP of 1969 consists of a single extended line, however, this line has a smaller than 45° angle. Note that the CRPs shown here are no longer square due to the different duration of the compared time series in the x-axis, which is one of the advantages of using CRP approach.

This example of assessing the pairwise similarity of hydrographs can be extended to evaluate the rarity of each flood in terms of its runoff dynamics by intercomparing it to all other floods in the event set. This results in a matrix of *DET* values of all pairwise hydrograph intercomparisons (see Fig. B.2 in Appendix B.2) which can be summarized statistically. Fig. 4.9 shows such an intercomparison; each flood hydrograph of February and March from 1901 to 2010 is compared to all the other events, and the median *DET* value is used as rarity measure. Events with low median *DET* values have hydrograph

shapes that reoccur rarely within the event set, whereas high values suggest that these events have common hydrograph shapes. In case the hydrograph shape is a signature of the underlying flood generation processes, then the median *DET* value can be used to indicate unusual events in terms of flood generation. The two events with the highest and lowest median *DET* values, respectively, are marked in Fig. 4.9a and their hydrographs and phase space trajectories are shown in Fig. 4.9b – e and Fig. 4.9h. In addition, the peak discharge and the median *DET* values of all events are plotted against their empirical exceedance probability in Fig. 4.9f and g.

The 1940 event (Fig. 4.9c) has the lowest median *DET* value (zero), indicating that this is the most unusual event in the whole flood series. It contains a first peak whereas the increase and recession are very steep and the peak magnitude shows the highest value of all February and March events of the period 1901-2010. Its second peak has completely different characteristics. After a steep increasing limb the hydrograph shows almost constant values for ten days. The historical archive [Schuh, 2011] reports that this event was a rare ice jam flood caused by accumulated ice debris slightly downstream of the gauging station. The unusual hydrograph shape suggests that, by the time of the second peak, the ice debris had accumulated and jammed the river, so that the high flood water level of the river was kept constant for an unusually long duration.

The 1909 flood (Fig. 4.9b) has the second lowest median *DET* value and the 4th highest peak discharge. This event was also recorded in the archive as unusual; very heavy rain was combined with icy and deep frozen ground [Röttcher and Deutsch, 2009, Schuh, 2011]. The rainfall intensity was unusually high for this season; such high intensities are rather observed in the summer season in the Elbe catchment [Petrow et al., 2007]. The superposition of intensive rainfall with frozen ground led to an exceptionally peakish hydrograph shape with steep rising and falling slope. Interestingly, the antecedent catchment conditions were rather dry. The streamflow at the event start was $90 m^3/s$, while the median of all annual maximal floods in February and March is $200 m^3/s$. This event was caused by different flood generation processes compared to the typical rain-on-snow floods [Merz and Blöschl, 2003] in February and March at the gauge Dresden, where snowmelt prior or during the flood event increases the catchment wetness and amplifies the impact of moderate rainfall [Nied et al., 2017].

The floods in 1995 and 2005 (Fig. 4.9d–e) have the highest median *DET* values, which suggests that these events represent the most common flood runoff dynamics. Their hydrographs show a rather prolonged recession. Fig. 4.9h compares the phase space trajectories of these four events. The events in 1995 and 2005 are rather similar to each other, while the events in 1909 and 1940 with the lowest median *DET* values have very different trajectories.

The two events with the lowest median *DET* value have the highest and 4th highest peak discharge. This could suggest a link between unusual runoff dynamics and extreme

discharge in the sense that the extremes are generated by different processes compared to the majority of floods. Fig. 4.10(a) plots peak discharge versus median *DET* values. There is a moderate correlation (Pearson correlation coefficient r = -0.44), significant at the 1% level. Hence, there is a tendency that floods with extreme peak discharges have unusual runoff dynamics as shown by the floods 1940 and 1909 which are both within the top 5 of the indices (shaded orange), and that moderate or low peaks have rather common runoff dynamics (e.g. floods 2005 and 1995). However, not all events with extreme peaks are characterized by rare runoff dynamics and vice versa. For instance, the 1924 flood has a considerable peak discharge above 2000 m^3/s (peak discharge rank 7) but a common hydrograph shape (median *DET* rank 42), while the 1901 event with low peak discharge (peak discharge rank 34) shows a rather unusual runoff dynamics (median *DET* rank 8) with five peaks and unusual fluctuations within the event. Multiple peaks are not necessarily unusual; for instance, the event 1952 has a rather common hydrograph with three sub-events that are smooth in their transition (median *DET* rank 43).

To further assess the proposed CRP-based measure against frequently used hydrological signatures, we compare it against the baseflow index, the rising and falling slope, and the volume and duration of the hydrograph. The rising and falling slope ΔQ_{rise} and ΔQ_{fall} are calculated as the gradient during the flood event prior to the peak (i.e. from the start of the event to the peak) and after the peak (i.e. from the peak to the end of the event), respectively. The volume V is calculated as an approximate integral of the total discharge using the trapezoidal method, and the baseflow index BFI is the ratio of baseflow and total discharge volume, also derived using the same integral approximation.

We plot each signature against the median *DET* value for the flood event set (Fig. 4.11), and measure its correlation using the Pearson correlation coefficient R. Falling slope and baseflow index show a positive correlation, significant at the 1% level, i.e. events with rare runoff dynamics show steeper recessions and a lower fraction of baseflow. This result can be explained by the dominant flood generation processes. Floods in February and March are typically snow-melt events or rain-on-snow events with moderate to low rainfall leading to slow recessions. Hence, events with mild falling slopes are not considered as rare or unusual. These dominant flood types also explain the relation between BFI and median *DET*. Winter floods are often characterized by a high fraction of baseflow. The remaining signatures do not show a significant relation with median *DET*.

Table 4.1 compares the top 5 events for each index. For visual comparison, all hydrographs can be found in Figure B.3 in the Appendix. The most unusual event identified by the CRP-based measure, the 1940 flood, is also unusual in terms of high peak discharge, steep rising slope and high volume. Although its shape is clearly an outlier with a steep first peak and a second peak which is held constant for ten days due to ice blocking the river, the falling slope index does not suggest that this event is unusual, since both slopes are aggregated into one value hiding the very specific event characteristics. The second

and fourth unusual events, the floods in 1909 and 1956, are set apart from the other events by their unusually steep rising and falling slopes and low baseflow index. The third unusual event, the 1906 flood, is not within the top 5 events of any of the hydrological signatures. In terms of these signatures, this event is not particularly unusual. However, it has indeed an unsual shape with a long upfront limb with comparatively low variability. The 1942 event, the fifth unusual flood, is also characterized as particular by the volume and duration.

The comparison of the CRP-based similarity measure with the conventional hydrological signatures shows that it characterizes different events as unusual. It shows moderate correlation with the falling slope, baseflow index and peak discharge, but no significant relation to the other signatures. These differences can be explained by the different conceptual approaches: *DET* quantifies the event runoff dynamics by taking into account the temporal evolution of the discharge values of the entire event. In contrast, the conventional hydrograph signatures consider either one specific component of the hydrograph or are an aggregated value. Hence, they provide a less comprehensive picture, as they either focus on a specific component or lump across several characteristics, such as the slope averaged across several sub-events. It is interesting to note that the proposed CRP-based measure does not only characterize events with very particular hydrograph shapes as unsual, such as the double-peak 1940 flood where the second peak is almost constant for ten days due to ice blocking the river. It also detects events that have a common single-peak shape, but are unusual in terms of low baseflow and steep slopes, such as the 1909 event. An advantage of the hydrological signatures is that they provide an explanation why they characterize an event as unusual. However, due to their specific nature several signatures need to be considered jointly to judge whether a hydrograph is unusual.

Table 4.1: Top 5 most unusual events in terms of median *DET* and different hydrological signatures. The last three columns show the match between median *DET* and the hydrological signatures.

No	Index	1st	2nd	3rd	4th	5th	Exact Match	Match diff. rank	Total Match
1	Median *DET* - lowest	1940	1909	1906	1956	1942			
2	Peak discharge - highest	1940	1923	1947	1909	1946	1	1	2
3	Rising slope (ΔQ_{rise}) - steepest	1940	1956	1909	1916	1923	1	2	3
4	Falling slope (ΔQ_{fall}) - steepest	1909	1923	1956	1931	1948	-	2	2
5	Volume - highest	1988	1940	1937	1942	1947	-	2	2
6	Baseflow index (BFI) - lowest	1909	1956	1933	1922	1945	-	2	2
7	Duration - longest	1937	1942	1988	2009	1914	-	1	1

To compare our approach with a well-established method, we utilize these signatures as

a joint index to identify rare events through clustering. We use hierarchical clustering with the euclidean distance as classification factor. Each signature is normalized before the clustering. Figure 4.12a shows a of the three main event clusters and the five outliers. of the three main event clusters and the five outliers. Their variation across the hydrological signatures is given in Figure4.12b The outliers 1 (1940), 2 (1909) and 3 (1956) are characterized by high rising slope ΔQ_{rise} and also moderate to high discharge peak, while outliers 4 (1988) and 5 (1937) are associated with high baseflow index, long duration and overall volume. With reference to the events' median DET, three of these outliers are within the lowest five, except events 1988 and 1937 with median DET are ranked 11^{th} and 12^{th} respectively.

Despite the close characteristics of these 1988 and 1937 events from their conventional signatures and hence combined into a cluster, their hydrographs look visibly dissimilar. The reason of such misleading similarity assessment lies on the calculation of certain index instead of the clustering method. For instance ΔQ_{rise}, where the existence of several sub-events and hence variation of magnitudes before the flood peak enlarges the uncertainty of the slope value as it is averaged by a slope of single line drawn from the starts of events to their peaks. In contrast, the CRP between these 2 hydrographs show hardly any clear diagonal lines and very low DET value indicating dissimilarity (see Fig.4.13).

4.4 Conclusions

Based on the concept of Recurrence Plots, we propose a novel hydrograph similarity measure. The event runoff dynamics is characterized by its continuous time sequence, i.e. the entire hydrograph shape is represented as phase space trajectory. Since the phase space vector is reconstructed using multidimensional time delay embedding, each point of the phase space trajectory contains the relation of several points in time within the event hydrograph, including for example, the initial flow conditions caused by antecedent rainfall. The phase space vectors of two events are then analyzed and compared directly for their similarity using Cross Recurrence Plots instead of being summarized as an index first before comparison. Thereafter the resulted CRPs are summarized using one of the Recurrence Quantification Analysis measures called determinism (DET).

The closest concept to this similarity assessment using CRP and DET is a scatter plot between two time series and its correlation coefficient. The comparison between these two concepts demonstrates the benefit of the proposed method. In contrast to scatter plots and correlation analysis, the CRP-based method allows comparing time series of different duration, and it detects similar or identical signals that are shifted in time. In contrast to correlation analysis, CRP is not limited to monotonic , linear relations and the time when similar patterns occur, i.e. as long as both trajectories are common. The most important benefit stems, however, from the fundamentally different approach of

the CRP-based method to quantify similarity based on the multi-dimensional relation of different magnitudes in time within an event.

We further provide recommendations how to parameterize CRP. This includes the adaptation of a method recently proposed by Wendi et al. (2018) to properly select the time delay and embedding dimension to prevent artifacts in the analysis. This suggests the use of measure called *DET* distance to evaluate the safety of an embedding parameter set within an acceptable embedding loss (i.e. $\leq 10\%$ of hydrograph length). The choice of embedding dimension (m) can be subjective as well to the user's requirements, such as how complex should each vector in the phase space represent, e.g. to include the implications of a minimum number of antecedents conditions. For instance, a vector in a 4 dimensional phase space can describe the relationship between flood peak discharge and 3 other prior discharge values i.e. at τ, 2τ, and 3τ earlier. From our experience with the application example, we noticed that hydrographs with longer durations and multi-peaks generally require higher embedding dimension to attain maximum *DET* distance. We also suggest the use of the local minima method with a phase distance threshold [Schultz et al., 2011, Wendi and Marwan, 2018a] to define the recurrence points for a more robust CRP, i.e. which is less dependent on the threshold ε and avoid thick lines artifacts.

In the application example, we show that through inter-comparing every flood hydrograph in a pairwise manner, we can evaluate whether an event is unusual in terms of its runoff dynamics as assessed using median values of their *DETs*. Interestingly, the two floods with the lowest median *DET*, suggesting the most unusual runoff dynamics, are events that are also described as unusual in the historical archives in terms of their flood generation processes. The double-peak 1940 flood contains an almost constant second peak for several days caused by blockage of the river due to ice debris. The second most unusual event, the 1909 flood, was caused by the superposition of very heavy rainfall on frozen ground. This rainfall can be described as unseasonal, as such high intensites are unusual in this season in the study catchment.

The comparison of the proposed hydrograph similarity measure with conventional hydrological signatures individually shows that each measure defines different events as unusual. This was expected as each measures puts the focus on different aspects when measuring similarity. The conventional hydrological signatures focus on particular components of the hydrograph or lump characteristics into an aggregate value. This provides a partial quantification of similarity only and may lead to wrong conclusions, for instance, by hiding specific hydrograph characteristics through the aggregation.Further, our example shows that multi-variate indices, which combine several hydrological signatures, can still mis-identify similar hydrographs. The cause of this mis-identication is the aggregation into a single value before the comparison.. Since the proposed measure compares phase space trajectories that builds on time delay embedding, and hence, directly compares the entire set of hydrograph magnitudes and their unique time sequence, we

argue that it provides a more comprehensive similarity measure

However, when working with real world observations, the presence of noise might cause the diagonal in CRP to be discontinuous and hence decreases the *DET* values or herein used as similarity index. Therefore, if noise presence is known to be prominent, user should consider noise reduction of the signal before conducting CRP analysis. In addition, unlike the comparison of using commonly signatures, the similarity index DET does not easily provide intuitive and specific meaning to the similarity found in the hydrograph. Besides, reference in the application of hydrology is not yet available

To our knowledge, this is the first application of (Cross) Recurrence Plots and Recurrence Quantification Analysis in catchment hydrology. We project these methods have a large application potential in hydrology. A straightforward extension would be to analyze longer periods, such as annual or seasonal hydrographs instead of just events, in order to evaluate if there has been a change in the hydrological regime over time. These methods could also be used to calibrate and validate hydrological and hydrodynamic simulation models, by applying them as measure to quantify the agreement between simulation results and observations.

Acknowledgments

This research was carried out within the Research Training Group "Natural Hazards and Risks in a Changing World" (NatRiskChange; GRK 2043/1) funded by the Deutsche Forschungsgemeinschaft (DFG).

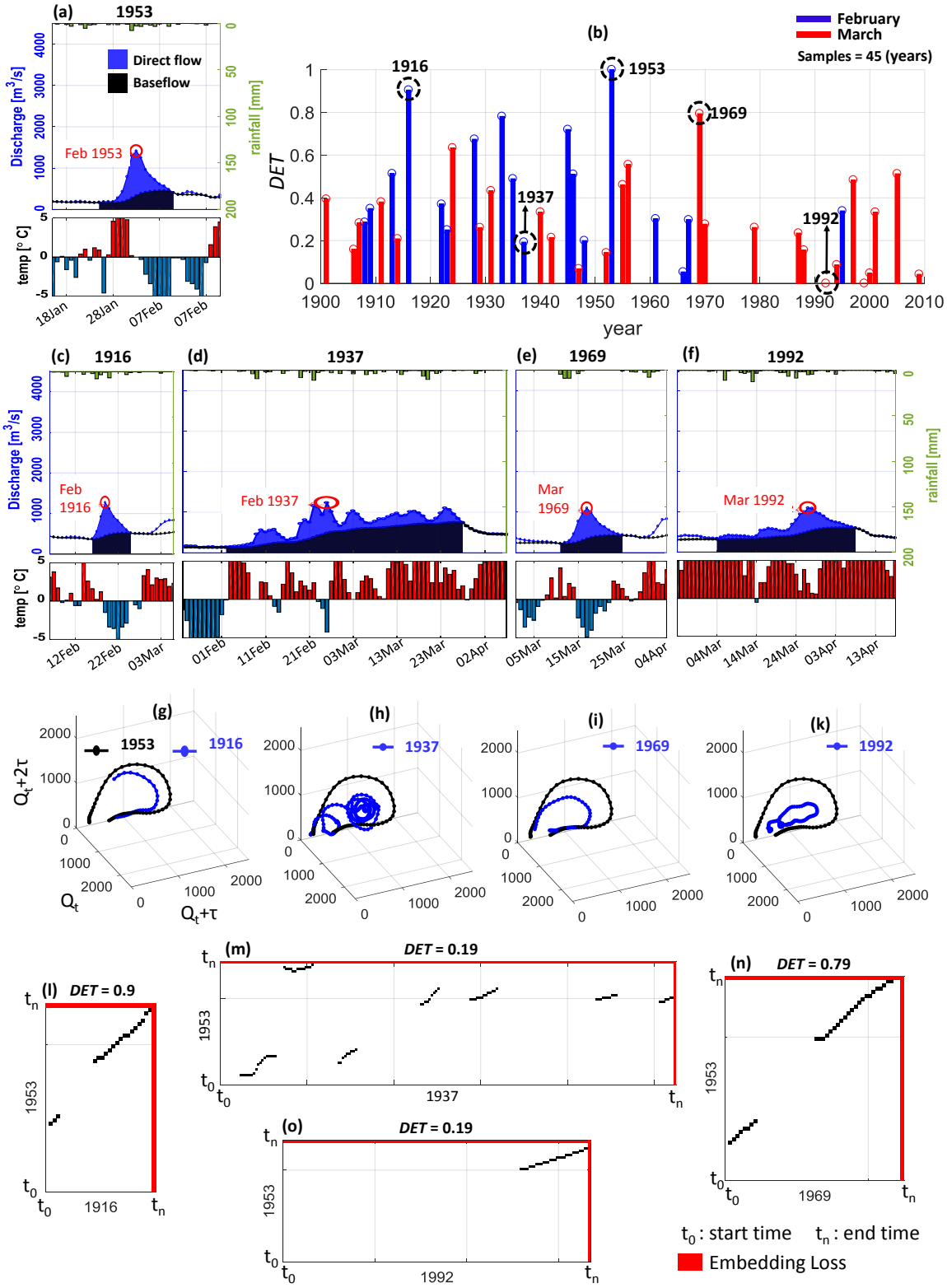

Figure 4.8: Comparing the February 1953 event to all other annual maxima that occurred in February and March. (a) Reference hydrograph 1953; (b) *DET* values resulting from the pairwise comparison; (c, e) example hydrographs with high *DET* values; (d, f) example hydrographs with low *DET* values; (g – k) phase space trajectories of the example hydrographs and the 1953 event; (l – o) CRP plots comparing 1953 to the example hydrographs. Note that the CRP grid are plotted with equal x and y tick axis distance of 10days

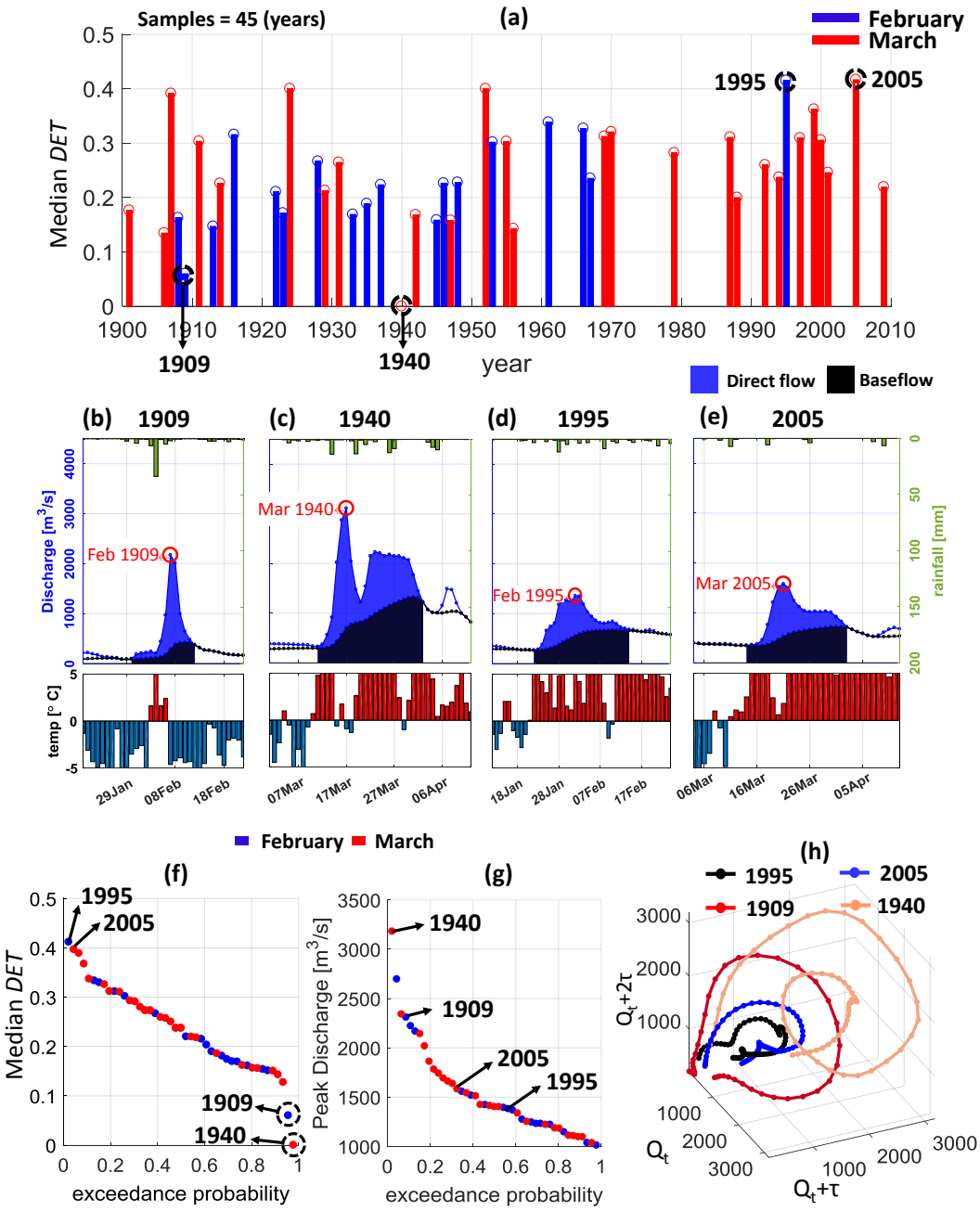

Figure 4.9: Intercomparison of all February and March flood hydrographs: (a) median *DET* values; (b, c) hydrographs of the two events with the lowest median *DET* values; (d, e) hydrographs of the two events with the highest *DET* values; (f – g) empirical distribution of peak discharge and median *DET* values; (h) phase space trajectories for the events with the two highest and lowest median *DET* values.

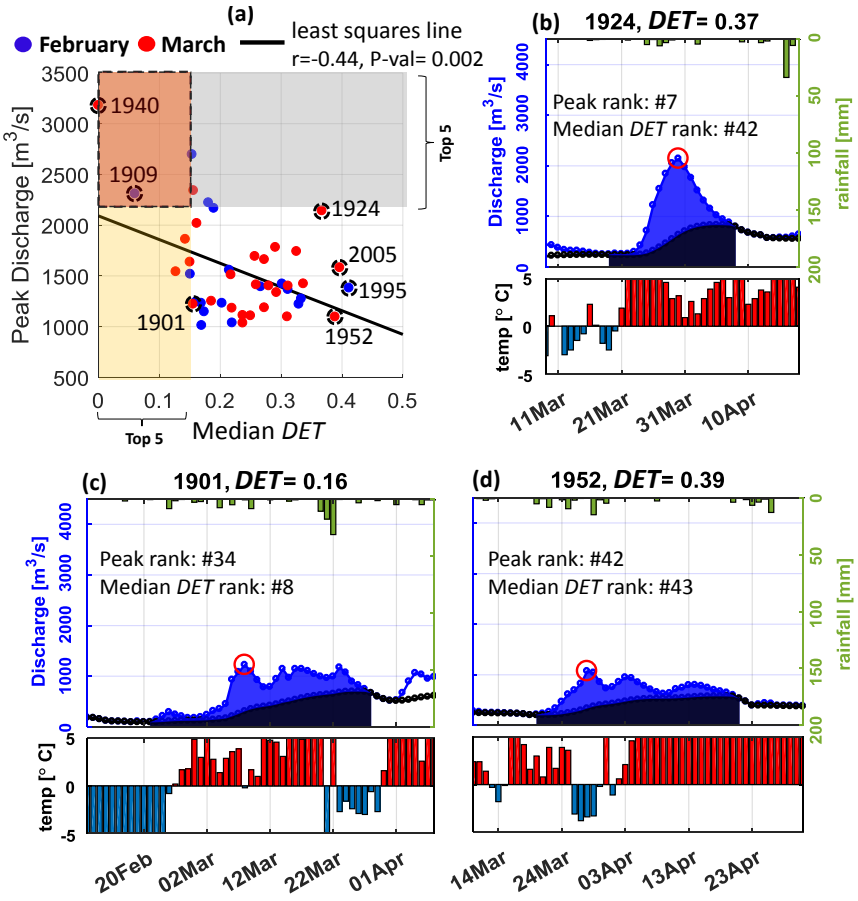

Figure 4.10: Relationship between flood peak discharge and median *DET* (a) with each top 5 of the index being shaded (grey: high discharge, yellow: low values of median *DET*, orange: overlap of both top 5). Three further examples of event hydrographs with common (b, d) and rare (c) runoff dynamics.

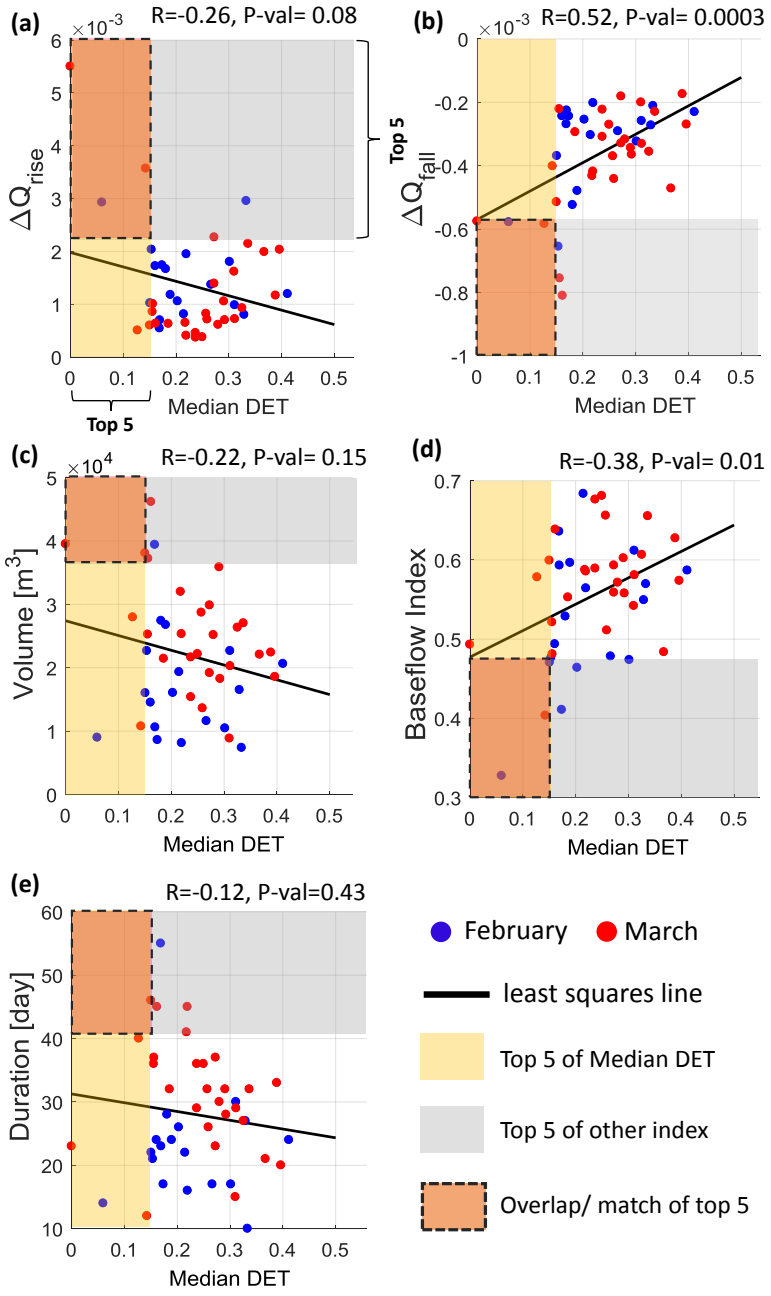

Figure 4.11: Scatterplots of hydrological signatures versus median *DET*: (a) rising slope ΔQ_{rise}, (b) falling slope ΔQ_{fall}, (c) event volume, (d) baseflow index BFI, (e) event duration. The shaded areas show the top 5 events for each signature index. In addition, the Pearson correlation coefficient R and the P-value are given.

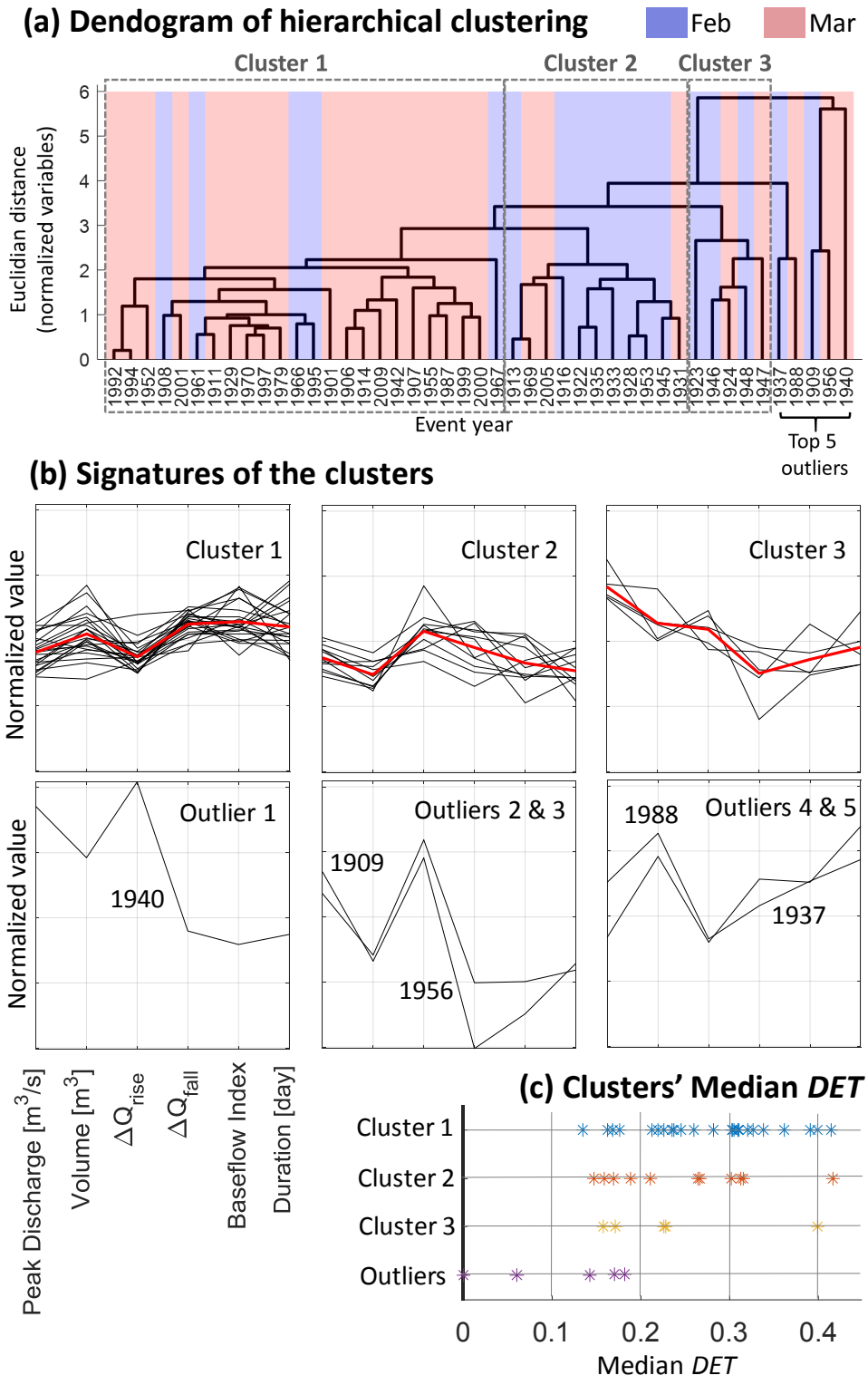

Figure 4.12: Clusters of events by considering the joint-indices of their conventional signatures through hierarchical clustering method with euclidean distance. (a) Dendogram of the hierarchical clusters and the considered outliers, (b) Signatures of each cluster and the outliers, (c) Median *DET* values of the clusters and outliers

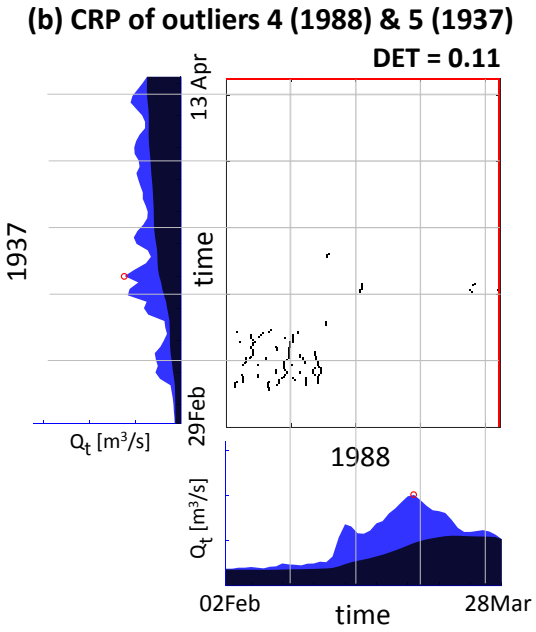

Figure 4.13: CRP between the cluster of outlier 4 (year 1988) and 5 (year 1937)

5 Synthesis and Conclusions

In the following, the main findings and conclusions based on the formulated specific research questions are summarized and discussed according to the topical structure presented in Fig. 1.6 of the introduction chapter.

5.1 Phase Space Reconstruction & Parameterization

The main research done in this topic is presented in Chapter 2 of the thesis and also published as [Wendi et al., 2018].

RQ-2. How to determine a safe parameters set when creating a phase space trajectory using time delay embedding?

Artifacts can result as a wrong parameterization of time delay embedding (i.e. m and τ) when reconstructing a phase space trajectory, and therefore misleads an RP and RQA. An example is when a stochastic or a random signal that should result in zero or very low DET in an RQA, show a contrary high DET value, and therefore imply a deterministic feature (i.e. being predictable). This artifacts are shown in the RP as dominant clear and defined diagonal lines instead of the expected scattered singular points. With regards to the mentioned artifacts, the study in Chapter 2 proposes a practical and easy to use approach to evaluate if a embedding parameters set used to reconstruct phase space trajectory is safe from artifact or not. This approach exploits a sequence shuffling technique that destroys the original information contained in the applied signal or time series, and convert the signal into a stochastic series. In order to evaluate the parameters set, a measure called *median DET Distance* that varies from 0 to 1, obtained by calculating the median of differences between the original deterministic signal DET and the numerously shuffled version of the signal. The larger the *median DET Distance*, i.e. the closer to 1, the safer the parameter set is to avoid potential artifacts. Sets of parameters that exhibit high *median DET Distance* can be inferred to as artifact-safe region, and can be used alongside with standard approaches such as FNN and and MI to derive an optimal parameters set. Although not discussed in Chapter 2, this method is also applicable when using CRP, a variation of RP which compares two phase space trajectories. Similar to the concept of RP, when comparing two identical signal using CRP, the resulted DET should be 1, and if the two signals are of completely different dynamics then DET should be 0. By shuffling only one of the two series, we ensure that both signal dynamics are different, therefore

the CRP analysis should result in 0 or a very low *DET*. The *median DET Distance* corresponding to a certain parameter sets can then be calculated by numerously shuffling one of the identical signals. Matrix of *median DET Distance* can therefore be constructed for different combination sets of parameters (i.e. m and τ). From this matrix, the user is provided with options and bounds of artifact-safe parameters sets corresponding to high *median DET Distance* values. However, the user should also be cautioned that high values of parameters could result in embedding loss and therefore the resulting RP is no longer reliable. The method is both tested for synthetic data and real observation i.e. runoff series and shown to be effective. Therefore, this parameterization tool can also be used for other signals or time series. Noise however, needs to be taken care of, when using such method as it decreases the robustness of the parameters, and in general when using RP and RQA measures. RP and RQA sensitivity to noise then became the focal point of the Chapter 3 and summarized in the next main finding.

5.2 Robustness of RP and RQA for Observation Data

The main research done in this topic is presented in Chapter 3 of the thesis, and also published as Wendi and Marwan [2018b].

RQ-3. How to define a threshold for similar runoff dynamics in order to properly construct an RP and what are the pitfalls to avoid?

When constructing an RP, a reliable distance threshold is required to define similar phase space trajectories. This parameter can also introduce artifacts when it is not defined properly, such that unnecessary thick lines and lumps of recurrence points can occur in the RP, and cause the corresponding RQA to be unreliable. Such thick lines for instance artificially introduces more diagonal lines and hence a misleadingly increase the *DET* value. Furthermore, additional points in the lumps of recurrence points can also decrease the *DET* value, while these lumps could artificially form other structures like horizontal or vertical lines that mislead other RQAs. To overcome these artifacts, the study in Chapter 3 proposes and recommends constructing an RP using an improved version of the original local minima (LM) approach bySchultz et al. [2011] with additional parameters called LM2P. The LM2P is shown to be superior over the LM approach that the RP becomes less sensitive to the choice of the threshold parameter, and could avoid the mentioned artifacts caused by artificial thick lines and lumps of recurrence points. This is also applicable to the CRP as introduced in Chapter 4 of the study.

RQ-4. Are the current RP and RQA methods robust for noise-present observational series and how to improve its robustness to prevent artifacts?

However, despite the resolved artifacts of thick lines and block structures in the RP, a problem persists when analyzing noisy signal, such as the disrupted and deviated diagonal lines in the RP. To take on this challenge, an extended RQA approach for accounting disrupted and deviated diagonal lines is proposed with the use of sliding diagonal window when quantifying the characteristics of RP. This sliding diagonal window is defined with minimal window size to tolerate the mentioned deviated diagonal lines and considers the gaps in the disrupted lines. In particular, this approach provides an alternative measure for determinism, and called $DDET$ that is effective to analyze noisy signals.

Throughout extensive test sets of Lorenz chaotic series (for varying parameter ρ from 80 to 110), unlike the conventional DET, this new measure is able to capture the deterministic property despite the induced noise, and clearly distinguishes the stochastic signals from the deterministic ones. Of course, provided that the signal to noise ratio (SNR) is within a reasonable range, for instance the SNR of 20dB is still shown to visibly capture the periodic characteristics of Lorenz series whereas the DET measure fails to do so.

This new approach is also shown to minimize the requirement of embedding dimension in contrast to the conventional approach, and therefore reduces the potential embedding loss. However, the range of $DDET$ values different to those of conventional DET measure that are more intuitive to interpret (between 0 and 1). Nevertheless, this extended version of RQA is concluded to be a promising concept when analyzing noisy signals. Due to the more extensive calculation approach, the complex parameters required by the additional sliding window, and the immaturity of this extended RP and RQA, I do not attempt to introduce this as yet to the hydrological application, especially when understanding to the simpler RP and RQA concept is yet to be established. Therefore, in the current stage, I would recommend the traditional approach of noise filtering technique [Elshorbagy et al., 2002] that is more intuitive to tackle the prominent noise presence in the time series.

Despite the application interest for the method is targeted towards analyzing streamflow dataset, the extended RP and RQA in Chapter 3 can also be adopted by other signals with similar characteristics, i.e. deterministic and continuous, with known issues of noise contamination.

5.3 Application for Hydrograph Similarity & Rare Flood Dynamics

The main research done in this topic is presented in Chapter 4 of the thesis, and also submitted for *Water Resources Research (WRR)* in Sept 2018.

RQ-1. What does phase space trajectory and time delay embedding mean for hydrological time series

As a fingerprint of the processes involved in the rainfall-runoff event, a hydrograph is a substantial proxy to distinguish the mechanism typology of a certain flood. However,

as the traditional hydrological signatures that describe hydrograph are quite limited to only contain partial characteristics, and its derivation method is known to lump several multi-peaks or sub-events characteristics within an event hydrograph, e.g. slopes. Therefore, I develop a method to consider a more elaborate characteristics of hydrographs when quantifying their similarity or dissimilarity, i.e. to envelope its temporal evolution or shape and referred to as runoff dynamics. To do so, similarity between two hydrographs can be quantified from the perspective of phase space trajectory. Trajectories that fall within a defined distance threshold can be considered to be similar. Moreover, Taken's time delay embedding allows a higher dimensional phase space trajectories to be reconstructed [Takens, 1981]. This means relationship of different and multiple magnitudes in time can be referred to as a vector in the phase space. This approach takes the temporal succession of discharge values into consideration, such that the impact of the initial conditions on the runoff events are considered as a characteristics vector in the multi-dimensional phase space. Therefore the reconstructed phase space now contains more information typical to a certain process of runoff generation, including the dependency of each discharge level to the others. As the phase space with dimension above 3 can no longer be directly visualized by human eyes, this study proposes the means of CRP and its RQA i.e. DET index to summarize the similarity between two trajectories.

RQ-5. How to apply RP and RQA to evaluate similar runoff dynamics between floods?

CRP as a variation of RP allows the comparisons of two hydrograph's runoff dynamics and therefore their similarity to be visualized by a 2-dimensional binary matrix, where the occurrence of clear diagonal lines in the plot is the indication of similar dynamics. In addition, the similarity structures (diagonal lines) in CRP can also be quantified by DET index as part of an RQA. This index ranges intuitively between 0 and 1 to indicate different dynamics to full similarity respectively. As to illustrate the concept of CRP, we demonstrated its difference to the widely used scatter plot and the cross correlation analysis using Pearson index (R). The strengths of CRP and DET as compared to scatter plot and R are their ability to detect similarity and the synchronization despite the different time of occurrence, i.e. when the compared identical hydrograph is shifted with time delay, and without the need of the two compared series sharing the same duration or length. In addition, CRP and DET are also shown to be superior when distinguishing two completely different dynamics.

RQ-6. How to adapt the method to evaluate a common or rare flood runoff dynamics?

The assessment of the pairwise hydrograph similarity can be extended to evaluate the rarity of each flood runoff dynamics by inter-comparing it to all other floods in the event

set or samples. This results in a DET matrix from all the CRPs of the pair-wise flood hydrographs, and can be summarized statistically, e.g., using median as an index of common or rare dynamics. In case the hydrograph shape and the relationship of difference discharge points in time are signatures of the underlying flood generation processes, then the *median* DET value is a good indication for unusual or rare flood typology related to the flood process mechanism.

RQ-7. What are the advantages of using such approach to quantify similar runoff dynamics, and how does it compare with other existing similarity index, e.g. hydrological signatures?

The comparison of the median DET with conventional hydrological signatures shows that each measure defines different events as unusual. This was expected as each measures puts the focus on different aspects when measuring similarity. As the conventional hydrological signatures focus on particular components of the hydrograph, the quantified similarity is therefore not a complete set of the event characteristics. Furthermore, as some of the signatures are derived as a statistical aggregate of a particular element, lets say the rising slope of multi peak hydrograph, they can lead to a wrong representation. The proposed measure on the other hand includes a more complete characteristics of the hydrograph, such as its continuous shape, and the complex relationship between each discharge magnitudes to the others in time. Therefore the approach account a temporal continuity of how a discharge evolve in time as a function of the catchment processes involved. Therefore, I argue that runoff dynamics and its similarity measure DET are better proxies to distinguish different flood typologies with regards to their process mechanism, and hence more reliable to detect rare flood processes.

RQ-8. What is the implication of rare runoff dynamics in its relation to causative mechanism?

The application example showed that events with low *median* DET values have hydrograph shapes that reoccur rarely within the event set, whereas high values suggest that these events have common hydrograph shapes. Interestingly, the two unusual flood described in the historical archives based on their generation processes, are captured by the measure of *median DET Distance*, i.e. being the two lowest, suggesting their most unusual runoff dynamics. The double-peak 1940 flood contains an almost constant second peak for several days caused by blockage of the river due to ice debris. The second most unusual event, the 1909 flood, was caused by the superposition of very heavy rainfall on frozen ground. This rainfall can be described as unseasonal, as such high intensities are unusual in this season in the study catchment.

However, validation with historical archive is not an easy task, as they are not easily available especially when the even happened more than decades ago. In addition, such

archive is also expected to document only events with prominent flood peaks or water levels, and hence reduces the availability of validation sets. Although other datasets like meteorological conditions e.g. precipitation and temperature can be beneficial to infer some mechanism of the flood events, they could only offer the perspective from the meteorological forcings. Besides, deriving catchment rainfall information for instance is subject to large spatial uncertainty especially when the density of rainfall gauges is low to represent spatial variations. Although, physically based flood model would arguably be the better option to simulate change of a flood process mechanism, a meso- and above scale study requires extensive resources of dataset and computation to consider the full interaction of different runoff generating parameters from the atmosphere to catchment and the river in space and time. Their complex data inputs and parameters are also subject to uncertainties. In contrast, the proposed approach and measures in this study, require only streamflow series as proxy to learn about changes in flood processes and therefore of a minimal resource requirement.

It should be noted as well that although the study argues that the consideration of runoff dynamics in phase space for the quantification of rarity is more superior to using conventional hydrological indices extracted from a hydrograph, the conventional indices are more intuitive to describe the unusual characteristics of the flood. For instance, a steep rising slope of the hydrograph is related to the fast response time of the catchment, and the constituent of the discharge are mainly surface or direct runoff. Therefore, I would recommend the consideration of runoff dynamics alongside all the other hydrological signatures to provide a better picture for the analysis of rare or unusual flood.

6 Outlook

To our knowledge, this is the first application of (Cross) Recurrence Plots and Recurrence Quantification Analysis in hydrology. We believe that these methods have a large application potential in hydrology. As the main motivation behind this method development was to analyze the change in flood dynamics with a more specific questions that if we experience more or less rare flood typology with regards to its runoff dynamics and hence possible attribution of change to climate, landuse, and river alteration, a wider extent of the analysis could be of substantial interest. A straightforward extension would be to analyze longer periods, such as annual or seasonal hydrographs instead of events, in order to evaluate if there has been a change in the general hydrological regime over time instead of just flood dynamics.

Flood change in German catchments for instance is a future study interest. Along with the reported increase of overall precipitation especially the increase rainfall intensity during winter, runoff dynamics is expected to have changed, especially in term of the seasonality of with respect to event typologies. As the use of RP and RQA measures offer a more comprehensive characteristics of runoff processes being captured in the analysis, they might be able to provide additional insight that reflects the change in hydrological processes in relation to the changes of the land use and river as well. The Elbe catchment for instance, IKSE [2005] has shown an extensive dam development upstream of the catchment especially after 1950 in the parts of Czech Republic (see in Fig. 6.1). Therefore, the impact of such development towards the change of flood dynamics downstream, e.g. Dresden, might be observable from the available dataset period and is therefore a substantial research interest.

In addition, RP and RQA could also be used to calibrate and validate hydrological and hydrodynamic simulation models, by applying them as a measure to quantify the agreement between simulation results and observations to be more representative towards the rainfall runoff generation dynamics. In addition, the runoff dynamics similarity index can also be used as an or additional objective function. This is especially when source of model parameters uncertainty is related to the performance criteria used to evaluate and calibrate the model. The commonly objective functions range from the usual root mean squared error ($RMSE$), coefficient of determination (r^2), peak error, to a more elaborated one like Nash Sutcliffe index/ efficiency (NSE), and Kling-Gupta efficiency (KGE) as modified version of NSE. However, these objective functions are also known to have their shortcomings. For instance, Gupta et al. [2009] mentioned that a maximized

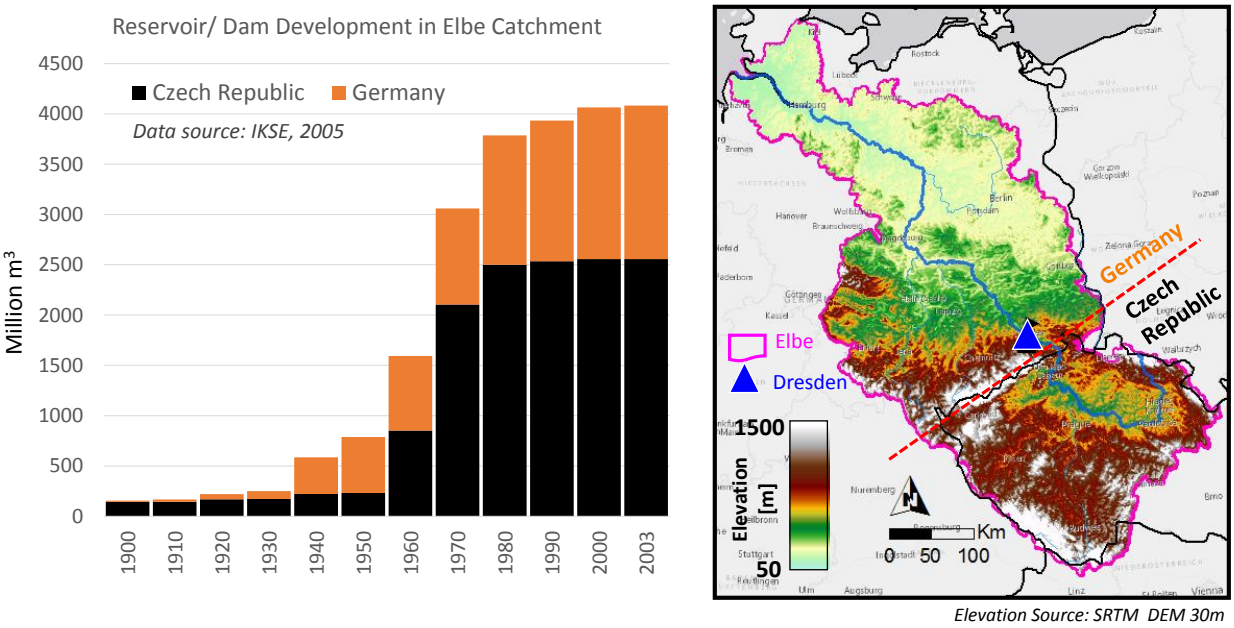

Figure 6.1: Development of Dam/ Reservoir in the Elbe Catchment from 1900-2003 with the contribution from Germany and Czech Republic, with data sourced from IKSE [2005]

NSE compromises variability and both NSE and KGE tend to underestimate peak runoff. Furthermore, these indices are mostly designed to evaluate an aggregated error with regards to their overall magnitude. Despite the advancement of multi-criteria calibration approach, the specific physically meaningful hydrograph shape accuracy might still be compromised. Therefore, by using the a more elaborate index such as *DET*, a more physical process representative model and the underlying parameters can be expected. This however requires further analysis and test cases to confirm the assumption. This performance indicator can also be compared with those of the recent advancements, such as the *series distance metric* developed by Ehret and Zehe [2011], where similarity in terms of occurrence, amplitude and timing of hydrological events can be captured.

Furthermore, the series of artifact-safe parameterization framework and the extended RP and RQA are not necessarily applicable just for discharge dataset. Other signals or observation series of the same kind of dynamics, i.e., continuous and deterministic, can also adopt these developed approach to avoid pitfalls in using RPs and RQA.

Bibliography

Marco A. Aceves-Fernandez., Juan M. Ramos-Arreguín, J. Carlos Pedraza-Ortega, Artemio Sotomayor-Olmedo., and Saúl Tovar-Arriaga. Finding Trends of Airborne Harmful Pollutants by Using Recurrence Quantification Analysis. *American Journal of Environmental Engineering*, 1(1):10–14, aug 2012. ISSN 2166-4633. doi: 10.5923/j.ajee.20110101.02. URL http://article.sapub.org/10.5923.j.ajee.20110101.02.html.

A. Bárdossy. Calibration of hydrological model parameters for ungauged catchments. *Hydrology and Earth System Sciences*, 3(3):1105–1124, 2006. ISSN 1607-7938. doi: 10.5194/hess-11-703-2007. URL https://www.hydrol-earth-syst-sci.net/11/703/2007/.

Günter Blöschl, Murugesu Sivapalan, Thorsten Wagener, Alberto Viglione, and Hubert Savenije. *Runoff prediction in ungauged basins: Synthesis across processes, places and scales*. Cambridge University Press, Cambridge, 2011. ISBN 9781139235761. doi: 10.1017/CBO9781139235761. URL http://ebooks.cambridge.org/ref/id/CBO9781139235761.

BMU/ BfN. Auenzustandsbericht: Flussauen in Deutschland. Technical report, Berlin, 2009. URL https://www.bfn.de/fileadmin/MDB/documents/themen/wasser/Auenzustandsbericht.pdf.

Helge Bormann, Nicholas Pinter, and Simon Elfert. Hydrological signatures of flood trends on German rivers: Flood frequencies, flood heights and specific stages. *Journal of Hydrology*, 404(1-2):50–66, jun 2011. ISSN 0022-1694. doi: 10.1016/J.JHYDROL.2011.04.019. URL https://www.sciencedirect.com/science/article/pii/S0022169411002605.

W. C. Boughton. A hydrograph-based model for estimating the water yield of ungauged catchments. In *Hydrology and Water Resources Symposium: Towards the 21st Century*, 1993.

Guy P. Brasseur, Daniela Jacob, and Susanne Schuck-Zoeller. *Klimawandel in Deutschland - Entwicklung, Folgen, Risiken und Perspektiven*, volume 51. Springer, 2017. ISBN 978-3-662-50396-6. doi: 10.1002/ciuz.201790001.

Axel Bronstert, A. Bárdossy, C. Bismuth, H. Buiteveld, M. Disse, H. Engel, U. Fritsch, Y. Hundecha, R. Lammersen, D. Niehoff, and N. Ritter. Multi-scale modelling of

land-use change and river training effects on floods in the Rhine basin. *River Research and Applications*, 23(10):1102–1125, 2007. ISSN 15351459. doi: 10.1002/rra.1036. URL www.interscience.wiley.com.

Manuela I. Brunner, Daniel Viviroli, Anna E. Sikorska, Olivier Vannier, Anne-Catherine Favre, and Jan Seibert. Flood type specific construction of synthetic design hydrographs. *Water Resources Research*, 53(2):1390–1406, feb 2017. ISSN 00431397. doi: 10.1002/2016WR019535. URL http://doi.wiley.com/10.1002/2016WR019535.

Th. Buzug and G. Pfister. Comparison of algorithms calculating optimal embedding parameters for delay time coordinates. *Physica D: Nonlinear Phenomena*, 58(1-4): 127–137, sep 1992. ISSN 01672789. doi: 10.1016/0167-2789(92)90104-U. URL http://linkinghub.elsevier.com/retrieve/pii/016727899290104U.

Simona Carrubba, Clifton Frilot, Andrew L. Chesson, and Andrew A. Marino. Mobile-phone pulse triggers evoked potentials. *Neuroscience Letters*, 469(1):164–168, jan 2010. ISSN 0304-3940. doi: 10.1016/J.NEULET.2009.11.068. URL http://www.sciencedirect.com/science/article/pii/S0304394009015596?via{%}3Dihub.

P M Crowley. Analyzing convergence and synchronicity of business and growth cycles in the euro area using cross recurrence plots. *European Physical Journal – Special Topics*, 164(1):67–84, 2008. doi: 10.1140/epjst/e2008-00835-3.

J.-P. Eckmann, S Oliffson Kamphorst, D Ruelle, S Oliffson Kamphorst, and D Ruelle. Recurrence Plots of Dynamical Systems. *EPL (Europhysics Letters)*, 4(9):973, 1987. URL http://stacks.iop.org/0295-5075/4/i=9/a=004http://iopscience.iop.org/0295-5075/4/9/004.

U. Ehret and E. Zehe. Series distance – an intuitive metric to quantify hydrograph similarity in terms of occurrence, amplitude and timing of hydrological events. *Hydrology and Earth System Sciences*, 15(3):877–896, mar 2011. ISSN 1607-7938. doi: 10.5194/hess-15-877-2011. URL http://www.hydrol-earth-syst-sci.net/15/877/2011/.

A. Elshorbagy, S.P. Simonovic, and U.S. Panu. Noise reduction in chaotic hydrologic time series: facts and doubts. *Journal of Hydrology*, 256(3-4):147–165, jan 2002. ISSN 0022-1694. doi: 10.1016/S0022-1694(01)00534-0. URL https://www.sciencedirect.com/science/article/pii/S0022169401005340.

D Eroglu, F H McRobie, I Ozken, T Stemler, K.-H. Wyrwoll, S F M Breitenbach, N Marwan, and J Kurths. See-saw relationship of the Holocene East Asian-Australian summer monsoon. *Nature Communications*, 7:12929, 2016. doi: 10.1038/ncomms12929.

European Commission. In-depth Reports: Soil Sealing. Technical report, European Comission, 2012. URL http://ec.europa.eu/environment/archives/soil/pdf/sealing/SoilSealingIn-depthReportMarchversion{_}final.pdf.

Federal Ministry of Food Agriculture and Consumer Protection (BMELV). German forests - Nature and economic factor. Technical report, Bonn, Germany, 2011. URL https://www.bmel.de/SharedDocs/Downloads/EN/Publications/GermanForests.pdf?{_}{_}blob=publicationFile.

Klaus Follner, Thomas Ehlert, and Bernd Neukirchen. The status report on German floodplains. *Proceeding of 38th IAD Conference*, 2010. URL https://www.bfn.de/fileadmin/MDB/documents/themen/wasser/Follner{_}etalAbstractIADconference.pdf.

Andrew M. Fraser and Harry L. Swinney. Independent coordinates for strange attractors from mutual information. *Physical Review A*, 33(2):1134–1140, feb 1986. ISSN 0556-2791. doi: 10.1103/PhysRevA.33.1134. URL http://link.aps.org/doi/10.1103/PhysRevA.33.1134.

L. Gaál, J. Szolgay, S. Kohnová, K. Hlavčová, J. Parajka, A. Viglione, R. Merz, and G. Blöschl. Dependence between flood peaks and volumes: a case study on climate and hydrological controls. *Hydrological Sciences Journal*, 60(6):968–984, 2015. ISSN 21503435. doi: 10.1080/02626667.2014.951361. URL https://www.tandfonline.com/doi/pdf/10.1080/02626667.2014.951361?needAccess=true.

Bedartha Goswami, Niklas Boers, Aljoscha Rheinwalt, Norbert Marwan, Jobst Heitzig, Sebastian F. M. Breitenbach, and Jürgen Kurths. Abrupt transitions in time series with uncertainties. *Nature Communications*, 9(1):48, dec 2018. ISSN 2041-1723. doi: 10.1038/s41467-017-02456-6. URL http://www.nature.com/articles/s41467-017-02456-6.

Hoshin V. Gupta, Harald Kling, Koray K. Yilmaz, and Guillermo F. Martinez. Decomposition of the mean squared error and NSE performance criteria: Implications for improving hydrological modelling. *Journal of Hydrology*, 377(1-2):80–91, oct 2009. ISSN 00221694. doi: 10.1016/j.jhydrol.2009.08.003. URL http://linkinghub.elsevier.com/retrieve/pii/S0022169409004843.

Ezra Haaf and Roland Barthel. An inter-comparison of similarity-based methods for organisation and classification of groundwater hydrographs. *Journal of Hydrology*, 559: 222–237, apr 2018. ISSN 0022-1694. doi: 10.1016/J.JHYDROL.2018.02.035. URL https://www.sciencedirect.com/science/article/pii/S0022169418301112{#}b0075.

J. Hall, B. Arheimer, M. Borga, R. Brázdil, P. Claps, A. Kiss, T. R. Kjeldsen, J. Kriaučiūnienė, Z. W. Kundzewicz, M. Lang, M. C. Llasat, N. Macdonald, N. McIntyre,

L. Mediero, B. Merz, R. Merz, P. Molnar, A. Montanari, C. Neuhold, J. Parajka, R. A. P. Perdigão, L. Plavcová, M. Rogger, J. L. Salinas, E. Sauquet, C. Schär, J. Szolgay, A. Viglione, G. Blöschl, R. Br??zdil, P. Claps, A. Kiss, T. R. Kjeldsen, J. Kriau??uniene, Z. W. Kundzewicz, M. Lang, M. C. Llasat, N. Macdonald, N. McIntyre, L. Mediero, B. Merz, R. Merz, P. Molnar, A. Montanari, C. Neuhold, J. Parajka, R. A P Perdig??o, L. Plavcov??, M. Rogger, J. L. Salinas, E. Sauquet, C. Sch??r, J. Szolgay, A. Viglione, and G. Bl??schl. Understanding flood regime changes in Europe: a state-of-the-art assessment. *Hydrology and Earth System Sciences*, 18(7):2735–2772, jul 2014. ISSN 1607-7938. doi: 10.5194/hess-18-2735-2014. URL http://www.hydrol-earth-syst-sci.net/18/2735/2014/.

David M. Hannah, Barnaby P. G. Smith, Angela M. Gurnell, and Glenn R. McGregor. An approach to hydrograph classification. *Hydrological Processes*, 14(2):317–338, feb 2000. ISSN 0885-6087. doi: 10.1002/(SICI)1099-1085(20000215)14:2<317::AID-HYP929>3.0.CO;2-T. URL http://doi.wiley.com/10.1002/{%}28SICI{%}291099-1085{%}2820000215{%}2914{%}3A2{%}3C317{%}3A{%}3AAID-HYP929{%}3E3.0.CO{%}3B2-T.

Neil M. Harris, Angela M. Gurnell, David M. Hannah, and Geoff E. Petts. Classification of river regimes: a context for hydroecology. *Hydrological Processes*, 14(16-17):2831–2848, nov 2000. ISSN 0885-6087. doi: 10.1002/1099-1085(200011/12)14:16/17<2831::AID-HYP122>3.0.CO;2-O. URL http://doi.wiley.com/10.1002/1099-1085{%}28200011/12{%}2914{%}3A16/17{%}3C2831{%}3A{%}3AAID-HYP122{%}3E3.0.CO{%}3B2-O.

F F Hattermann, S Huang, O Burghoff, W Willems, H Österle, M Büchner, and Z Kundzewicz. Modelling flood damages under climate change conditions – a case study for Germany. *Nat. Hazards Earth Syst. Sci*, 14:3151–3169, 2014. doi: 10.5194/nhess-14-3151-2014. URL www.nat-hazards-earth-syst-sci.net/14/3151/2014/.

M Hrachowitz, H H G Savenije, G Blöschl, J J Mcdonnell, M Sivapalan, J W Pomeroy, B Arheimer, T Blume, M P Clark, U Ehret, F Fenicia, J E Freer, A Gelfan, H V Gupta, D A Hughes, R W Hut, A Montanari, S Pande, D Tetzlaff, P A Troch, S Uhlenbrook, T Wagener, H C Winsemius, R A Woods, E Zehe, C Cudennec, and H G Savenije. A decade of Predictions in Ungauged Basins (PUB)-a review. *Hydrological Sciences Journal*, 58(6):1198–1255, 2013. ISSN 2150-3435. doi: 10.1080/02626667.2013.803183. URL http://www.tandfonline.com/action/journalInformation?journalCode=thsj20.

IKSE. Die Elbe und ihr Einzugsgebiet: ein geographisch-hydrologischer und wasserwirtschaftlicher Überblick. Technical report, Internationale Kommission zum Schutz der Elbe, 2005.

Holger Kantz and Thomas. Schreiber. Nonlinear Time Series Analysis. *Technometrics*, 47(3):381–381, 2005. ISSN 0040-1706. doi: 10.1198/tech.2005.s306. URL `http://www.tandfonline.com/doi/abs/10.1198/tech.2005.s306`.

Matthew B. Kennel, Reggie Brown, and Henry D. I. Abarbanel. Determining embedding dimension for phase-space reconstruction using a geometrical construction. *Physical Review A*, 45(6):3403–3411, mar 1992. ISSN 1050-2947. doi: 10.1103/PhysRevA.45.3403. URL `http://link.aps.org/doi/10.1103/PhysRevA.45.3403`.

K H Krämer, R V Donner, J Heitzig, and N Marwan. Recurrence threshold selection for obtaining robust recurrence characteristics in different embedding dimensions. *Chaos*, 28(8):085720, 2018. ISSN 1054-1500. doi: 10.1063/1.5024914.

Edward N. Lorenz. Deterministic nonperiodic flow. *Journal of the Atmospheric Sciences*, 20(March 1963):130–141, 1963. URL `http://dx.doi.org/10.1175/1520-0469(1963)020{%}3C0130:DNF{%}3E2.0.CO;2http://dx.doi.org/10.1175/1520-0469(1963)020{%}7B{%}25{%}7D3C0130:DNF{%}7B{%}25{%}7D3E2.0.CO;2`.

Otache Yusuf Martins, Mohammed Abubakar Sadeeq, and Isiguzo Edwin Ahaneku. Nonlinear Deterministic Chaos in Benue River Flow Daily Time Sequence. *Journal of Water Resource and Protection*, 3:747–757, 2011. ISSN 1945-3094. doi: 10.4236/jwarp.2011.310085. URL `http://www.scirp.org/journal/jwarp`.

N Marwan and A Meinke. Extended recurrence plot analysis and its application to ERP data. *International Journal of Bifurcation and Chaos*, 14(2):761–771, feb 2004. doi: 10.1142/S0218127404009454.

N. Marwan, M. Thiel, and N. R. Nowaczyk. Cross Recurrence Plot Based Synchronization of Time Series. *Nonlinear Processes in Geophysics*, 9(3/4):325–331, 2002a. ISSN 1607-7946. doi: 10.5194/npg-9-325-2002. URL `https://www.nonlin-processes-geophys.net/9/325/2002/npg-9-325-2002.pdfhttp://www.nonlin-processes-geophys.net/9/325/2002/`.

N Marwan, N Wessel, U Meyerfeldt, A Schirdewan, and J Kurths. Recurrence Plot Based Measures of Complexity and its Application to Heart Rate Variability Data. *Physical Review E*, 66(2):26702, 2002b. doi: 10.1103/PhysRevE.66.026702.

NORBERT Marwan. How to avoid potential pitfalls in recurrence plot based data analysis. *International Journal of Bifurcation and Chaos*, 21(04):1003–1017, jul 2010. ISSN 0218-1274. doi: 10.1142/S0218127411029008. URL `http://arxiv.org/abs/1007.2215http://dx.doi.org/10.1142/S0218127411029008http://arxiv.org/abs/1007.2215{%}0Ahttp://dx.doi.org/10.1142/S0218127411029008http://www.worldscientific.com/doi/abs/10.1142/S0218127411029008`.

Norbert Marwan, M. Carmen Romano, Marco Thiel, and Juergen Kurths. Recurrence plots for the analysis of complex systems. *Physics Reports*, 438(5-6):237–329, jan 2007. ISSN 03701573. doi: 10.1016/j.physrep.2006.11.001. URL `http://linkinghub.elsevier.com/retrieve/pii/S0370157306004066`.

Bettina Matti, Helen E Dahlke, | Bastien Dieppois, Damian M Lawler, and Steve W Lyon. Flood seasonality across Scandinavia-Evidence of a shifting hydrograph? 2017. doi: 10.1002/hyp.11365. URL `https://onlinelibrary.wiley.com/doi/pdf/10.1002/hyp.11365`.

R. Merz and G. Blöschl. A process typology of regional floods. *Water Resources Research*, 39(12), dec 2003. ISSN 00431397. doi: 10.1029/2002WR001952. URL `http://doi.wiley.com/10.1029/2002WR001952`.

Manuela Nied, Kai Schröter, Stefan Lüdtke, Viet Dung Nguyen, and Bruno Merz. What are the hydro-meteorological controls on flood characteristics? *Journal of Hydrology*, 545:310–326, feb 2017. ISSN 0022-1694. doi: 10.1016/J.JHYDROL.2016.12.003. URL `https://www.sciencedirect.com/science/article/pii/S0022169416307922`.

S Oberst and J C S Lai. Nonlinear transient and chaotic interactions in disc brake squeal. *Journal of Sound and Vibration*, 342:272–289, 2015. doi: 10.1016/j.jsv.2015.01.005.

Ugur Ozturk, Dadiyorto Wendi, Irene Crisologo, Adrian Riemer, Ankit Agarwal, Kristin Vogel, José Andrés López-Tarazón, and Oliver Korup. Rare flash floods and debris flows in southern Germany. *Science of The Total Environment*, 626:941–952, jun 2018. ISSN 0048-9697. doi: 10.1016/J.SCITOTENV.2018.01.172. URL `https://www.sciencedirect.com/science/article/pii/S0048969718302109`.

N. H. Packard, J. P. Crutchfield, J. D. Farmer, and R. S. Shaw. Geometry from a Time Series. *Phys. Rev. Lett.*, 45(9):712–716, sep 1980. ISSN 00319007. doi: 10.1103/PhysRevLett.45.712. URL `http://link.aps.org/doi/10.1103/PhysRevLett.45.712`.

Murray C. Peel and Günter Blöschl. Hydrological modelling in a changing world. *Progress in Physical Geography*, 35(2):249–261, 2011. ISSN 0309-1333. doi: 10.1177/0309133311402550. URL `http://journals.sagepub.com/doi/10.1177/0309133311402550http://www.hydro.tuwien.ac.at/fileadmin/mediapool-hydro/Publikationen/bloeschl/2011{_}Peel{_}ppg.pdf`.

Th. Petrow, B. Merz, K.-E. Lindenschmidt, and A. H. Thieken. Aspects of seasonality and flood generating circulation patterns in a mountainous catchment in south-eastern

Germany. *Hydrology and Earth System Sciences*, 11(4):1455–1468, jul 2007. ISSN 1607-7938. doi: 10.5194/hess-11-1455-2007. URL http://www.hydrol-earth-syst-sci.net/11/1455/2007/.

Theresia Petrow and Bruno Merz. Trends in flood magnitude, frequency and seasonality in Germany in the period 1951-2002. *Journal of Hydrology*, 371(1-4):129–141, jun 2009. ISSN 00221694. doi: 10.1016/j.jhydrol.2009.03.024. URL http://www.sciencedirect.com/science/article/pii/S0022169409001917{#}fig2.

Amilcare Porporato and Luca Ridolfi. Nonlinear analysis of river flow time sequences. *Water Resources Research*, 33(6):1353–1367, jun 1997. ISSN 00431397. doi: 10.1029/96WR03535. URL http://doi.wiley.com/10.1029/96WR03535.

Klaus Röttcher and Mathias Deutsch. 100 Jahre Hochwasser 1909 – Was interessiert uns das heute noch? *Zeitschrift: WasserWirtschaft*, page 42/ 43, may 2009.

K. A. Sawicz, C. Kelleher, T. Wagener, P. Troch, M. Sivapalan, and G. Carrillo. Characterizing hydrologic change through catchment classification. *Hydrology and Earth System Sciences*, 18(1):273–285, jan 2014. ISSN 1607-7938. doi: 10.5194/hess-18-273-2014. URL http://www.hydrol-earth-syst-sci.net/18/273/2014/.

Alfred Schuh. *Eishochwasser an Oder und Elbe aus historischen und meteorologischen Gesichtspunkten und im Hinblick auf mögliche Gefährdungen*. PhD thesis, Brandenburgischen Technischen Universität Cottbus, 2011. URL https://opus4.kobv.de/opus4-btu/frontdoor/index/index/docId/2274.

Aaron P. Schultz, Yong Zou, Norbert Marwan, and Michael T. Turvey. Local Minima-Based Recurrence Plots for Continuous Dynamical Systems. *International Journal of Bifurcation and Chaos*, 21(04):1065–1075, apr 2011. ISSN 0218-1274. doi: 10.1142/S0218127411029045. URL http://www.worldscientific.com/doi/abs/10.1142/S0218127411029045.

B Sivakumar. Chaos theory in hydrology: important issues and interpretations. *Journal of Hydrology*, 227(1):1–20, 2000. ISSN 00221694. doi: 10.1016/S0022-1694(99)00186-9. URL http://www.sciencedirect.com/science/article/pii/S0022169499001869.

Colin Sparrow. *The Lorenz Equations: Bifurcations, Chaos, and Strange Attractors*, volume 41 of *Applied Mathematical Sciences*. Springer New York, New York, NY, 1982. ISBN 978-0-387-90775-8. doi: 10.1007/978-1-4612-5767-7. URL http://link.springer.com/10.1007/978-1-4612-5767-7.

Floris Takens. Detecting strange attractors in turbulence. In *Dynamical Systems and Turbulence, Warwick 1980, Lecture Notes in Mathematics, Volume 898. ISBN 978-3-540-11171-9. Springer-Verlag, 1981, p. 366*, volume 898, pages 366–381. 1981. ISBN

978-3-540-11171-9. doi: 10.1007/BFb0091924. URL http://link.springer.com/10.1007/BFb0091924.

Camille Ternynck, Mohamed Ali Ben Alaya, Fateh Chebana, Sophie Dabo-Niang, Taha B. M. J. Ouarda, Camille Ternynck, Mohamed Ali Ben Alaya, Fateh Chebana, Sophie Dabo-Niang, and Taha B. M. J. Ouarda. Streamflow Hydrograph Classification Using Functional Data Analysis. *Journal of Hydrometeorology*, 17(1):327–344, jan 2016. ISSN 1525-755X. doi: 10.1175/JHM-D-14-0200.1. URL http://journals.ametsoc.org/doi/10.1175/JHM-D-14-0200.1.

Marco Thiel, M. Carmen Romano, J??rgen Kurths, Riccardo Meucci, Enrico Allaria, and F. Tito Arecchi. Influence of observational noise on the recurrence quantification analysis. *Physica D: Nonlinear Phenomena*, 171(3):138–152, oct 2002. ISSN 01672789. doi: 10.1016/S0167-2789(02)00586-9. URL http://www.sciencedirect.com/science/article/pii/S0167278902005869.

L. L. Trulla, A. Giuliani, J. P. Zbilut, and C. L. Webber. Recurrence quantification analysis of the logistic equation with transients. *Physics Letters, Section A: General, Atomic and Solid State Physics*, 223(4):255–260, dec 1996. ISSN 03759601. doi: 10.1016/S0375-9601(96)00741-4. URL http://linkinghub.elsevier.com/retrieve/pii/S0375960196007414.

UBA/ UBA. Water Resource Management in Germany - Part 1 & 2. Technical report, Federal Ministry for the Environment, Nature Conservation and Nuclear Safety and Federal Environment Agency, Dessau-Roßlau, Germany, 2013. URL http://www.umweltbundesamt.de/sites/default/files/medien/publikation/long/3770.pdf.

K Vormoor, D Lawrence, M Heistermann, and A Bronstert. Climate change impacts on the seasonality and generation processes of floods-projections and uncertainties for catchments with mixed snowmelt/rainfall regimes. *Hydrol. Earth Syst. Sci*, 19:913–931, 2015. doi: 10.5194/hess-19-913-2015. URL www.hydrol-earth-syst-sci.net/19/913/2015/.

S Vorogushyn and B Merz. Flood trends along the Rhine: the role of river training. *Hydrol. Earth Syst. Sci*, 17:3871–3884, 2013. doi: 10.5194/hess-17-3871-2013. URL www.hydrol-earth-syst-sci.net/17/3871/2013/.

Dadiyorto Wendi and Norbert Marwan. Extended Recurrence Plot and Quantification for Noisy Continuous Dynamical Systems. *Chaos*, 28(8):085722, aug 2018a. ISSN 1054-1500. doi: 10.1063/1.5025485. URL http://aip.scitation.org/doi/10.1063/1.5025485.

Dadiyorto Wendi and Norbert Marwan. Extended recurrence plot and quantification for noisy continuous dynamical systems. *Chaos: An Interdisciplinary Journal of Nonlinear*

Science, 28(8):085722, aug 2018b. ISSN 1054-1500. doi: 10.1063/1.5025485. URL http://aip.scitation.org/doi/10.1063/1.5025485.

Dadiyorto Wendi, Norbert Marwan, and Bruno Merz. In Search of Determinism-Sensitive Region to Avoid Artefacts in Recurrence Plots. *International Journal of Bifurcation and Chaos*, 28(01):1850007, jan 2018. ISSN 0218-1274. doi: 10.1142/S0218127418500074. URL http://www.worldscientific.com/doi/abs/10.1142/S0218127418500074https://www.worldscientific.com/doi/pdf/10.1142/S0218127418500074.

I. K. Westerberg and H. K. McMillan. Uncertainty in hydrological signatures. *Hydrology and Earth System Sciences*, 19(9):3951–3968, sep 2015. ISSN 16077938. doi: 10.5194/hess-19-3951-2015. URL www.hydrol-earth-syst-sci.net/19/3951/2015/http://www.hydrol-earth-syst-sci.net/19/3951/2015/.

Ida K. Westerberg, Thorsten Wagener, Gemma Coxon, Hilary K. McMillan, Attilio Castellarin, Alberto Montanari, and Jim Freer. Uncertainty in hydrological signatures for gauged and ungauged catchments. *Water Resources Research*, 52(3):1847–1865, mar 2016. ISSN 00431397. doi: 10.1002/2015WR017635. URL http://doi.wiley.com/10.1002/2015WR017635.

Joseph P Zbilut and Charles L Webber. Embeddings and delays as derived from quantification of recurrence plots. *Physics Letters A*, 171:199–203, 1992. URL http://ac.els-cdn.com/037596019290426M/1-s2.0-037596019290426M-main.pdf?{_}tid=48a957c0-1953-11e7-bc5c-00000aab0f26{&}acdnat=1491323295{_}de10e55394d4a5f3f221977fd25abbc4http://ac.els-cdn.com/037596019290426M/1-s2.0-037596019290426M-main.pdf?{%}7B{_}{%}7Dtid=48a957c.

A Appendix for Chapter 2

A.1 Impact of the Recurrence Threshold

Figure A.1 describes the impact of recurrence threshold (i.e. recurrence rate) on the determinism distance between the original and all shuffled Lorenz time series. It can be seen that large recurrence threshold would lead the recurrence plot into artefact as implied by its low determinism distance (fig. A.1 b, c, e and f). Similarly when $\tau = 1$, $m > 1$, the increase of recurrence rate further decrease the determinism distance (fig. A.1 d). This confirms us to ignore the use of such parameter value regardless of the choice of recurrence threshold. However when $m = 1$, there is an increase of determinism distance i.e peaking at 20% recurrence rate and decreases thereafter (fig. A.1 d). Despite the increase, the determinism distance is still regarded low (i.e. below 0.5).

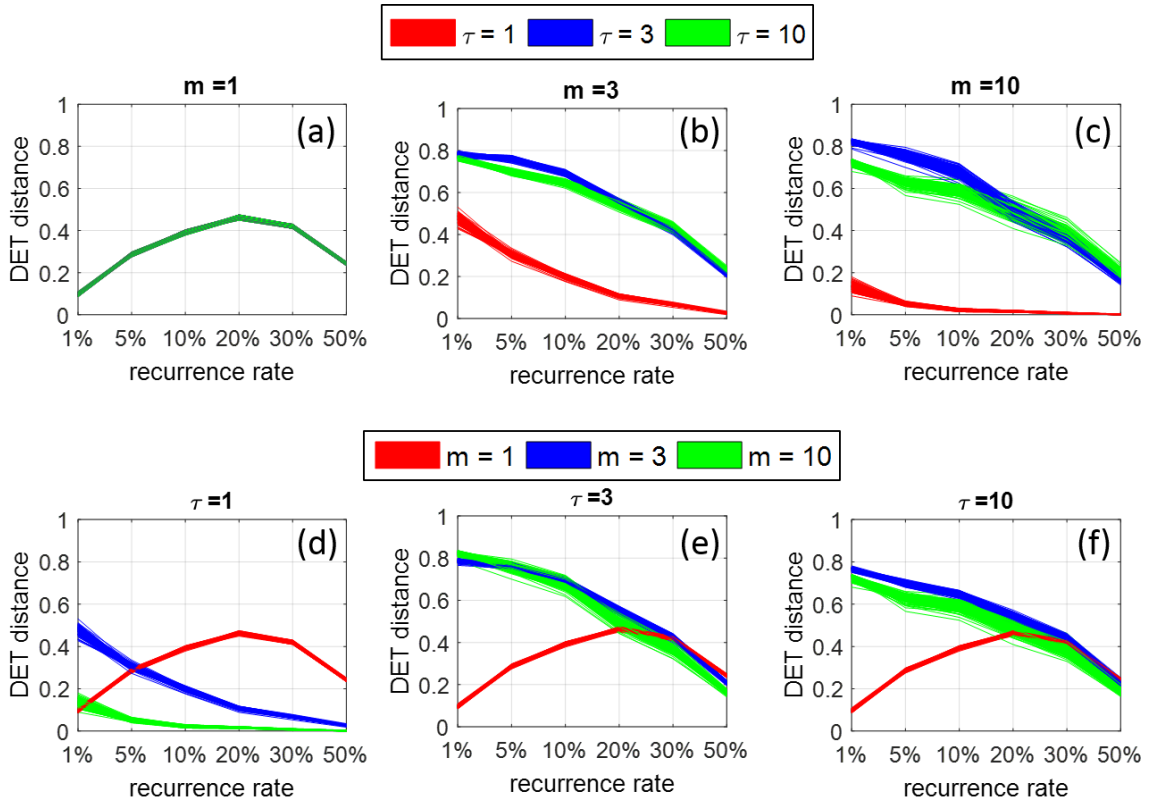

Figure A.1: Impact of recurrence threshold (i.e. recurrence rate) on determinism distances (100 shuffles) corresponding to different embedding parameters. Note: on sub-figure a, red and blue band lines are overlapped by green bands, hence not visible

Both original and shuffled time series experience increase of their DET values when recurrence rate is increased (fig. A.2 a, b, and c). However, when $m > 1$ the increase of DET values is rather sharp, changing significantly from low to high. The shuffled series recurrence plots with $m = 1$, and recurrence rate of 20% (i.e. at the peak of DET distance) still do not present any noteworthy deterministic features (fig. A.2 d, e, and f). In this case, users should avoid using large threshold values and special attention should be made on using such shuffling technique (i.e. when choosing $m = 1$).

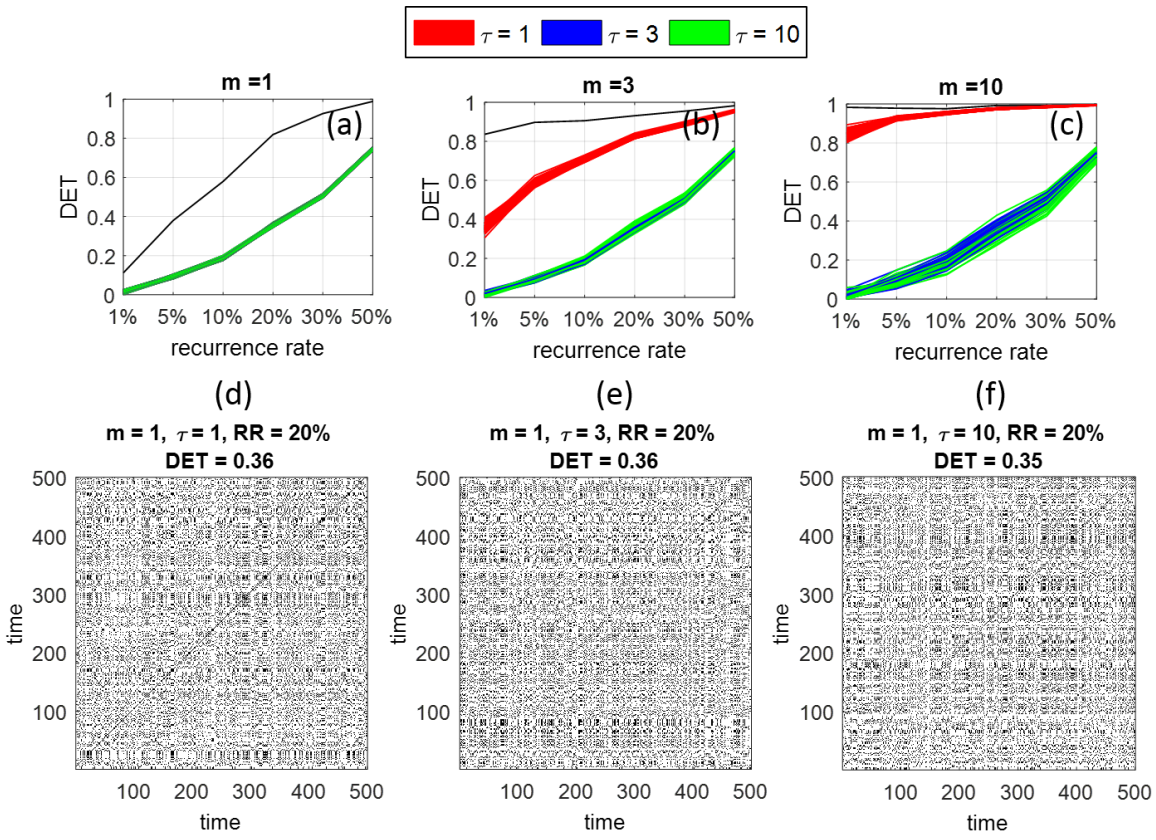

Figure A.2: Impact of recurrence threshold (i.e. recurrence rate) on DET (black line is resulted from original Lorenz time series, while the each coloured ones are resulted from the shuffled series (n=100), while the color corresponds to different selection of τ) with m =1, 3 and 10 respectively for sub-figures a, b and c .Sub-figures d to e present an extracted sample of the shuffled recurrence plot with fixed $m = 1$ and $\tau = 1$, 3, and 10 respectively. Note: on sub-figure a, red and blue band lines are overlapped by green bands, hence not visible

A.2 DET for Correlated Random Series (AR1)

In this following we include the evaluation of DET values of a correlated random series (exemplified using AR1 series) in contrast with uncorrelated random series and Lorenz to showcase that the high DET values is indeed associated with deterministic system instead of its auto-correlation structures (see fig. A.3 and A.4). Although there are also cases at

certain embedding parameter set where diagonal lines of RP artificially increase. Similar to random uncorrelated series, when tau equals 1, AR1 appears to artificially induce long diagonal lines and hence high DET when embedding dimension gets higher. Meanwhile, in addition to mentioned, there appear some (but rare) relatively high DET at certain parameter sets, e.g. when $6 \leq m \leq 10$ and $\tau = 7$ (See fig. A.3 and fig. A.4). However, there is possibility that we have excluded some rare structures of a non-deterministic signal that also showcase high DET values. Therefore, it is important to note that this proposed technique is intended to be used when the user know that the dynamical system is deterministic.

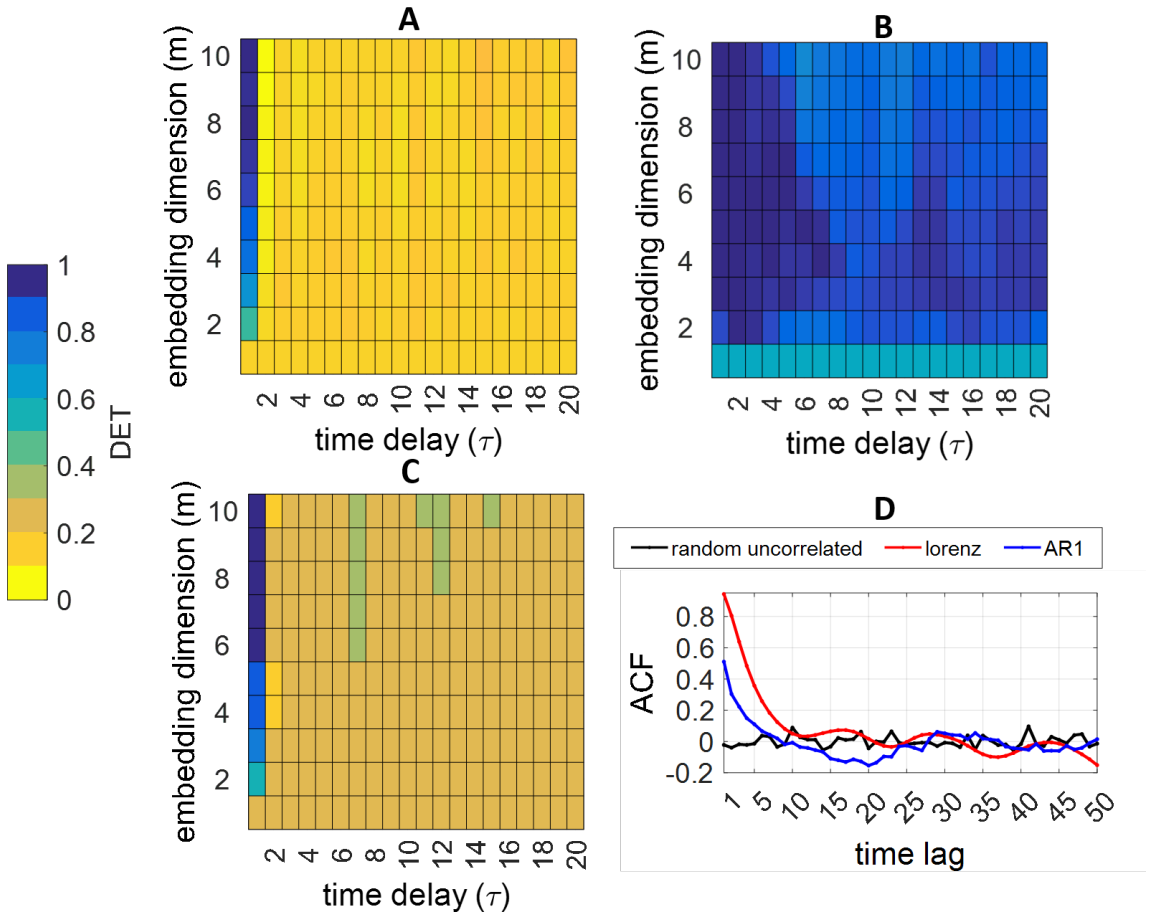

Figure A.3: DET of (A) random uncorrelated series (B) Lorenz and (C) AR1 and their corresponding autocorrelation (D)

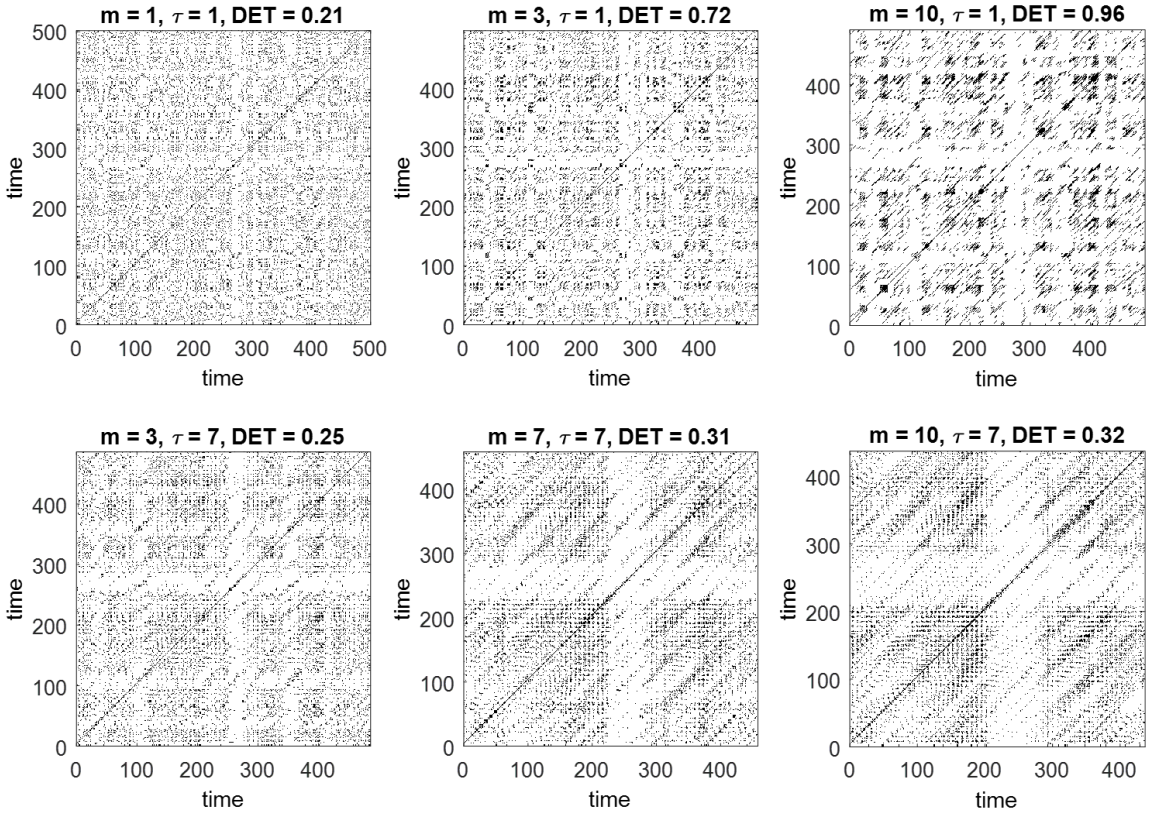

Figure A.4: Selected recurrence plots of AR1 with different embedding parameter sets to showcase the artificial increase of diagonal lines

B Appendix for Chapter 4

B.1 Parameters evaluation for all events using *DET* distance

Figure B.1 shows the parameter set evaluations of all events through DET distance with both the selected set of $m = 3$ and $\tau = 30$hours and sets that allow maximum DET distance. Two events with the lowest DET distances were identified to have the hydrographs with longest duration and highest number of multi-peaks. For these two events to result in higher DET distance, higher embedding dimension m with different tau are required. In general events hydrographs with longer duration that contains more multi-peaks tend to have lower DET distance and therefore would require a higher m.

B.2 *DET* Matrix of All Pairwise Flood Hydrographs

Figure B.2 shows the DET Matrix of all pairwise flood hydrographs that is used for median DET summary.

B.3 Extracted Hydrographs in Dresden Station

Figure B.3 contains all the extracted hydrographs sorted based on their median DET values (from low that indicates rare runoff dynamics to high that indicates common runoff dynamics).

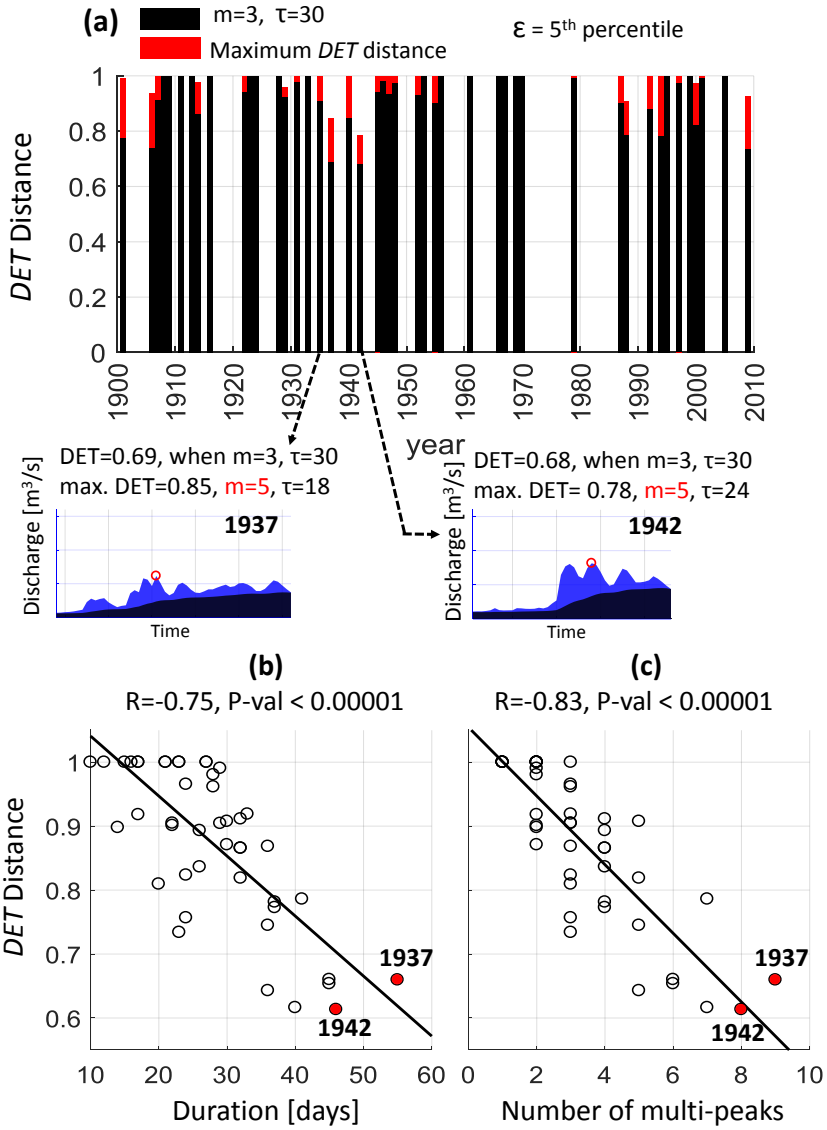

Figure B.1: Parameters evaluation for all events: (a)*DET* distances of all events based on the selected parameters set of $m = 3$ and $\tau = 30$hours (black bar), and maximum *DET* distances from possible sets of parameters within $1 \leq m \leq 10$ and $6 \leq \tau \leq 60$ hours.Examples are shown for event 1937 and 1942 where its maximum *DET* distance can be achieved by using higher m; (b) and (c) are scatter plots and correlations between *DET* distance and event duration and number of multi- peaks in the hydrographs.

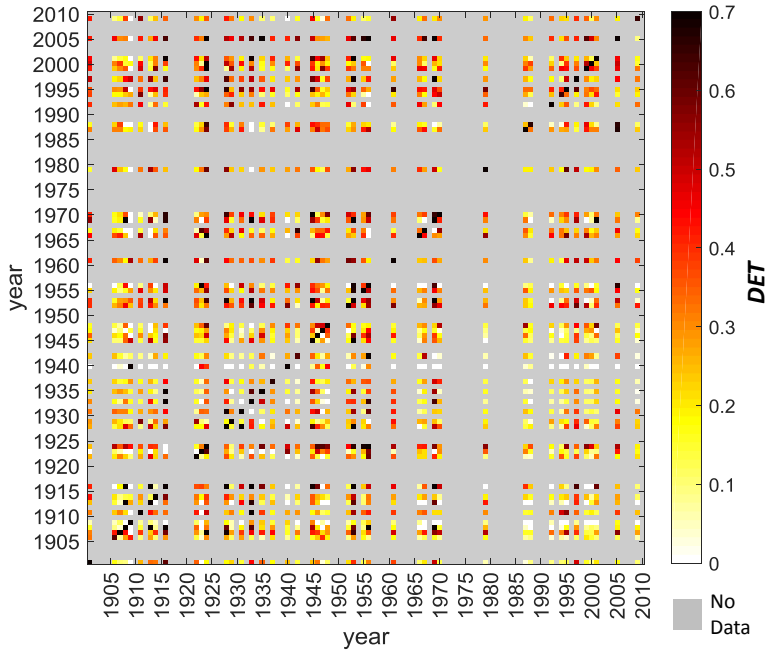

Figure B.2: *DET* Matrix of all pairwise flood hydrographs in February and March extracted from Dresden station from 1901 to 2010. Grey indicates no event satisfied the selection criteria.

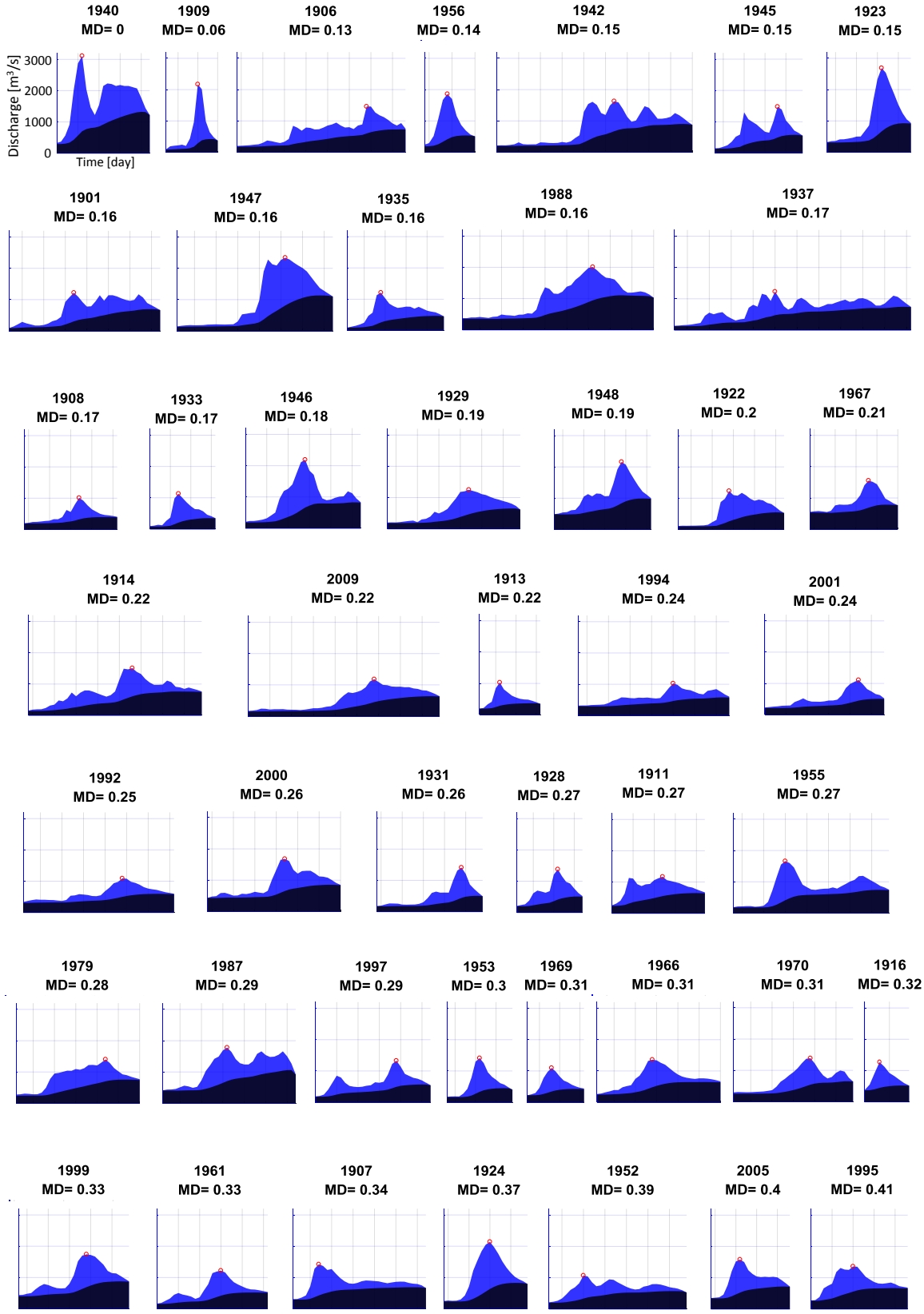

Figure B.3: Hydrographs of all selected February and March floods sorted by median *DET* (MD). Smaller MD values characterize more unusual events in terms of runoff dynamics.